Pēteris Pavlovskis

ANALYSIS OF TWO ACTUAL PROBLEMS OF INTERLAMINAR FRACTURE ASSESSMENT OF LAYERED COMPOSITE

Doctoral Thesis

RIGA TECHNICAL UNIVERSITY
1862

RIGA TECHNICAL UNIVERSITY

Faculty of Mechanical Engineering, Transport and Aeronautics
Institute of Aeronautics

Pēteris Pavlovskis

Doctoral Student of the Study Program
"Transport"

ANALYSIS OF TWO ACTUAL PROBLEMS OF INTERLAMINAR FRACTURE ASSESSMENT OF LAYERED COMPOSITE

Doctoral Thesis

Scientific supervisor
Dr. habil. sc. ing.
VITALIJS PAVELKO

Riga 2022

ABSTRACT

The doctoral thesis presents the results of solving two actual problems of layered composite materials associated with tests for obtaining strength characteristics.

Problem 1: two types of specimens were studied based on applying the nonlinear theory of flexible plates to obtain the interlaminar fracture toughness of layered composites. For a specimen of the thin sub-layer type, a theoretical solution was obtained in relation to the determination of the interlaminar fracture toughness for a mixed II/I mode. The fundamental possibility of using this solution in test practice was confirmed, an assessment of the advantages was given, and the problems associated with the practical implementation of tests based on this type of specimen were noted. The application of the nonlinear theory of flexible plates to the well-known standard specimen of the double-cantilever beam (DCB) was studied in more detail. A theoretical solution was obtained, an iterative algorithm for processing test results based on MATLAB code was developed, highly flexible glass fiber reinforced polymer (GFRP) specimens were tested and their comparison with the results of processing according to the ASTM D-5528-01 standard with correction of the linear solution was given.

Problem 2: there was performed the experimental study of effect of plasticity of process of interlaminar delamination propagation in the layered composite of the elastic-plastic material of a matrix. Two groups of DCB glass fiber reinforced polymer specimens with brittle and plastic matrix were used. Remaining stress and strain were observed for the specimen of second group as well as smooth process of delamination growth near maximum of load.

ANOTĀCIJA

Promocijas darbs parāda divu aktuālo problēmu risinājumu saistībā ar slāņveida kompozītmateriāliem, tos apstiprinot ar testiem, kas parāda izturības īpašības.

1. problēma: tika pētīti divu veidu paraugi, pamatojoties uz elastīgu plākšņu nelineāro teoriju, lai iegūtu slāņveida kompozītmateriālu starpslāņa lūzumu izturību. Plāna apakšslāņa tipa paraugam tika iegūts teorētisks risinājums attiecībā uz starpslāņu lūzuma izturības noteikšanu jauktai II/I Modai. Tika apstiprināta fundamentālā iespēja izmantot šo risinājumu testēšanas praksē, sniegts priekšrocību novērtējums un atzīmētas problēmas, kas saistītas ar testu praktisko ieviešanu, pamatojoties uz šāda veida paraugiem. Sīkāk tika pētīta elastīgo plākšņu nelineārās teorijas pielietošana labi zināmajam dubultkonsoles sijas (DCB) standarta paraugam. Iegūts teorētiskais risinājums, izstrādāts iteratīvs algoritms testa rezultātu apstrādei, pamatojoties uz MATLAB kodu, pārbaudīti ļoti elastīgi stiklašķiedras pastiprināta polimēra (GFRP) paraugi un dots to salīdzinājums ar apstrādes rezultātiem pēc ASTM D-5528-01 standarta ar lineārā risinājuma korekciju.

2. uzdevums: tika veikts eksperimentāls pētījums par plastiskuma ietekmi uz starpslāņainu atslāņošanās izplatīšanās procesu matricas elastīgi-plastiskā materiāla slāņainā kompozītmateriālā. Tika izmantotas divas GFRP paraugu DCB veida grupas ar trauslu un plastisku matricu. Otrās grupas paraugam tika novērots atlikušais spriegums un deformācija, kā arī vienmērīgs atslāņošanās augšanas process tuvu slodzes maksimumam.

CONTENT

LIST OF ABBREVIATIONS

4ENF – four-point bend end-notched flexure
AITM – Airbus Industries Test Method
ASTM – American Society for Testing and Materials
ARALL - aramid reinforced aluminum laminate
BFRP– basalt fiber reinforced polymer
CCM – compliance calibration method
CFRML – carbon fiber reinforced metal laminates
CFRP – carbon fiber reinforced polymer
CNC – computer numerical control
CT – compact tensile
CZM – cohesive zone models
DCB – double-cantilever beam
DEN – double edge notched
ELS – end-loaded split
ENF – end-notched flexure
ESIS – European Structural Integrity Society
FE – finite element
FEA – finite element analysis
FJF – Joggle Flat Joint
FML – fiber metal laminates
FRMM – fixed ratio mixed mode
GFRP – glass fiber reinforced polymer
ISO – International Organization for Standardization
JIS – Japanese Industry Standards
MBT – modified beam theory
MCC – modified compliance calibration method
MMB – mixed mode bend
NL – deviation from linearity
PEEK – polyether ether ketone
PES – polyether sulphone
SC – surface-cracked
SEM – scanning electron microscope
SEN – single edge notched
SLJ – single lap joint
UDL – uniformly distributed load
VIS – visual observation
WIF – wedge-insert-fracture

INTRODUCTION

In last decades composite structures, like glass fiber and carbon fiber has gained popularity in many fields like aviation, automobile, sport and marine. One of the main advantages over other materials are weight to strength ratio as well as shapes and design possibilities. For engineering purposes huge part of a design is connection of these carbon fibre materials. A lot of times adhesive bonding is used instead of usual practices like fasteners and rivets. As there are more composite structures in usage, the repair sector is also becoming increasingly larger [1–5].

As the author of the diploma thesis has major experience in ultralight aircraft manufacturing, there is interest in delamination and its predictability. In ultralight aircraft all of the bearing parts usually are made exclusively from carbon fiber and all of them are bonded (Figure 1.1). It is of great importance for the engineer to predict and take into consideration all of the risks of delamination when designing the aircraft. From work in this field, it is also clear that part of it is repairing already used and damaged aircraft parts. Usually, materials used in the repair process are very thin (not more than 1 mm), as the aero shape of the part should not be changed. This also puts great risk of nonlinear delamination to occur.
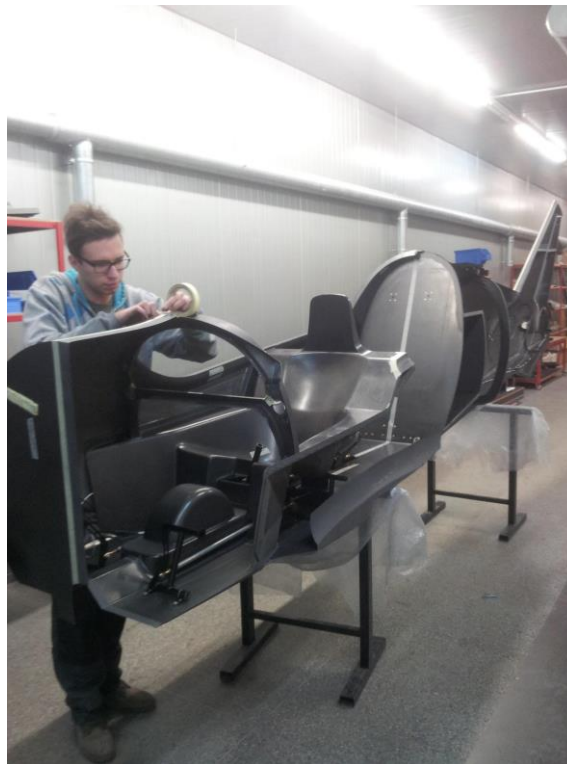
Figure 1.1. Bonding of composite fuselage of "Tarragon" aircraft.

From an engineering and design standpoint even slightest improvement and accuracy of calculation and predictability can give huge gains in aircraft final design. As it can be lighter, cheaper, and most importantly – safer.

However, the aim of this diploma thesis is not to recalculate given ultralight aircraft or make any improvements in its structure.

Effective methods of finite element analysis of the stress-strain state of complex parts of the bearing structure have been created, which allow them to predict their strength and rigidity with high accuracy. Methods and standards have been developed for determining the mechanical characteristics of materials, which are a key component of the calculation complex for assessing the bearing capacity of a modern aircraft.

Naturally, the computational and design complex of the aircraft structure is in continuous development and improvement as the scientific problems put forward by practice are solved.

In particular, to determine the interlaminar fracture toughness of a layered composite, there is an ASTM standard based on the use of a linear model of bending of a DCB specimen [6]. The standard contains several restrictions and corrections for its use, which, however, do not guarantee an accurate determination of the specified mechanical characteristic for a specimen of increased flexibility. This drawback of the standard can be eliminated by using a nonlinear model that allows to obtain an exact solution to the problem of bending the DCB specimen [3-6].

Another problem is related to the deformation properties of the layered composite matrix. A huge number of tests have been carried out on laminated composites with a brittle polymer matrix. In the literature, however, there are practically no publications on the study of interlaminar fracture toughness of a layered composite with an elastic-plastic matrix. Therefore, a purposeful study of the behavior of such composite is of great interest, especially for perspective types of layered composite material.

The above mentioned two relevant problems determine the purpose of this work.

Main goal of this work is research that is focused to analysis and solution of two actual problems of fracture mechanics of layered composites:
1. Improvement of method of interlaminar fracture toughness measurement by using nonlinear DCB specimen, corresponding technology, and software of test data processing.
2. Estimation of effect of plasticity to process of interlaminar delamination propagation in the layered composite of the elastic-plastic material of a matrix.

To achieve this goal author has put forward the following objectives of the work:
1. Literature analysis of composite materials, testing methods and standards, as well as research of tests performed so far.
2. Analysis of the effect of DCB specimen non-linearity to the interlaminar fracture toughness measurement.
3. Theoretical model of the interlaminar fracture toughness for mixed I/II mode, based on the nonlinear theory of flexible plates.
4. Development of mathematical model of non-linear DCB specimen for the interlaminar fracture toughness measurement.
5. Experimental study of the interlaminar fracture toughness measurement of layered composite of high flexibility using the DCB specimen: material selection, specimen designing and manufacturing technology, procedure of testing.

6. Algorithm and MATLAB software of test results processing using non-linear DCB specimen.
7. Experimental study: effect of plasticity to process of interlaminar delamination propagation in the layered composite of the elastic-plastic material of a matrix.
8. Test results processing and main features extraction on the effect of plasticity to the interlaminar fracture toughness of layered composite.

Thesis presents following scientific novelty:
1. Analysis of the effect of DCB specimen non-linearity to the interlaminar fracture toughness measurement is performed.
2. Development of theoretical model of the interlaminar fracture toughness for mixed I/II mode, based on the nonlinear theory of flexible plates.
3. Development of mathematical model of non-linear DCB specimens for the interlaminar fracture toughness measurement is achieved using nonlinear theory of flexible beam bending.
4. It was established that formally defined, the mode-I interlaminar fracture toughness is not a material constant and monotonically decreases as a function of delamination length [7].
5. It has been found that at constant extension rate the relationships between strain energy release rate, load and rate of delamination growth in the elastoplastic stage of loading are complex and mutually disproportionate [7].
6. Experimental results are evaluated.

Practical significance of thesis is as follows:
1. The use of a nonlinear model of the DCB specimen and the corresponding program MATLAB code allows to directly obtain the experimental value of the interlaminar fracture toughness of a layered material of low rigidity (low thickness or low modulus of elasticity of the composite).
2. The DCB model of the specimen and the corresponding program MATLAB code can also be useful in assessing the interlaminar fracture toughness that is obtained from the linear DCB model, and the nonlinearity corrections proposed by the standard.
3. The effects of the elastic-plastic properties of the matrix of the layered composite, revealed during the tests and a thorough analysis of their results, require a significant correction of the procedures for the calculated assessment of the interlaminar fracture toughness of the layered composite with the elastic-plastic properties of the matrix.

The following methods of the research are used in thesis:
1. Theory of elasticity of anisotropic materials.
2. Layered composites mechanics.
3. Strength theory of layered composites.
4. Non-linear theory of bending of flexible beams.
5. Fracture mechanics.

6. Experimental fracture mechanics.
7. Mathematic statistics.

Main results of thesis include:
1. Development of theoretical model of the interlaminar fracture toughness for mixed I/II mode, based on the nonlinear theory of flexible plates.
2. Development of mathematical model of non-linear DCB specimens for the interlaminar fracture toughness measurement is achieved using nonlinear theory of flexible beam bending.
3. Algorithm and MATLAB software of test results processing using non-linear DCB specimen was created.
4. A satisfactory result can be obtained by using an equation that implies correction of the formal expression of G_{Ic} according to the linear model by its multiplication by the standard correction factor [8].
5. Results confirm the suitability of the nonlinear model of DCB specimen for determination of the G_{Ic} quantity of a composite within the limits of applicability of the standard test methods based on the Euler theory of bending of beams [8].
6. Experimental study: effect of plasticity to process of interlaminar delamination propagation in the layered composite of the elastic-plastic material of a matrix is performed.

Doctoral thesis contains introduction, 5 chapters, conclusions, and references. Thesis volume includes 99 printed pages, 61 figures, 3 tables and bibliography containing 108 titles.

In the period of making of the thesis 5 publications have been published in international journals:

Scientific publications
1. Pavelko V., Lapsa K., Pavlovskis P. The Effect of Plasticity to Interlaminar Fracture Toughness of Adhesive Bond of Composite. IOP Conference Series: Materials Science and Engineering, 2017, Vol.251: 3rd International Conference on Innovative Materials, Structures and Technologies (IMST 2017), pp.012081.-012081 ISSN 1757-8981. e-ISSN 1757-899X. Available: doi:10.1088/1757-899X/251/1/012081
2. Pavelko V., Lapsa K., Pavlovskis P. Determination of the Mode I Interlaminar Fracture Toughness by using a Nonlinear Double-Cantilever Beam Specimen. Mechanics of Composite Materials, 2016, Vol.52, No.3, pp. 347.–358. ISSN 0191-5665. e-ISSN 1573-8922. Available: doi:10.1007/s11029-016-9587-y

Conferences papers
1. Pavelko V., Kuzņecovs S., Lapsa K., Pavlovskis P. The Effect of Plasticity to Interlaminar Fracture Toughness of Adhesive Bond of Composite. No: Матеріали XIII міжнародної науково-технічної конференції "ABIA-2017", Ukraina, Kiev, April 19.–21., 2017. Kiev: 2017, pp. 17.38.–17.43.

2. Pavelko V., Lapsa K., Pavlovskis P. The Effect of Plasticity to Interlaminar Fracture Toughness of Adhesive Bond of Composite. No: 3rd International Conference "Innovative Materials, Structures and Technologies: (Abstracts)", Latvia, Riga, September 27–29, 2017. Riga: RTU Izdevniecība, 2017, p. 126.

3. Pavelko V., Lapsa K., Pavlovskis P. Определение вязкости межслойного разрушения первой моды с помощью нелинейного двухконсольного балочного образца. Механика композитных материалов = Mechanics of Composite Materials, 2016, Vol. 52, No. 3, pp. 491.–506. ISSN 0203-1272

1 GENERAL OVERVIEW

1.1 Composite materials. Functions and structure

The present study focuses on the analysis of interlaminar fracture of layered composites and the improvement of methods of measurement of interlaminar resistance. And since the phenomenon under study and the mechanical characteristics depend on the choice of primary components of the composite, its structure, manufacturing technology, application conditions, the Chapter 1 provides an overview of research on these aspects in terms of their effect on the of interlaminar resistance of layered composites.

There is a lot of information about composite materials, structure, manufacturing methods from books, internet resources, studies and nowadays even videos online. Composites consist of individual materials called components. There are two main components: matrix and reinforcement. Both are needed. The matrix material, for example epoxy resin holds the reinforcement materials, maintaining their position. Reinforcements give their mechanical and physical properties for example strength, to improve the properties of the matrix. Synergy creates material properties that are not available from individual components. There are different combinations of matrices and reinforcements used to achieve what is needed [7-9].

A vacuum infusion produces a final product with around 40 % resin and 60 % fiber. The durability of a part is highly dependent on this relationship [10].

The matrices usually consist of two components – resin itself and hardener, that must be mixed in right proportion and very carefully, before using usually refilled to different container, so there is no chance of using resin without hardener that may accumulate on the sides of the container of mixing.

The matrix types mostly used for composite structure production are:

- Polyester resins, that are relatively low cost but tend to react by ultraviolet radiation and degrade over time [10].
- Vinyl Ester resins are purple greenish. These resins are more flexible than polyester resins and have lower viscosity, as well as more transparency. There is also less decomposition compared to polyester resins [10].
- Epoxy resins are the type of resin that author has used in his time working in aviation production and in this thesis experimental part. When they are fully cured, they are almost transparent, so in finished product the reinforcements, like carbon or glass fibers are clearly visible. The downsides of this type is brittleness and physical property decrease if moisture is present. This is the most used type of resin for aviation and structural purposes [7–10].

Reinforcement usually increases the stiffness and significantly prevents the propagation of cracks. The main concern and decisive factor are bond between reinforcement and matrix. The bond between both components is one of main factors for finished parts final properties. Huge role here is played by production methods used [10, 11]. This aspect is briefly viewed later in this chapter.

There are two main types of fibre reinforcement materials:

- Short fibre-reinforced, from authors experience a lot less used for aviation purposes, as strength to weight ratio is not as good as second type. Still there are a lot of uses for this type and many upsides of using it.
- Continuous fibre-reinforced. This type is used a lot in aviation purposes, it comes in different weaves and thicknesses. Example of rolls of carbon fiber reinforced material is shown in Figure 1.2.

Figure 1.2. Rolls of continuous carbon fiber reinforced material.

By using type of component that is shown in Figure 1.2 there is possibility to make final product from layers of the carbon fiber reinforced sheets. There are many variables like thickness, numbers of sheets, direction of sheets and material of sheets that allows engineers to design parts with exact needed properties [1, 10].

Great way to make quality parts is by using prepreg type of carbon fiber sheets. This is material type that is already consisting of both matrix and reinforcement in right proportion. It is easy to work with and provides better quality final products. It is also more expensive and requires temperature and pressure treatment for production of parts. Almost all the "Tarragon" aircraft structure was made from this type of composite.

Other reinforcement methods are also being used. One of examples is making ARALL, it consists of metal sheets in between aramid/epoxy layers. One of advantages of this structure is impact damage and resistance to fatigue cracking. Example of this type of layered composite material is shown in Figure 1.3 [2, 5].
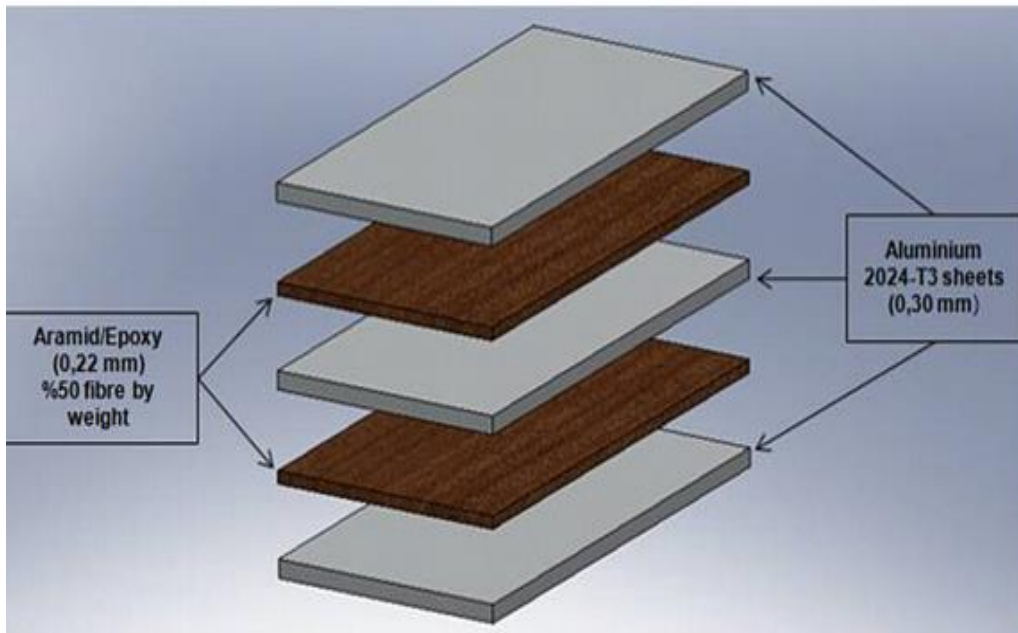
Figure 1.3. Presentation of fibre metal laminate (ARALL 2).

There is huge variety of sandwich type of composite structures as shown in Figure 1.4 below. One of examples is to use honeycomb or foam type of material in between carbon fiber outer layers. This provides great strength to weight ratio. Downside of this type of structure is the possibility of damage in case of direct impact to the surface [2, 3].

Figure 1.4. Sandwich structure with foam between carbon fiber sheets.

In a study by Khurram and Xu et al. the report provides a summary of techniques for making a 3D structure of graphene and examples of how these foam structures are used as a core to form the relevant polymer composites [3].

Usually, one monolayer of composite is substantially anisotropic. Therefore, a very important aspect of the structure of the layered composite is the order of layers stacking. If maximum tensile strength is to be ensured, most layers must be stacked with an orientation angle of 0° in the direction of the required maximum strength of the composite. However, layers

with a stacking of 90° will be exposed to the risk of cross-ply destruction during the delamination of the composite.

1.2 Composites manufacturing methods

There are different production methods [9]. Picture below (Figure 1.5) shows production of composite aircraft parts by the author of thesis.

Figure 1.5. Production of carbon fiber composite part from authors personal photo archive.

There are many different production and molding strategies used depending on shape, size, materials and final product properties and surface quality needed. Some parts, like wind turbine blades are very large compared to small brackets made for ultralight aircrafts or bicycle frames. Production also depends on automatization and human labor and tooling [9].

Like in many industries, the cost greatly increases with quality, higher weight to strength ratio and over all better properties of the produced parts. There is also higher cost of producing low amount of parts as tooling, like mold production in the first place, plays huge role on total cost. From authors personal experience that is sometimes the case to go against using composite parts and find different solutions.

If prepreg is not used, the production of composite parts usually consists of mixing resin with hardener in right proportion before joining it with reinforcements, for example glass fiber sheets, production of parts like that is shown in Figure 1.6.

Figure 1.6. Production of parts by using wet lay-up technology.

There are few ways to do it, for example before or after the sheets are shaped in molds. Depending on this, there are different names for each of the production methods. Here are some of the most common ones:

- Wet lay-up when reinforcements are joined with matrix and then laid into molds and shaped.
- Vacuum Infusion, when sheets are laid into molds and shaped, later vacuum is applied and resin is being sucked in. This method ensures that structure has less excess resin and better weight to strength ratio, also chance of voids are lower.

Depending on the method used there may be need for vacuum bag used as shown in Figure 1.6 above, that greatly improves the quality and dimensions of the part, by also reducing weight. Also, to fasten the curing rate, heat may be used [10].

Molds are made from different materials, that include composite materials, metals, woods, dense foam. Sometimes its hand shaped, but usually done by CNC machinery. The other way to make mold is to machine or shape model of the part, that is with right dimensions and make mold from composite materials directly from it.

Sometimes molds are made from same material, that part will be made from, as in case of using heat for post-curing process the expansion rate is same and final dimensions are right. This is very important when final product is made from prepreg, as post curing is always needed.

When producing part and mold for it, there is importance of which side of final product is more important, as that is the side, that should face the mold. It's usually called – A face.

Mold can also consist of many parts itself, as it is of great importance that later the finished product can be removed from the mold. Mold should also have extra surfaces and flanges for cutting lines of finished parts and places to attach vacuum bag if needed.

Vacuum molding greatly improves quality of part as there is less chance for air gaps between layers. It also improves geometry of product, especially in corners and edges. For seal between vacuum bag and mold there is special sealing tape used.

Opposite to vacuum, pressure also can be used. In case of prepreg products autoclave is used. There is usage of both, pressure, and vacuum in same time, this is achieved by using heated and pressurized oven, where mold is being placed. In same time, in this oven, there is also connections to vacuum system. All the parameters must be strictly controlled to meet manufacturing specifications. This procedure allows to make very high-quality composite parts, that can be safely used for aircraft operations.

Vacuum infusion type of production can use molds that are from both sides of the produced part, making both sides – A face (or one side as A face is vacuum bag is used). In this method reinforcement is first put in between molds, and only after system is sealed and vacuum is used, then resin is being sucked into produced part in between fibers. This process also can benefit from elevated temperature to speed up the curing process.

Before part can me produced in made, there are also steps to prepare the mold, for example by waxing it, so part does not stick to the mold in process of curing. These steps are very important to follow, otherwise mold and part may be damaged or destroyed.

After part is cured and can be extruded from the mold, there are usually more steps to achieve final result. For example: drilling holes, cutting part to right dimensions, applying surface coatings. It depends when CNC drilling and milling is used and when it is done by human. Sometimes templates are used to make the process faster and more precise [4].

1.3 Physical properties, failure, and testing

The physical properties of composite materials are anisotropic, that means different in different directions. That is one of its biggest advantages compared to metals, that are isotropic materials. This allows engineers to design components with minimalistic material used, that can lead to great weight savings [10].

If both the fibers and the resin are facing parallel to the direction of loading, the deformation of both phases will be the same. This condition shows an upper limit on the strength of the composite and is determined by the rule of mixtures, as shown in the equation (1.1) [11]:

$$E_c = \sum_{i=1} V_i E_i, \tag{1.1}$$

where E_c is the effective composite Young's modulus, and V_i and E_i are the volume fraction and Young's moduli, respectively, of the composite phases.

For example, for a mixed material consisting of α and β phases with iso-strain, the Young's modulus is as follows in equation (1.2) [11]:

$$E_c = V_\alpha E_\alpha + V_\beta E_\beta, \tag{1.2}$$

where V_α and V_β are the respective volume fractions of each phase.

The lower limit is determined by the iso-stress conditions when the fibers and the matrix are oriented perpendicular to the direction of loading – equation (1.3) [11]:

$$\frac{1}{E_c} = \Sigma_{i=1} \frac{V_i}{E_i}. \tag{1.3}$$

Following the above example, if there were a composite material consisting of α and β phases under iso-stress conditions, the Young's modulus of the composition would be as in this equation (1.4) [11]:

$$E_c = (E_\alpha E_\beta)/(V_\alpha E_\beta + V_\beta E_\alpha). \tag{1.4}$$

The isostrain condition means that when loaded, both parts experience the same stress levels but will experience different loads. Under relatively iso-stress conditions, both phases will experience the same stress, but the strains will be different in each phase [10, 11].

Stiffness of the composite material is increased if the fibers are aligned in the same direction as the loading. There is also possibility of tensile fracture of the fibers in the same time, if the tensile strength is greater than the strength of the matrix. If the fiber has incorrect orientation angle θ, there are many possible Modes. The change of tensile strength compared to angle of orientation is briefly shown in Figure 1.7 [12].
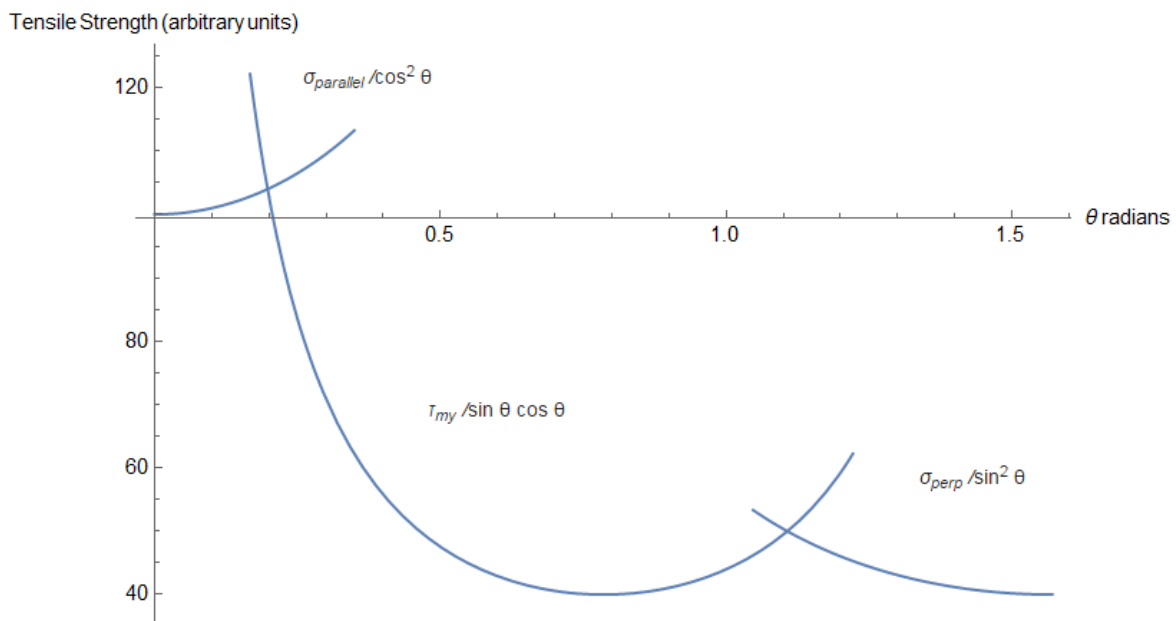
Figure 1.7. The diagram shows the three fracture modes that composites can have, depending on the angle of misalignment with respect to the alignment of the fibers in parallel with the applied stress [12].

Most commercial composites are formed by randomly dispersing fiber scattering and orientation, in which case the composite Young's modulus falls between the isostrain and isostress boundaries. In aviation industry strength to weight ratio must be as good as possible,

so orientation of fibers are strictly controlled. Documentation of product sheet layer angles is called ply-book [9-12].

The rigidity of the panel also depends on the construction of the panel. For example, the fiber reinforcement and resin, the paneling method, the thermosetting to the thermoplastic material and the type of weave [10, 12].

As of repeated stress cycles the material can fail between the layers. This is called delamination. Same can happen in case of impact on surface, there is more detail about this failure type at the start of the second chapter of thesis.

Compared to metals composite materials may be much more fragile to impact damage, it depends on the design of composite part. There can also be some microscopic scale voids when the composite part is produced. It is very important to detect these errors in quality control process of manufacturing. On larger scale the damaged parts of composite parts are visible by eye or by using non-destructive testing methods [2, 4, 10].

There are many parameters that affect the performance of the bonded joints. As bonding is becoming more and more used method in joining wide range of materials. For example in "Tarragon" aircraft that author of the thesis has worked on, most of the separate composite component parts where bonded together to achieve all the aircraft structure components, as shown in Figure 1.8.

Figure 1.8. From many parts bonded structure of aircraft "Tarragon" fuselage.

As bonding is a viable method for joining a wide range of materials. Today, however, there is a great demand to increase service life, reduce costs and improve structural safety. Therefore, making of new resins or additives that can be easily recycled, heal or self-heal connected structures is of great interest to the industry [13-17]. However, one of the main challenges facing the aerospace industry with advanced composites, given their inherent complex handling of damage, is structural repairs [18-24]. Many research papers have been done about this self healing and bonding theme in general in recent years [25 – 27].

One of the examples is based on a microencapsulated drug and catalyst into the polymer resin (see Figure 1.9). As the crack spreads through the capsules, the monomer accumulated in them is released along the crack, where it meets the dispersed catalyst, initiating polymerization and thus regenerating [23].

Self-healing of layered composite is perspective method of increasing of the interlaminar resistance of layered composites.
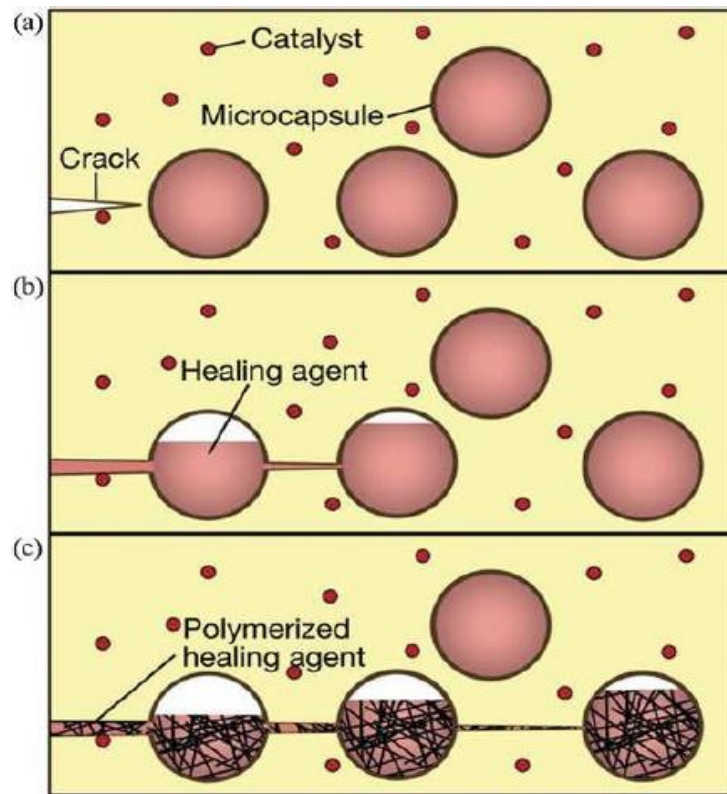
Figure 1.9. Microcapsule-based self-healing concept [23].

Testing and calculations are usually done for the weakest type of stress or weakest link of the chain. As peel stress is the most unfavorable, testing of it, usually gives the best evaluation of bonded joints structural integrity. If heat resistance is an important requirement for the adhesive, a creep testing should be done. In addition, aging tests are performed to assess longevity [23].

Structural adhesives are increasingly being used in new applications, replacing conventional bonding methods. As they become more and more popular, there is more interest in studying the subject and development for improvement of toughness [24].

When designing bonded structures and choosing what adhesive to use, there are many different properties, like usage temperature, cost, loads, moisture also plays huge factor in lowering fracture toughness [25].

At design stage the bond testing can be done by manufacturer and designer in the way they see the best fit and need. Alternative is to use universal testing methods that are well known and documented [16, 26–29].

In the figure below (Figure 1.10) is shown most popular bonded joint types of composite structures. Usually, they are two dimensional that is sufficient as stresses in direction of load is far higher than in the width [30]. The effects of overlap length and adhesive thickness must also be taken into account. Predicting the failure load of connected connections is an important issue to increase confidence in the design [19].
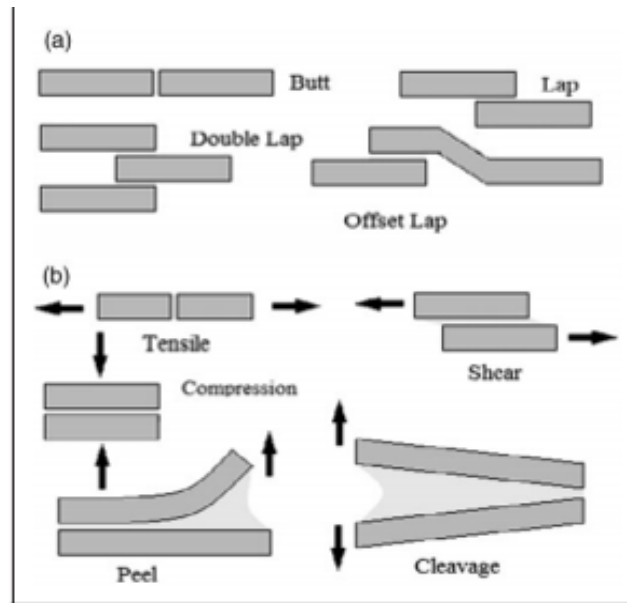
Figure 1.10. Schematic of (a) common joint structures and appropriate (b) types of joint stresses [30].

There is also great importance and reviews on adhesive contact calculation methods, focusing on general mechanical models of continuity for attractive interactions between solids, which are suitable for describing the binding and separation of arbitrary bodies [31, 32].

Changes in the stacking sequence also affects interlayer stresses and damage loads.

There are also article reviews related to the surface treatment of composite materials. The peel-ply is used as a removable layer in the composite material layout and is torn off to modify the surface for gluing [33]. From thesis authors personal experience only removing peel-ply was not enough to use the surface as ready for bonding and additional sanding and cleaning needed to be done. In order to ensure a clean and preferably active surface, primary and minimal pre-treatment of the surface is required before gluing. Modern advances achieve this by using either the peeling method or various machining operations.

When speaking about adhesive thickness, as it increases, the final tensile load decreases. In addition, the maximum allowable displacement of the adhesive to the adhesive when completely damaged is directly proportional to the thickness of the adhesive, which differs from that of the fragile adhesive.

Bonding has many advantages compared to other mechanical fastening types like riveting and bolting. Some of advantages are reduced production time, weight, and better design. Although surface preparation for bonding is critical part of the process. Sometimes both methods can be used together as failsafe system. Some of the common manufacturing bonding methods are shown in Figure 1.11 [25].
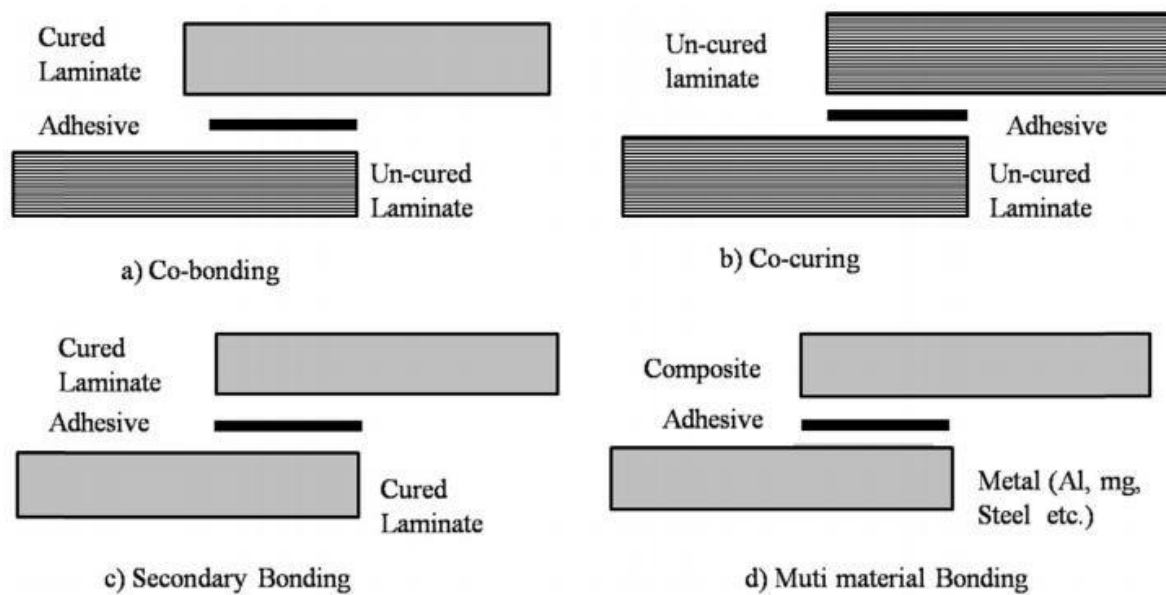
Figure 1.11. Mostly used bonding methods between two composite parts [25].

Using a double console beam test, the resistance of type I mode to fracture of one hardened and two secondary connected systems has been determined. The initial defect was found to have a large effect on the fracture toughness initiation values. It was also found that in both secondary connected systems, cohesive failure occurred predominantly, while the hardened joint failed at the interface [34–36].

As mentioned by the study of Khoshravan M. assessing and evaluating the adhesive bond is very important to achieve safety mode. Experimental testing and calculations show agreement about effectiveness of bonded joints [37].

Glued joints can provide a longer fatigue life than conventional joining methods, provided that a set of requirements is met. One of the most important requirements is the mechanical preparation of the glued joint surface, which improves the adhesion of the joint interface [38, 39].

Studies on investigating the effect of the macroscopic condition of the substrate surface on the strength of adhesive joints has been done. After analysis of the results, it was observed that in the case of brittle adhesive, the patterns can increase the bonding of untreated substrates [40].

A high-modulus CFRP system has recently been developed to improve the load-bearing capacity and usability. The results of the study indicate that the use of a silane compound significantly improved the strength of the bond. Although the presence of glass fibers helped to improve the initial strength of the system, it did not improve the strength of the bond. The use of both methods improved both the overall bond of the fastening system and the environmental resistance [41, 42].

Azari MPS and Spelt JK. studied the effect of surface roughness on the fatigue and fracture behavior of a hardened epoxy adhesive system and came to conclusion that its extremely important parameter for bond longevity [43].

Fracture energy is more sensitive to changes in thickness than strength [44, 45]. Studies also show that by increasing overlap length joints with flexible adhesive increase in strength almost proportionally [46, 47].

In experimental studies where lower joint strength has been achieved by larger bond line, the contributing factor may be more places for possible voids, adhesion, and other errors. In the same time with increased adhesive thickness the fracture toughness also increased [25, 48–50].

For bonded joints, especially with increased thickness, the Constance of thickness also plays huge role. Sometimes it can be achieved by using textile membrane into the adhesive layer. Shown in Figure 1.12 below.
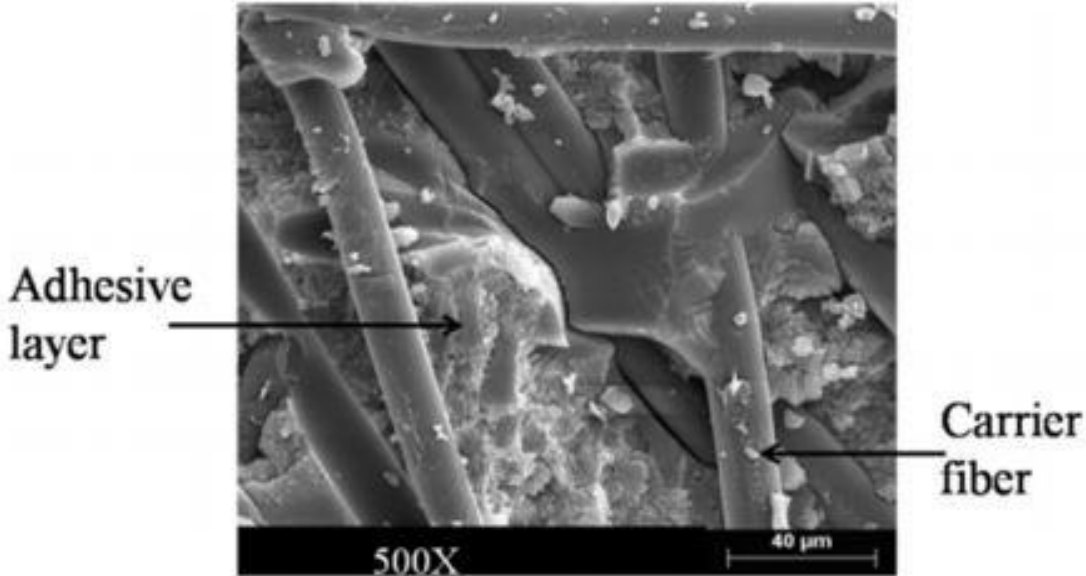
Figure 1.12. Fractured composite that shows the carrier fiber in adhesive film to support the bond line thickness [25].

It is shown that it is difficult to achieve uniform adhesive thickness, resulting in quite significant difference as shown in Figure 1.13 [25]. In summary geometrical parameters play huge role for bonded joints and must be taken into consideration. There are many unknown factors so far and many more tests and studies must be done in this field.
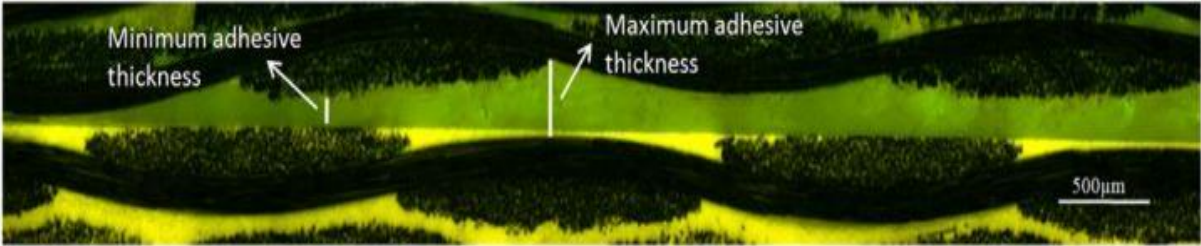
Figure 1.13. Variation in bonded joint thickness [25].

There are different ways to reduce problem of stress concentration at the end of the overlap. Many modifications have been made in geometry to achieve it. Engineering aim is to reduce the shear stress of the interface by using joined laminates to strengthen existing structures [51, 52].

The results of numerical analysis have been done, which show the advantages of using cones in the design of reinforced beams [53].

For example, Kishore et al. [54] transformed SLJ into a flat FJF (Figure 1.14), which overcomes eccentricity in the presence of a hoop to keep the loads in the plane and also to avoid the bending effect. There was a 90 % increase in the load on FJF bond connections when compared to flat connections.
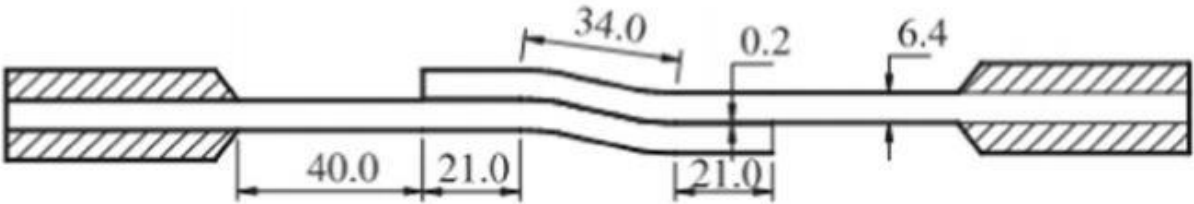
Figure 1.14. Flat joggle flat joint [54].

Dimensional modifications consist of flattening of the outer surface of the patch, thickening of the adhesive near the overlapping outer edge, filling of the slit with adhesive (plug filling) using fillets of different shapes and sizes at the ends of the patch, uncoupling of the outer and inner edges of the plate. With the correct connection configuration, the residual strength can be increased by 27 % for single lap connections and by 12 % for double lap connections [55].

Figure 1.15 below shows the gained effect of the conical end plate and the reduction of stress at the end of the overlap. However, as production is a difficult task. Thus, it was considered that instead of applying the cone over the whole bonded layer, it would be more efficient to apply it to a smaller portion [25].
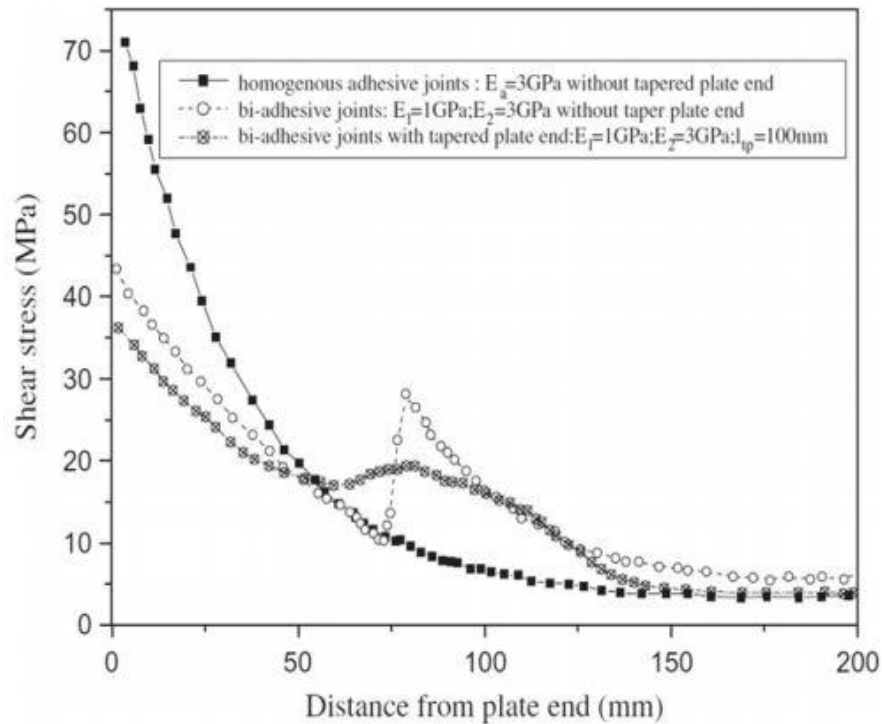
Figure 1.15. Shear stress distribution in the Carbon Fibre Reinforced Plastic strengthened steel beam with mixed adhesive joints under UDL load [25].

Engineers also need to be aware of the layer fiber orientation and sequence of them, when designing bonded joints. As stacking them in different order can affect failure mode [26], the bearing capacity and the fatigue resistance of the connected joints [25]. Another important factor is usage of the best possible stacking sequence of each of the parts produced. In the end it's clear that it is all geometrical parameters like cut angles, fillets, thickness and stacking sequence, play huge role in final quality and properties of the bond.

Studies have shown that by increasing overlap length, the strength also increases, but by increasing overlap width the load-bearing capacity increases. Width ranging from 5 m to 25 m and length from 5 mm to 25 mm were compared. It must also be mentioned that this is true only up to a certain dimension. There is also dependence on ratio of both values not only total adhesion area. Huge role is also played by adhesion stiffness, as it increases the torque force the bond can withstand. Studies had been done not only on composite, to composite, but also metals to metals and metals to composites bonds. From authors personal experience this is very important, as especially in aviation field there is huge need for connections of dissimilar material joints, for example – aluminum hinge bracket attachment to carbon fibre wing structure of an aircraft.

As composite structures or part of it become more and more popular, there is current need for better and improved adhesives. Also, as this field invents new composite material types, there is need to meet the new requirements for it.

An innovative method for bonding materials is usage of adhesive tape. Although from personal experience of author in real life usage the circumstances of, for exam0ple tolerances between parts, that concludes bond thickness sometimes are factor that dismisses possibility to

24

use such technologies. In same time there are many opportunities for technologies like this to be well suited for.

As world is moving towards better recycling methods, there has been research done with new developments on separation and reuse of bonded surfaces. This goes in hand with development of self-healing adhesives mentioned previously in this chapter. One of the self-healing adhesives is made by using carbon nanotubes, brief concept of it can be seen in Figure 1.16 [56, 57].
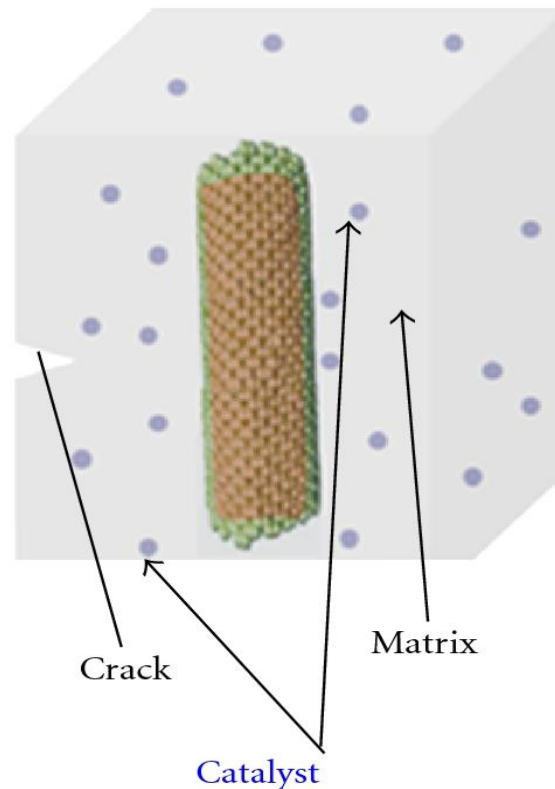
Figure 1.16. Concept of the self-healing process using carbon nanotubes [56].

To increase the fracture toughness of the polymer addition of microcapsules can be used. There are also alternative system that use double microcapsule epoxy resin chemistry in thermosetting epoxy. Still this research is in early stages of the technology and many problems needs to be addressed. One of them being installation of the systems on nowadays used bonding methods and adhesives used. Materials being bonded also is important factor.

Impact resistance is also important and interesting field of research at the moment. However, research into the use of self-healing materials for adhesive sutures is at an early stage and there are still many technical challenges to incorporating self-healing concepts into the adhesive bond [25].

For better testing and importance of comparison of results, there are several ASTM and ISO standard test methods available, to determine the properties of bonded materials [6]. However, there are still some shortcomings that need to be addressed. For example, crack fatigue monitoring is still not developed in the fatigue test standard, which is a challenging issue. Three

techniques (visual, compliance-based approach and effective delamination length) were used to monitor crack growth in the low fatigue mode [32]. This agreement suggests that further development of the test procedure to incorporate automated data acquisition and analysis may be worthwhile.

A procedure has been developed based on real-time monitoring of the conformity of the specimen to the experimental characterization of the fatigue strength of cracks in composite materials. The methodology was applied to the Mode II load in the three-point end incision flexibility test. The accuracy of this methodology allowed the detection of neglected phenomena such as thermal expansion of the test system or friction between the specimen and the reinforcement [56].

Recently, Chaves et al. proposed a new apparatus and method for determining the strength of adhesive joints in a mixed mode [25]. Mixed Mode I + II fracture characterization tests are performed with a dual actuator load device to obtain a fracture shell. The results of the experiment revealed that the linear energy criterion works well when describing the fracture sheath of these joined compounds [57].

There is huge need to also look at different chosen material types to be bonded, as that greatly changes final properties of the attachment to each other in case of using the same adhesive. The impact reaction of adhesive compounds has not received enough attention compared to quasi-static loading. Adhesives for joints with composite materials water showed little importance. In both tests, adhesive joints have occurred in joints with steel adhesions and delamination of joints associated with the composite material [58]. Environmental factors have been investigated on the shear and tensile strength of multi-material adhesive compounds. The specimens were made of carbon fiber – epoxy composites, aluminum and two types of improved steels: wear-resistant and high-strength. The freeze-thaw cycle had a negligible effect on both GFRP and BFRP tensile properties, but had an adverse effect on CFRP, resulting in a 16 % decrease in strength and an 18 % decrease in modulus after 90 freeze-thaw cycles. The deterioration of CFRP was associated with the sensitivity of carbon fiber and epoxy compounds to freeze-thaw cycles [59].

The freeze-thaw cycle showed almost to non existent effects on the tensile properties of both: boron fiber reinforced polymer and glass fiber reinforced polymer, but the effect on carbon fiber reinforced polymer was opposite. This further speaks of the problem, that material and adhesive design is playing huge role on over all strength of the bond [25, 59]. Values as internal fracture toughness plays huge importance in order to achieve the best properties of bonding different adhesives. Joint example showed in Figure 1.17 [25].
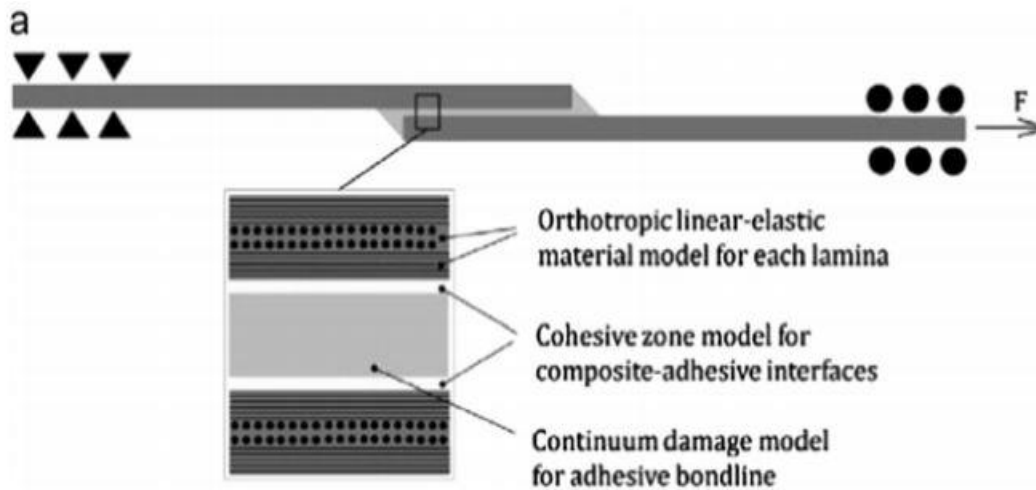
Figure 1.17. Materials used in a co-bonded adhesive joint with removal of wet peel-ply [25].

There are six failure modes according to the Airbus Internal Test Protocol. Described in detail in AITM1-0053 standard:

1) pre-hardened glue (delamination);
2) fiber / peeled resin adhering to the interface;
3) at the peeled layer adhesive interface;
4) adhesive inside the bond;
5) at the interface of the glued panel to be glued (wet-wet intermediate phase);
6) inside the glued panel (delamination).

Many researchers [34, 48, 51] have studied the parameters that affect the collapse regime of adhesive bonds. It has been observed that the disintegration mode and the properties of the connections are interrelated and are influenced by various parameters such as joining methods, moisture, temperature, type of adhesive, preparation of surfaces, dimensions, etc. [25, 60].

When compared to other parameters temperature as well as humidity have a larger effect on the failure of the glued join. So far it is studied that brittle fracture happens at lower temperature, while malleable crack has formed at high temperatures [25].

Celemin and Llorca has submitted research on bonds at normal and elevated temperature, up to 1200 °C. When using Al_2O_3 / Nicalon SiC composite the results showed that as temperature was higher, the tensile strength and modulus was seen decreasing. Study showed that around 800 °C temperature the properties were not changing any more. The final results also show the good connection between tests done and prediction of cracks spreading in the lesion area [61].

Some studies have been done with different materials but even higher temperatures, up to 1600 °C. Similar results to the one mentioned above was concluded after calculations and real-life tests. One of the main parameters measured was internal fracture toughness [62]. From thesis authors experience such high temperatures are never used for carbon fiber reinforced composite structure bonding in aircraft field, where he has been working as engineer.

2 INTERLAMINAR DELAMINATION OF LAYERED COMPOSITES

2.1. Causes and examples of composite delamination

This chapter primarily analyzes the physical and mechanical properties of layered composites related to strength and stiffness. The most popular test methods for obtaining these characteristics are also discussed in more detail.

The main difference between composites and traditional (primarily metal) structural materials is the possibility of their "design under a given load". The material designed according to this principle has maximum strength in the direction of action of the main load. And given the much higher specific strength (strength/density ratio), the designs of their high-strength composites are substantially lighter and, ultimately, more cost-effective. Structures made of high-strength composites are also less prone to fatigue and corrosion.

At the same time, a strong anisotropy of strength and elastic characteristics has negative consequences for use in operation in the case when, along with the main loads, side effects also occur. It is known that a typical quasi-isotropic carbon fiber reinforced epoxy laminate has a tensile strength in the plane of 700–1200 MPa, which depends on the exact arrangement, but the tensile strength through thickness can be as low as 50 MPa and the transparent permeability is also relatively low. Therefore, the thickness stress in the component can cause delamination to occur if they exceed the through-thickness strength. This can be cause of impact damages in aircraft operation.

Aircraft composite structures can be damaged in many ways. There is human factor, for example, if the aircraft is not serviced and handled properly. There is also risk of collision with another aircraft or other objects on the ground (see Figure 2.1) [63].

(a)

Figure 2.1. Risk of damaging aircraft fuselage on the ground when loading (a) and towing (b) [63].

When the aircraft is flying the damage to the structure can be done by bird strikes and hail (see Figure 2.2) [62].

(a)

29

(b)

Figure 2.2. Damage done to the aircraft fuselage by bird strikes (a) and hail (b) [62].

All this different kind of composite structure damage types lead to delamination of composite materials as shown in Figure 2.3 [63].
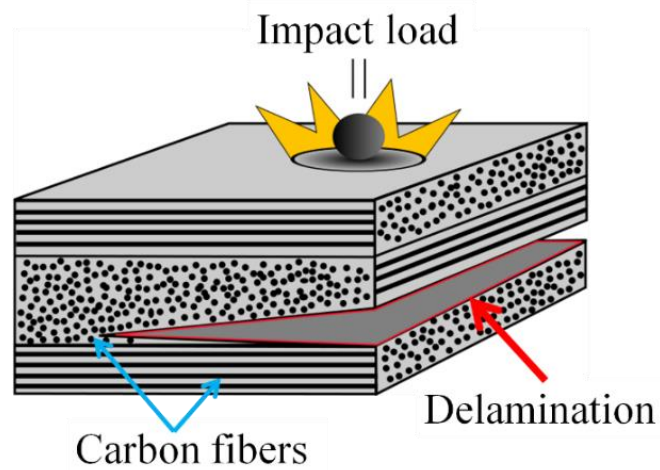
Figure 2.3. Delamination in composite structures caused by impact [63].

2.2 Interlaminar fracture toughness

Delamination can occur in composites that are made of carbon or glass fibers that are of high strength while being used with resin that is typically weaker.

Therefore, the thickness stress in the component (see Figure 2.4) can cause delamination to occur if they exceed the through-thickness strength [16].

Interlaminar fracture toughness is the main contributor of delamination propagation, it is not the thickness strength of the composite.
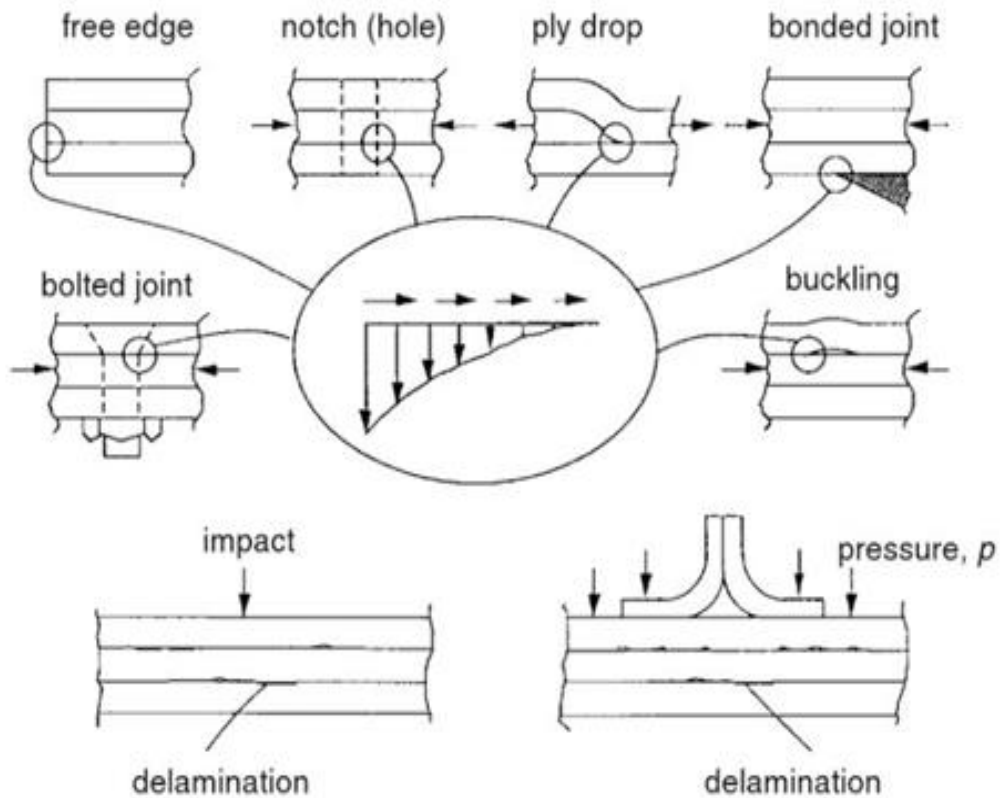
Figure 2.4. Thickness stresses that can initiate delamination [16].

The measurement used to express interlaminar fracture toughness is rate of release of critical energy G_c. It shows the rate of the energy that is used by the materials layers when the delamination occurs.

There are three main measuring styles (the Modes) used, shown in Figure 2.5. There is also possibility and need to sometimes use mixed style.
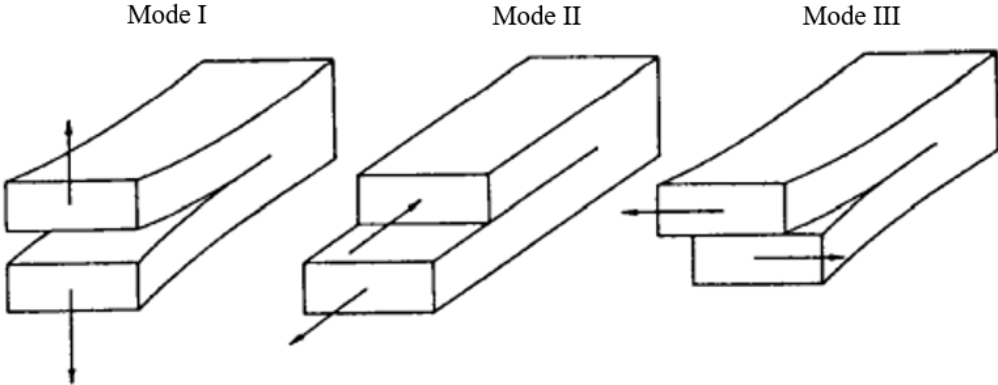
Figure 2.5. Picture showing Mode I – opening, Mode II – shear, Mode III – tearing [16].

For better assessment the units of interlaminar fracture toughness in different materials are shown below in Table 2.1 [16].

Table 2.1.

Possible values of interlaminar fracture toughness [16]

Material Fibre/matrix	Fracture toughness (kJ m^{-2})		
	Mode	Initiation	Propagation
T300/6376	Mode I	0,27	0,27
	Mode II (ELS)	0,60	-
	Mode II (ENF)	0,65	-
XAS/913	Mode I	0,28	0,28
	Mode II (ENF)	0,66	-
T300/914	Mode I	0,14	0,14
	Mode II (ENF)	0,72	-
T800/924	Mode I	0,22	0,25
	Mode II (ELS)	0,44	0,60
AS4/PES	Mode I	0,80	2,02
	Mode II (ELS)	1,23	1,84
	Mode II (ENF)	1,29	-
AS4/PEEK	Mode I	1,68	2,42
	Mode II (ELS)	1,74	3,16
	Mode II (ENF)	1,82	-

In composite materials, that are isotropic, the Interlaminar fracture toughness is usually given in Mode I because that even if it starts at Mode II, later it transforms into Mode I anyway. This is shown in Figure 2.6 (a) that later transforms into Figure 2.6 (b) [16]. If there is layered sufficiently anisotropic material, then usually it interlaminar resistance at the Mode II should be defined by independent constant G_{cII}.
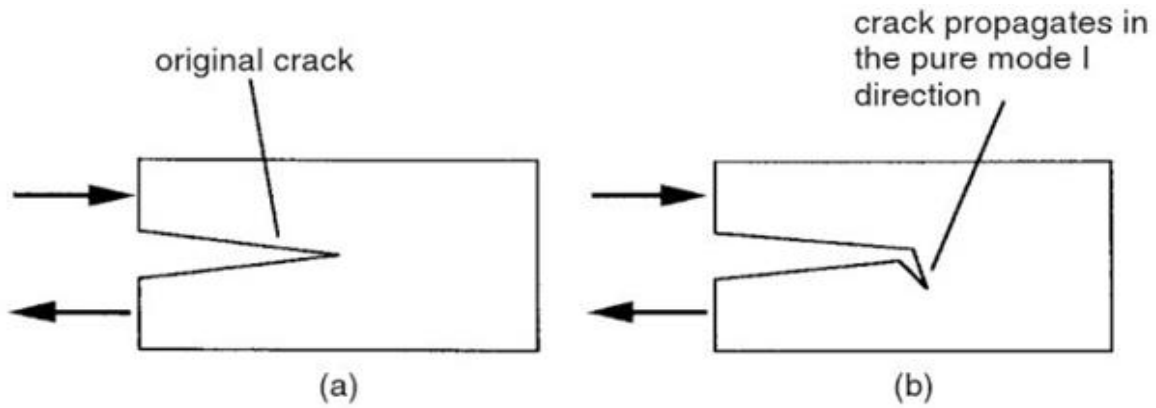
Figure 2.6. Crack propagation in an isotropic material [16].

Studies have been done around Mode I and Mode II, but it is known that in fact, composite structures are usually subjected to Mode I and Mode II combinations [62, 64–66].

It is known that static or dynamic strength depends on the speed. For defining of this dependence in measurement practice used of the Mode I load specimens are shown in Figures 2.7 and 2.8.

Specimen design	Compliance	Mode I fracture toughness
DCB	$C = \dfrac{8a^3}{WH^3 E_x}$	$G_I = \dfrac{12P^2 a^2}{W^2 H^3 E_x}$ $G_I = \dfrac{3P\delta}{2Wa}$
WIF	$C = \dfrac{8a^3}{WH^3 E_x}$	$G_I = \dfrac{12\left\{(P_x r \cos\theta)^2 + [P_y(a+e)]^2\right\}}{W^2 H^3 E_x}$

Figure 2.7. Test specimen design for Mode I testing [62].

Crack growth is stable if the cracked specimen is loaded perpendicular to the fibers. This method can be used to measure the fracture toughness of a crack excitation. In the DCB test (Figure 2.6), crack growth than is stable. In Figure 2.7 are shown two popular configurations of DCB specimen for the Mode I measurement. Irrespective of the frictional force in the WIF specimen, the same expression can be obtained as in the DCB specimen. The CT specimen (Figure 2.8) is only suitable for the investigation of induction lesions related to insufficient ligament length for further examination. The DEN, SEN and SC specimens (Figure 2.8), subjected to uniaxial stress, measure the fracture toughness of Mode I [62].
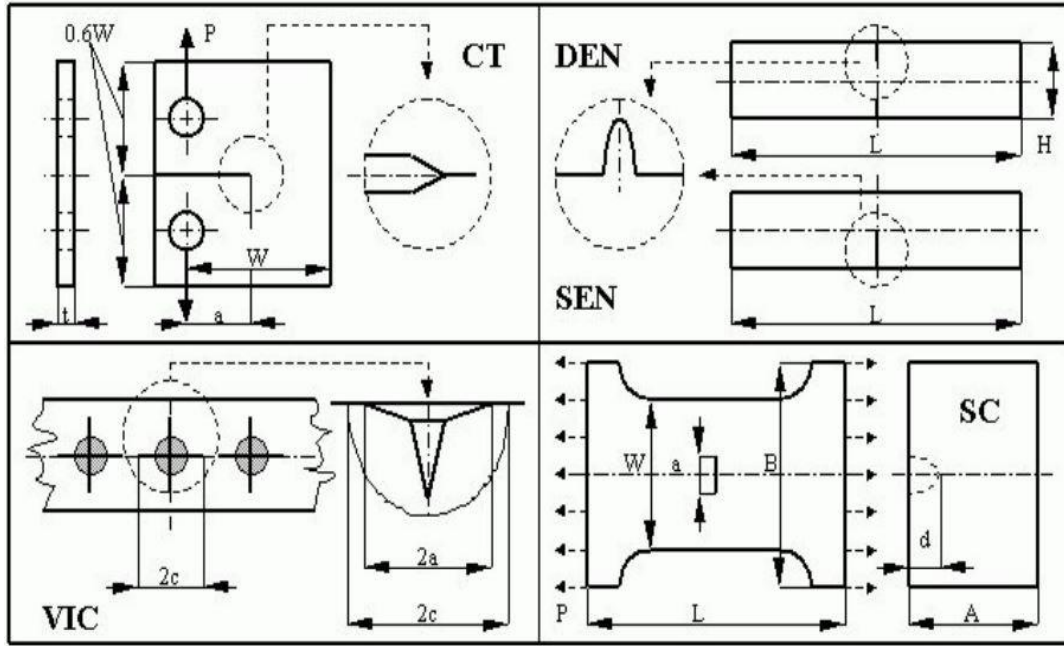
Figure 2.8. Specimens for Mode I loading [62].

To get a result from the fracture toughness equations the Beam theory can be used [62, 67]. Lawcock et al. studied the effect of adhesion bonding between Al sheets and prepreg of composite materials on mechanical properties of CFRMLs. The damage area increases together with impact energy increasing, by doing that, a different percentage decrease in strength can be observed. Thermoplastic FMLs have excellent impact resistance [62].

The critical stress intensity factor, K_c. is used as the other parameter of fracture toughness in metals and polymers. For linear flexible isotropic materials, K_{Ic} and G_{Ic} are related by the following expression for the plane strain case, as shown in the equation (2.1) [16]:

$$G_{Ic} = K_{Ic}^2 \frac{(1-v^2)}{E}, \tag{2.1}$$

where E is the Young's modulus and v the Poisson's ratio.

The load that is making Mode I crack to grow is proportional to the K_{Ic} of material. That shows that material stiffness does not play significant role. Equation (2.2) that for an isotropic material with a crack growing under plane deformation conditions in Mode I, the critical load P_c will be proportional to [16]:

$$\sqrt{\frac{G_{Ic}}{(1-v^2)}}. \tag{2.2}$$

This shows that if stiffness is kept the same, but G_{Ic} is increased two fold, than critical load is also increased times two. At the same time if the stiffness changes when using different material, than critical load will be changing proportionally.

The strain energy release rate and the stress intensity factor are the parameters those defined fatigue crack growth. For instance, the fatigue crack growth rate is expressed by the Paris-power law, as followed in equations (2.3 and 2.4) [62]:

$$\frac{da}{dt} = A(K_I)^m, \tag{2.3}$$

$$\frac{da}{dN} = B(\Delta G)^d, \tag{2.4}$$

where dt is the time increment, dN is the number of cycles increment, A, B, d and m are material constants [62].

2.3 Test methods and standards

By performing studies and exploring the field of testing, the strict testing methods has been developed and are expressed by several international and national Standards (USA ASTM D-5528-01, European ISO 15024:2001 and Japan's JIS K7086).

The most popular is the beam-type specimens for test which the aim is to determine the crack resistance. The main advantages of DCB specimen are using of a beam linear theory which gives simple equation for the test data processing and simplicity of testing and measuring. Theoretically at the loading of this specimen with extension (displacement) control the crack growth rate is stable, if the interlaminar fracture toughness is constant. From test results it is possible to estimate the interlaminar crack resistance.

For Mode I, the most common test uses the specimen of the DCB shown in Figure 2.9 [16].
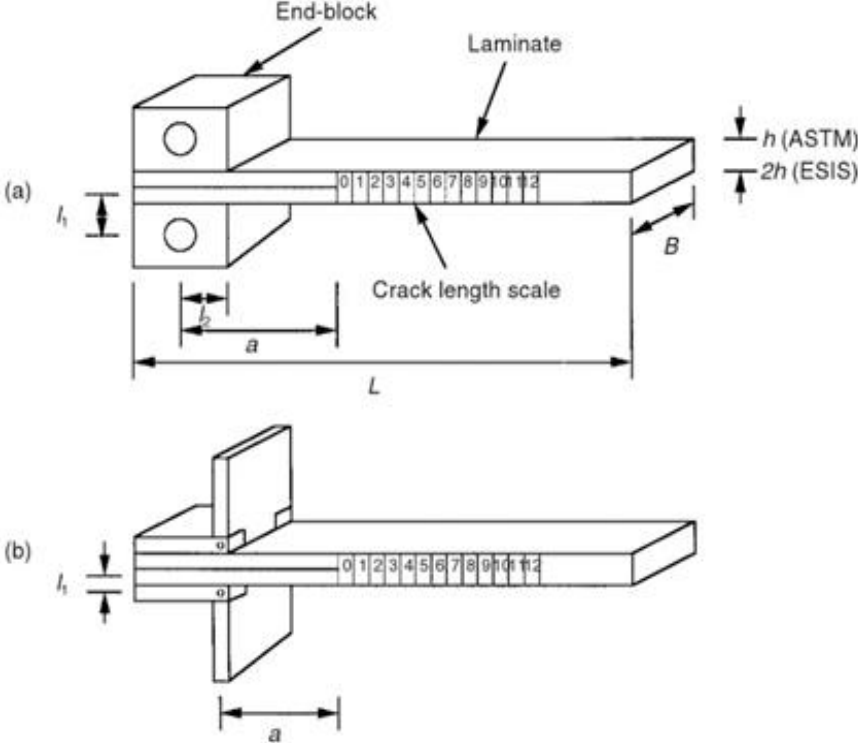
Figure 2.9. DCB specimen geometry, (a) end-blocks, (b) piano hinges [16].

Japanese Industrial Standard K7086 was published in 1993. American Society for Testing and Materials accepted their testing method D5528 in 1994 [6, 19]. For Mode I there is also tests than include DCB specimen width and taper testing. A Mode I test method was only accepted as an international standard by ISO in 2001 as 15024 [27].

If there are more than one Mode combined testing, it makes the measuring the interlaminar crack resistance a lot more interesting. One method is to use Mode I and II shown in Figure 2.10. It is called Fixed ratio mixed mode. Figure 2.11 shows another type of testing called Mixed mode curative method [16, 68–71].
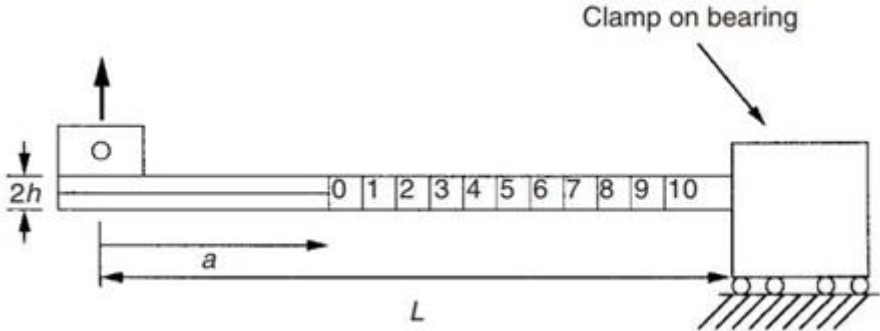
Figure 2.10. Fixed ratio mixed mode test method [16].
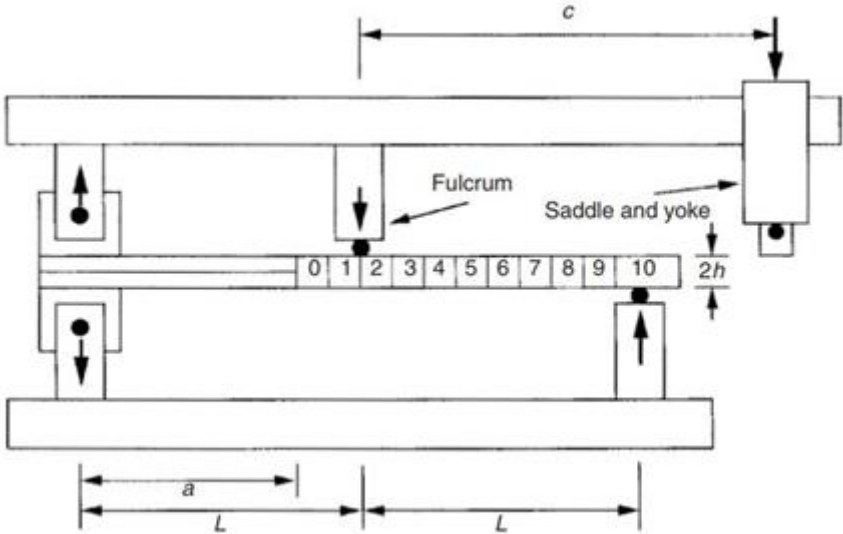
Figure 2.11. Mixed mode bend test method [16].

To make the testing of DCB specimen possible connection between specimen and laboratory equipment is necessary. There are two mainly used options of glued blocks or hinges used, shown in Figure 2.9. There are no special regulation from ASMT or ESIS about this point, except width can not be less than test specimen width. From testing done by author it must be mentioned that blocks and hinges dimensions must be kept in minimum size and also right kind of glue should be used for it to hold the small piano hinge in place. By using large size hinges the results of tests may be compromised. Rotation pin must be as close to the specimen as

possible, to not introduce changes in lever length. To calculate sire *l1* by ASTM standard the equation (2.5) is used [6, 16]:

$$l_1 = \frac{h}{4} + 0.01\sqrt{\frac{0.0434h^3E_{11}}{G_{Ic}} + a_o^2},$$ (2.5)

where *h* is the full thickness of the laminate and a_0 is the length of the layer measured from the load line.

If it is not possible to achieve the given l_1, correction must be used in later calculations.

The DCB example test higher load that is transferred by load attachments is relatively low, and can be calculated by equation (2.6) [16]:

$$P_{max} = \frac{B}{a}\sqrt{\frac{h^3E_{11}G_{Ic}}{96}},$$ (2.6)

where *B* is the width of the specimen and *h* is the full thickness of the laminate.

As mentioned in first chapter of this thesis, moisture can play great part of changing the properties of the test specimen, so getting constant rate is critical for later evaluation of data.

Test equipment plays huge role. First of all, it must be calibrated and at constant travel speed. The range of velocity should be 0.5 to 5 mm/min. Second important property is accuracy of the load sensing device over the relevant load range must be within ± 1 % of the specified value [16].

Best way is to use more than one camera and with markings on the side of the test specimen, the possibility to see 0.5 mm should be applied. The opening length is monitored by test equipment, so there is high precision already. It is advised to check both sides of the test specimen during the testing to later determine if test has been done correctly – symmetrical.

As testing specimen size is small than loads recorded are relatively low: around 100 to 200 N. From authors testing range of load can change depending on specimen materials, quality and even cure time. As it is known in time composites get stronger.

Important testing part is to zero all the equipment when the specimen is connected to it. Tolerances also must be taken into account. For example, if there is a free movement in hinges or loading block pins, that must be loaded and equipment set to zero at that point.

There are many options to determine G_{Ic} from testing results. By using this data it is possible to construct resistance curve by using calculated G value depending on crack length a, the curve is shown in Figure 2.12 [16].
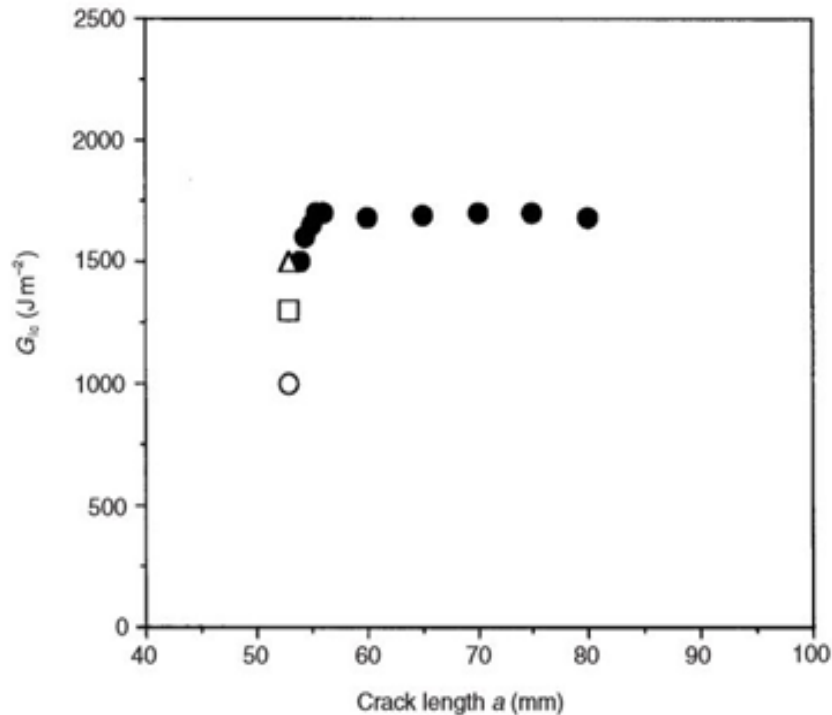
Figure 2.12. Typical R curve for Mode I fracture. ●, propagation values; ○, deviation from linearity; □ , visual onset; Δ , 5 % offset [16].

It has been mentioned above that it can be very difficult to pinpoint the start of delamination by visual inspection and in any case it is very up to the operator. As all of the tests done need to be repeatable, there has been three main methods used:

1. Initiation by visual observation (VIS). This method uses visual observation on both sides of the specimen. The G_{Ic} can be calculated from a and G values [16].

2. Initiation set on variation from linearity (NL). This method uses nonlinearity as the main point of start. For this method to work, the material tested must be fragile. Figure 2.13 (a), if the material is rigid than visual method can be used, as shown in Figure 2.13 (b) [16].

3. Initiation from 5 % offset/maximum load (5 % / MAX): G_{Ic} value can be calculated from the intersection values of the load-deposit curve with a line drawn from the beginning and compensated by a 5 % increase from the initial linear part of the load-deflection curve, as shown in Figure 2.13 (c) [16].
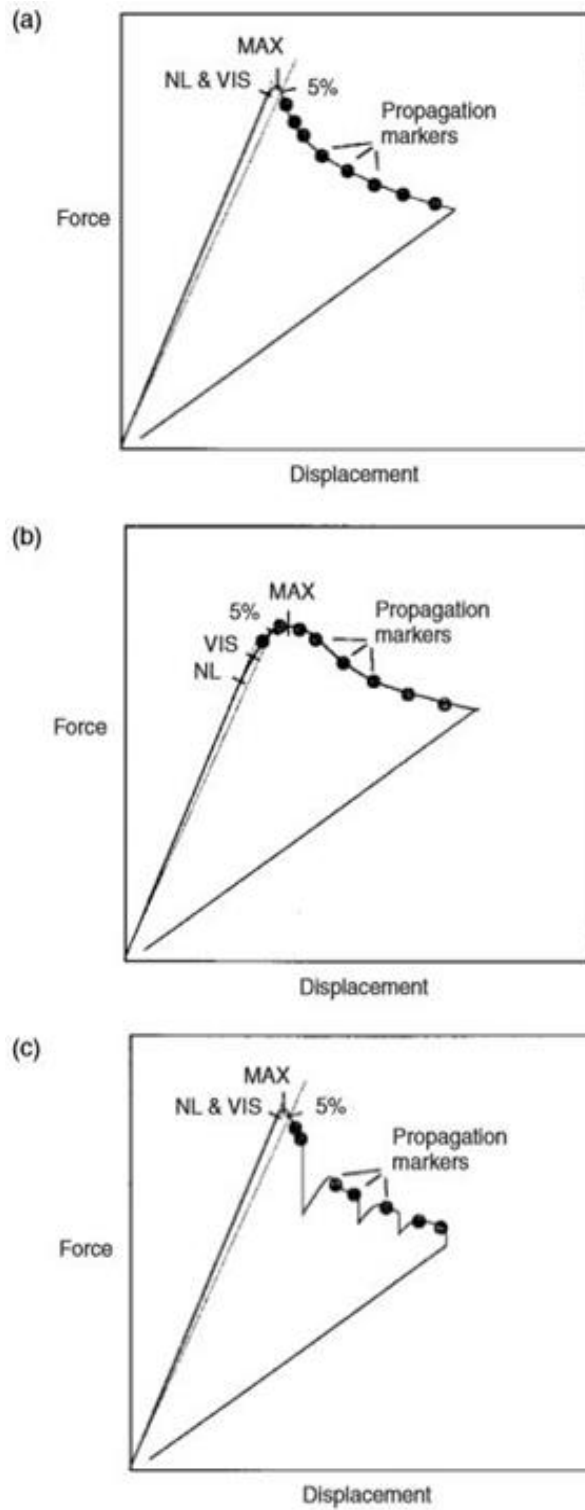
Figure 2.13. Test curves of load-displacement for DCB, (a) brittle matrix (b) tough matrix, showing stable crack growth, and (c) unstable crack growth [16].

The ASTM standard provides three G_I calculation methods and has been evaluated using a comprehensive test.

The DCB specimen is very useful for test, but there are some problems associated with difference from theoretical scheme:

1) The theoretical clam of a beam is not corresponding to practical realizing of DCB arms, because there is rotation of the cross-section of the arm in the front of a crack.
2) The linear theory of the beam bending must be restricted by maximum of allowable extension.

The first problem in Standard is resolved by using of three methods of test data processing:

- Modified beam theory (MBT) method.
- Compliance calibration method (CCM) (Berry's method).
- Modified compliance calibration method.

If MBT method is used to calculate energy release rate of the DCB specimen, equation (2.7) from simple beam theory can be used. If the arm of DCB is clamped at the delamination front, then

$$G_I = \frac{3P\delta}{2Ba}. \tag{2.7}$$

By inserting in the equation, the values of load, P and displacement δ associated with the increase in a given delamination length, a, the critical energy release rate G_{Ic} is calculated.

As a fact, the front of the delamination is rotating. This rotation effect can be explained by treating the DCB as if it contained a longer layer of each length, $a + \Delta$, and using equation (2.8) [16]:

$$G_{Ic} = \frac{3P\delta}{2B(a+\Delta)}, \tag{2.8}$$

Δ can be determined experimentally by fitting the root of the fit cube $C^{1/3}$ as a function of the delamination length, a (fit is the ratio of displacement to applied load, δ / P) Results as in Figure 2.14 below can be achieved [16].
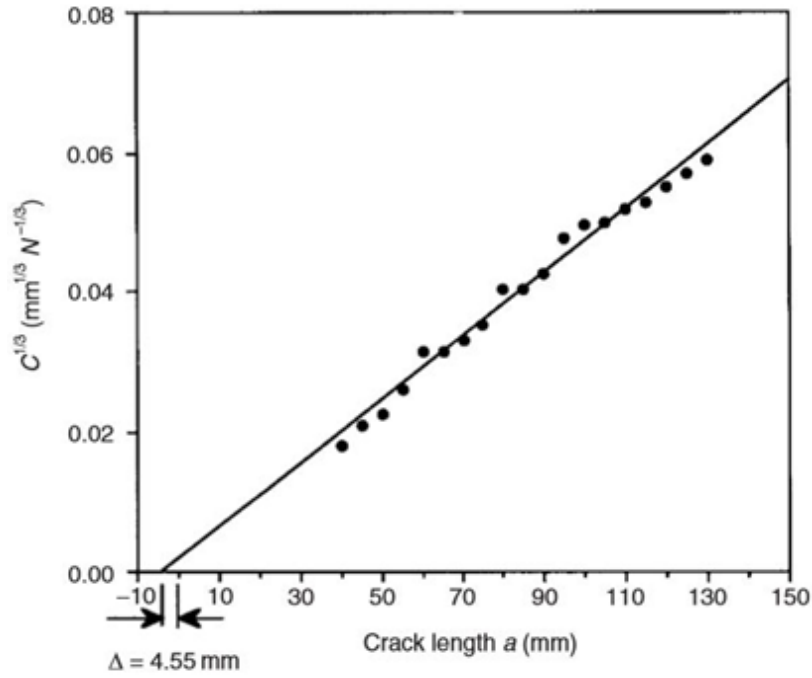
Figure 2.14. Calculation of Δ for the modified beam theory [16].

Approach like this also enables the determination of the flexural elastic modulus, E_{1f} shown in the equation (2.9):

$$E_{1f} = \frac{64(a+\Delta)^3 P}{\delta B h^3},$$
(2.9)

where, according to the ASTM convention, h is the full thickness of the laminate [16].

CCM (Berry's method). This way promotes the visual seen delamination initiation and cracking values δ and P with the corresponding delamination lengths, a. The graph is made from log (C) to log (a). The exponent n is the angle of the line as shown in Figure 2.15. The fracture toughness strength of Mode I interlayers is calculated from the equation (2.10) [16]:

$$G_{Ic} = \frac{nP\delta}{2Ba}.$$
(2.10)

Typical n values for a standard 3 mm thick CFRP specimen range from 2.7 to 2.9 mm (note that a simple beam theory gives $n = 3$) [16].
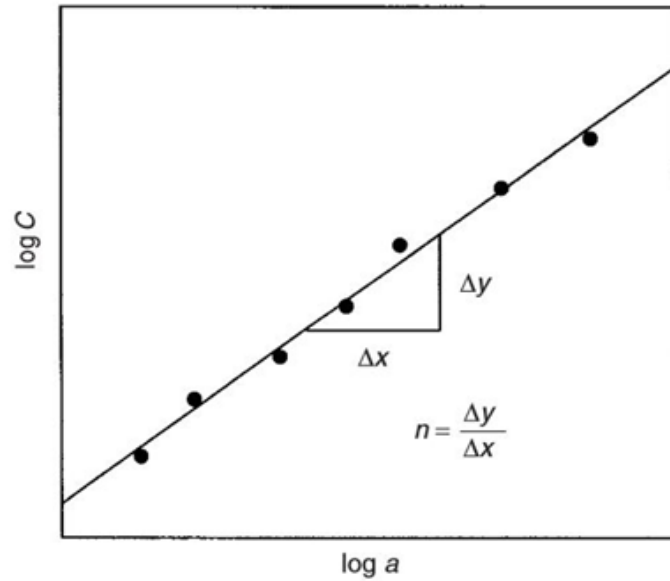
Figure 2.15. Calculation of n for the compliance calibration method [16].

Modified compliance calibration method. Fracture toughness can be calculated in different ways. Most used is conformity or conformity calibration method. Using this method fracture toughness can be determined as being function of the geometry, crack expansion and the load of test specimen. Critical fracture energy derived from the general Irvine-Kies expression [62]. The four-point bending end curvature elasticity test for delamination is also used to determine the Mode II delamination resistance. In previous studies [72, 73], 4ENF tests have given higher resistance to lamination than the more commonly used three-point bending end curved bend.

The ASTM method plots the delamination length normalized to the specimen thickness, a/h, as a function of the function of the matching cube root $C^{1/3}$, as shown in Figure 2.16 [16].
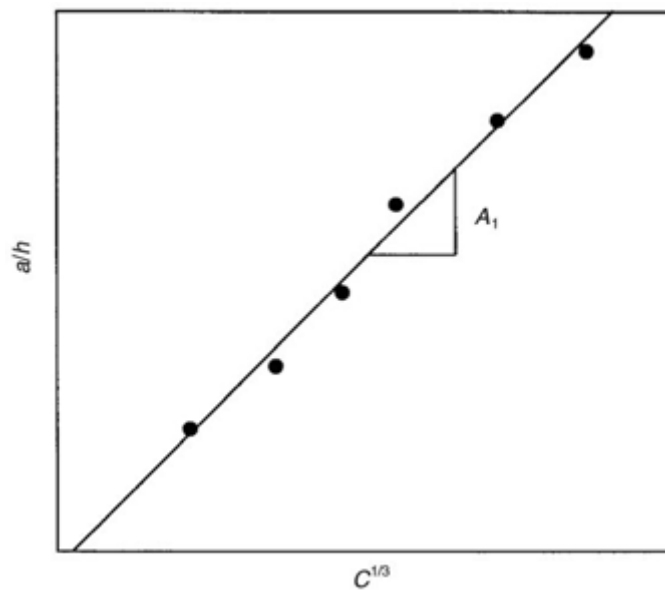
Figure 2.16. Modified compliance calibration [16].

The fracture toughness of Mode I interlayers is shown by the equation (2.11) [19]:

$$G_{Ic} = \frac{3m}{4h}\left(\frac{P}{B}\right)^2 (BC)^{2/3}. \tag{2.11}$$

For solution of second problem the Standard proposes correction of linear solution by introducing of some parameters.

Large shift effects must be corrected by the additional parameter F, in the calculation of G_I

$$F = 1 - \frac{3}{10}\left(\frac{\delta}{a}\right)^2 - \frac{3}{2}\left(\frac{\delta t}{a^2}\right), \tag{2.12}$$

where t is shown in equation (2.12) for piano hinges [19].

This parameter F forms both the torque lever communication and the tilt of the end blocks. For specimens with loading blocks, the distance from the end of the insert to the load line must be at least 50 mm so that the effect of the blocks is not taken into account. If no, the second parameter N must also be included, the displacement correction to take the stiffness of the specimen with blocks [19]:

$$N = 1 - \left(\frac{L'}{a}\right)^3 - \frac{9}{8}\left[1 - \left(\frac{L'}{a}\right)^2\right]\left(\frac{\delta t}{a^2}\right) - \frac{9}{35}\left(\frac{\delta}{a}\right)^2, \tag{2.13}$$

where t and L' are shown in equation (2.13) for end blocks [19].

Of course, this correction approach is approximate, and the alternative radical solution is proposed in this doctoral thesis in chapters 3 and 4 by using of non-linear theory of bending. The development of non-linear model of DCB specimen is one of aims of this doctoral thesis.

2.4 One application of flexible plate theory to the determination of interlaminar fracture toughness

The determination of interlaminar fracture toughness for a mixed mode is governed by the ASTM D 6671 – 01 standard, which is based on linear theory of plate and has several significant limitations related to the requirements for the characteristics of the specimen [6]. This paragraph below discusses some alternative option for determining the interlaminar fracture toughness for mixed loading mode, based on the nonlinear theory of flexible plates. A similar approach has been used in [74, 75] to predict the development of delamination and the destruction of thin flexible thin foil in a layered composite under nominal compression. The main purpose of the proposed analysis is to assess the advantages and disadvantages of the proposed approach compared to the standard. The results of using and evaluating the effectiveness of this approach for mode 1 are set out in the next chapter.

A layered elastic composite plate of thickness h contains number of horizontal layers which principal axes of elasticity coincident with axes x, y of Cartesian references system shown in Figure 2.17.

In a plate there is the through-width delamination of length l close to the upper horizontal surface of the plate. This delamination defines a sub-layer of constant thickness t. Because there

is assumed that the sub-layer thickness much less than the plate thickness ($t << h$), then the sub-layer influence to stress/strain state of a plate can be neglected. The plate is compressed in direction of axis x with control of displacement. There is the through-width delamination with length l. Global compressive strain of plate between tip cross-sections of part of a plate under delamination is equal to ε and defined by axial relative displacement between those cross-sections Δl (Figure. 2.17). So:

$$\varepsilon \approx \frac{\Delta l}{l}. \tag{2.14}$$

It is assumed that

$$\varepsilon > \varepsilon_{cr}$$

where ε_{cr} is the axial strain of sub-layer at critical force of buckling,

Easy to see that

$$\varepsilon_{cr} = \frac{\pi^2 t^2}{3l^2}. \tag{2.15}$$
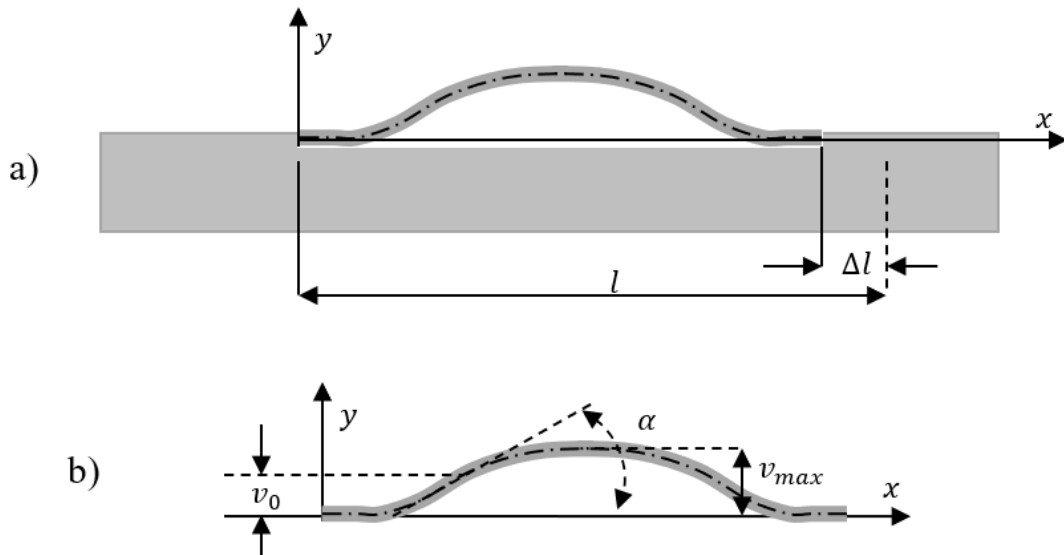
Figure 2.17. A layered composite plate with delamination (a) and the geometrical parameters of sub-layer (b).

The global longitudinal strain of sub-layer at the base l consists of two components: ε_c is related with action of compressive axial force (the compression strain) and ε_b is related with action of bending moment (bending strain):

$$\varepsilon = \varepsilon_c + \varepsilon_b. \tag{2.16}$$

The middle cylindrical surface of sub-layer has a generatrix which can be described by a exact differential equation of bending theory of flexible plate

$$D\frac{d\theta}{ds} = M(x) = M_0 - Pv(x), \tag{2.17}$$

where D cylindrical stiffness of sub-layer, s is the length of the generatrix of cylindrical surface;

$d\theta/ds$ is the curvature of the generatrix; $M(x)$ is the bending moment in equation (2.20), expressed in terms of its value M_0 at the source of cartesian references system and the compressive force P in the cross-section; $v(x)$ is the sub-layer deflection.

Similarly, to [75], the equation (2.17) can be transformed to the differential equation in natural form:

$$\frac{d\theta}{ds} = k\sqrt{2(\cos\theta - \cos\alpha)}, \tag{2.18}$$

where

$$\cos\alpha = 1 - \frac{M_0^2}{2DP} \quad and \quad k = \sqrt{\frac{P}{D}},$$

α is the maximum angle of the tangent of the generatrix of cylindrical surface of the sub-layer.

It can be seen, that this angle corresponds to the point of zero-curvature in Figure 1.17 b. k is defined by the compressive force and cylindrical stiffness of sub-layer.

It can be seen that:

$$k = \sqrt{\frac{P}{D}} = \frac{2\pi}{l}\sqrt{\bar{P}}, \tag{2.19}$$

where:

$$\bar{P} = \frac{P}{P_{cr}},$$

and the critical force

$$P_{cr} = \frac{4\pi^2 D}{l^2}.$$

After definition as given above several important parameters and total strains of a buckled sub-layer can be obtained. Internal forces in cross-section of sub-laminate is shown in Figure 2.18.

The differential of curved coordinate s from equation (2.18):

$$ds = \frac{d\theta}{k\sqrt{2}\sqrt{\cos\theta - \cos\alpha}}. \tag{2.20}$$

The parameter k can be expressed in terms of the complete elliptic integral $K(p^2)$ of the first kind:

$$k = \frac{4}{l}K(p^2),$$

and, the length of the generatrix

45

$$l = \int ds = \int \frac{d\theta}{k\sqrt{2}\sqrt{\cos\theta - \cos\alpha}} = \frac{4}{k}K(p^2), \tag{2.21}$$

where the parameter of the elliptic integral

$$p^2 = \frac{1}{2}(1 - \cos\alpha) = \sin^2\frac{\alpha}{2}. \tag{2.22}$$

The equation (2.19) and equation (2.22) give:

$$\bar{P} = \frac{P}{P_{cr}} = \frac{4}{\pi^2}K(p^2). \tag{2.23}$$
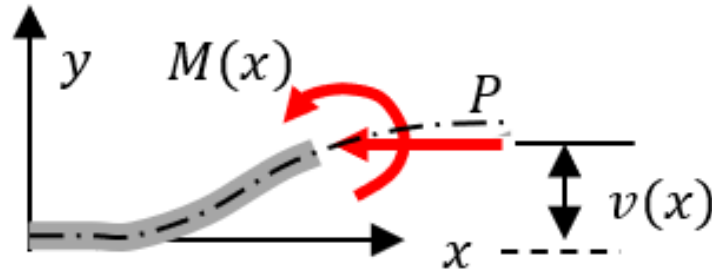
Figure 2.18. The internal forces in cross-section of sub-laminate.

The compression strain can be defined as follow:

$$\varepsilon_c = \frac{\Delta l_c}{l} = \frac{P}{E^* t}\int_0^l \cos^2\theta ds, \tag{2.24}$$

and after transformations

$$\varepsilon_c = \varepsilon_{cr}\bar{\varepsilon}_c, \tag{2.25}$$

where:

$$\bar{\varepsilon}_c = \frac{\varepsilon_c}{\varepsilon_{cr}} = \bar{P}\frac{[(4p^2 - 1)K(p^2) + 4(1 - 2p^2)E(p^2)]}{3K(p^2)}. \tag{2.26}$$

Average longitudinal strain caused by the bending is as follow:

$$\varepsilon_b = \frac{\Delta l_b}{l} = 1 - \int_0^l \cos\theta\, ds = 1 - \frac{4}{k\sqrt{2}}\int_0^\alpha \frac{\cos\theta\, d\theta}{\sqrt{\cos\theta - \cos\alpha}}, \tag{2.27}$$

and finally

$$\varepsilon_b = 2\left[1 - \frac{E(p^2)}{K(p^2)}\right], \tag{2.28}$$

where $E(p^2)$ is the complete elliptical integral of the second kind.

$$\varepsilon = \varepsilon_c + \varepsilon_b = \varepsilon_{cr}\bar{\varepsilon}_c + 2\left[1 - \frac{E(p^2)}{K(p^2)}\right]. \tag{2.29}$$

The deflection v_0 in the cross-section of zero-curvature is:

$$\bar{v}_0 = \frac{v_0}{l} = \frac{p}{\pi\sqrt{\bar{P}}}. \tag{2.30}$$

Now the strain energy released rate at delamination propagation condition can be considered.

The strain energy related with action of axial compressive force N (simply, compression energy):

$$U_c = \int_0^l \frac{N^2}{2E^*t}ds = \int_0^l \frac{(Pcos\theta)^2}{2E^*t}ds. \tag{2.31}$$

After integration and transformations:

$$U_c = \frac{1}{6}\frac{P^2l}{E^*t}\frac{[(4p^2 - 1)K(p^2) + 4(1 - 2p^2)E(p^2)]}{K(p^2)}. \tag{2.32}$$

In compact forms the compression energy is showed below in equation (2.33):

$$U_c = \frac{1}{2}E^*lt\bar{P}\varepsilon_{cr}\varepsilon_c = \frac{1}{2}E^*lt\bar{P}\varepsilon_{cr}^2\bar{\varepsilon}_c. \tag{2.33}$$

In equations above E is the elasticity modulus v is the Poisson's ratio of a sub-layer material and the elasticity modulus of plane strain stat

$$E^* = \frac{E}{1 - v^2}.$$

.

The strain energy connected with bending of the sub-layer (simply, bending energy)

$$U_b = \int_0^l \frac{M^2}{2D}ds = \frac{D}{2}\int_0^l \left(\frac{d\theta}{ds}\right)^2 ds, \tag{2.34}$$

but in terms of the complete elliptic integrals:

$$U_b = \frac{1}{2}E^*tl4[(p^2 - 1)K(p^2) + E(p^2)]\bar{P}\varepsilon_{cr}. \tag{2.35}$$

The compact form of a bending energy:

$$U_b = \frac{1}{2}E^*tl2(\varepsilon_\alpha - \varepsilon_b)\bar{P}\varepsilon_{cr}, \tag{2.36}$$

where $\varepsilon_\alpha = 1 - \cos\alpha = 2p^2$ can be interpreted as the superior limit of the longitudinal deformation due to bending.

The strain energy of the plate part with delamination is as follow:

$$U = U_0 - U_c - U_b, \tag{2.37}$$

where U_0 is strain energy with closed delamination

$$U_0 = \frac{1}{2} E^* l t \varepsilon^2. \tag{2.38}$$

Using equations (2.33, 2.35, 2.37) the strain energy released by buckling of a sub-layer can be represented as follows:

$$U = \frac{1}{2} E^* l t \left[\varepsilon^2 - \bar{P} \varepsilon_{cr} [\varepsilon - \varepsilon_b + 2(\varepsilon_\alpha - \varepsilon_b)] \right]. \tag{2.39}$$

At virtual extending of delamination, the total strain energy realize rate G is:

$$G = \frac{dU}{tdl} = \frac{1}{2} E^* \left\{ \varepsilon^2 + \varepsilon_{cr} \bar{P} [\varepsilon - \varepsilon_b + 2(\varepsilon_\alpha - \varepsilon_b)] - \varepsilon_{cr} \frac{d}{dl} [\bar{P} [\varepsilon_c + 2(\varepsilon_\alpha - \varepsilon_b)]] \right\}, \tag{2.40}$$

and finally

$$G = \frac{dU}{tdl} = \frac{1}{2} E t (\varepsilon^2 + a_1 \varepsilon_{cr} \varepsilon + a_2 \varepsilon_{cr}), \tag{2.41}$$

where $a_1 = \bar{P}$ and

$$a_2 = \bar{P} \left\{ 2\varepsilon_\alpha - 3\varepsilon_b - 2 \left[3 \frac{E'(p^2) K(p^2) - E(p^2) K'(p^2)}{K^2(p^2)} + 2 \right] \frac{2\varepsilon_{cr} \bar{\varepsilon}_c}{\varepsilon_{cr} \bar{\varepsilon}'_c + \varepsilon'_b} \right\}.$$

The equation (2.41) is the second order polynomial of the total longitudinal strain ε depend on the critical strain ε_{cr} and the parameter p^2 of the buckled shape of sub-layer.

The condition of delamination propagation is:

$$G = G_c, \tag{2.42}$$

where G_c is the critical strain energy realize rate postulated as a material constant on mixed I / II Modes.

Using equations (2.36 and 2.37) this condition can be presented as follows:

$$\varepsilon^2 + a_1 \varepsilon_{cr} \varepsilon + a_2 \varepsilon_{cr} = \varepsilon_0^2, \tag{2.43}$$

where:

$$\varepsilon_0^2 = \frac{2t G_c}{E^*}. \tag{2.44}$$

The strain energy release rate in equation (2.40) is a function of three variables: the total relative strain ε, the l/t ratio of the sub-layer, and the parameter p^2 of buckled shape. Therefore, to determine the critical configuration of the buckled sub-layer the following algorithm should be realized.

Using equation (2.29) the total strain should be excluded from equation (2.41):

$$(\varepsilon_{cr}\bar{\varepsilon}_c + \varepsilon_b)^2 + a_1\varepsilon_{cr}(\varepsilon_{cr}\bar{\varepsilon}_c + \varepsilon_b) + a_{21}\varepsilon_{cr} + a_{22}\varepsilon_{cr}^2 = \varepsilon_0^2, \qquad (2.45)$$

where:

$$a_{21} = \bar{P}(2\varepsilon_\alpha - 3\varepsilon_b),$$

$$a_{22} = \bar{P}\left\{-2\left[3\frac{E'(p^2)K(p^2) - E(p^2)K'(p^2)}{K^2(p^2)} + 2\right]\frac{2\bar{\varepsilon}_c}{\varepsilon_{cr}\bar{\varepsilon}_c' + \varepsilon_b'}\right\}.$$

Resolve of equation (2.45) and determinate of the critical strain ε_{cr} for selected values of the shape parameter.

Determinate of the total strain ε from equation (2.29).

Because the coefficient a_{22} depends on the critical strain ε_{cr} , then this algorithm requires of iteration procedure.

The pre-condition of successful test for measurement of the interlaminar fracture toughness of a mixed II/I mode using the specimen with thin delamination is sufficient strength of sub-layer at compression/banding combined load for which strength defined by ultimate strain ε_u. The problem of strength of sub-layer were considered in [74, 75].

From study done by V. Pavelko [75] in Figure 2.19 there is a graph showing the behavior of the compressed sub-layer with a gradual increase of total deformation for $\varepsilon_u/\varepsilon_0$=1 and ε_0=7.8·10⁻³. If the compressive strength of the plate and the sub-layer is similar, then for small values of the ratio $\bar{l} = l/t$ the destruction of the plate happen until buckling of sub-layer. In all cases, below the critical strain (dash-dotted line) sub-layer does not buckle. In the region above this line but below the combined solid line delamination is not propagated, and there is no its destruction. If the total deformation of the composite reaches a value corresponding to the combined bold line, there are two possible scenarios for the damage behavior. If the ratio length / thickness of the sub-layer is not more than $\bar{l}_*$ (equal to 72 in this case), the maximum compressive strain in a dangerous cross-section of the sub- layer reaches the limit ε_u and the sub- layer collapse [75].

If the ratio length / thickness of the sub- layer is not more than $\bar{l}_*$ (equal to 72 in this case), the maximum compressive strain in a dangerous cross-section of the sub-laminate reaches the limit ε_u and the sub-laminate collapse. If the length / thickness ratio is more than $\bar{l}_*$, then the stable propagation of delamination can be observed. If the total strain reaches of ε_0, then the breakaway of sub-layer occurs along the entire length of the composite [75].
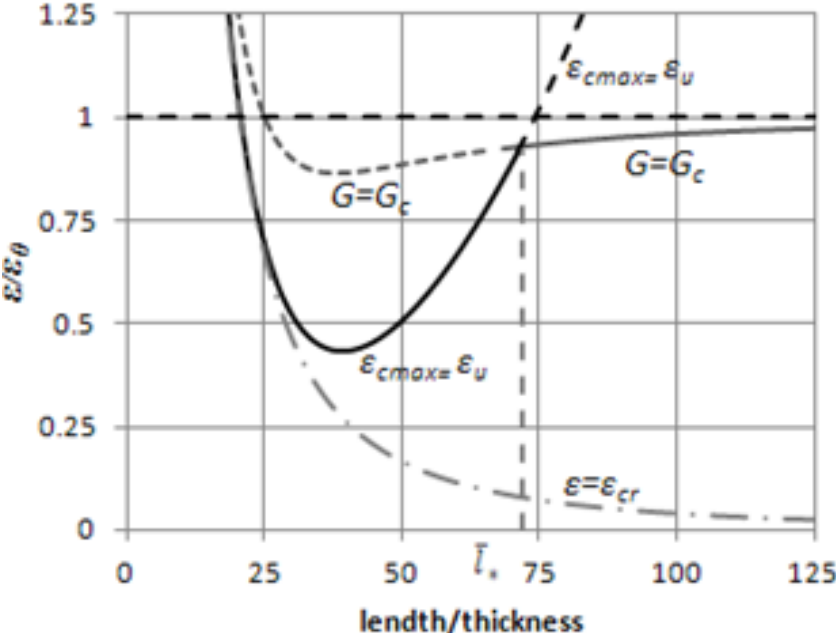
Figure 2.19. Sub-layer destruction – delamination propagation curve [75].

Results of calculation of the delamination propagation and the strength curves are presented in Figure 2.20 for different $\varepsilon_u/\varepsilon_0$ relations [75].
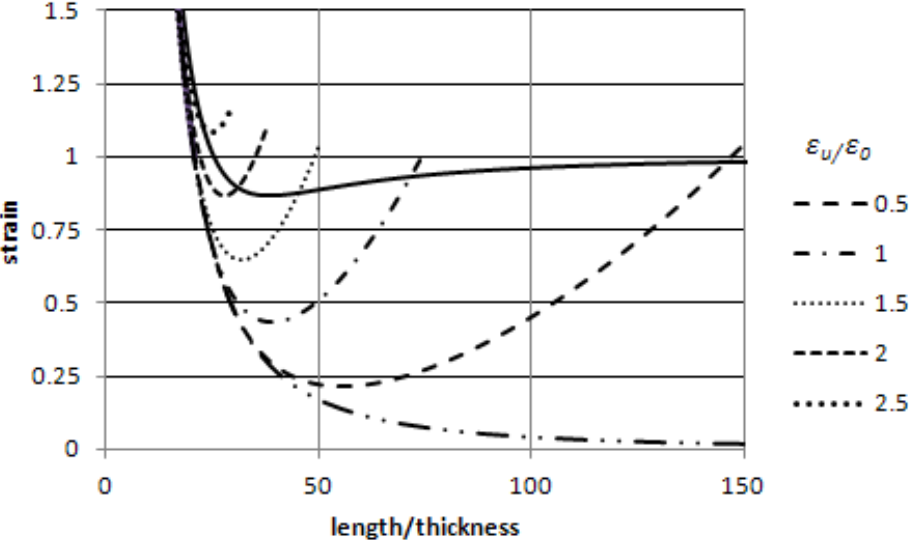
Figure. 2.20. Delamination propagation and strength curves [75].

Final conclusions:

1. The specimen with thin delamination is potentially useful for measurement of the interlaminar fracture toughness of layered composite: there is always the length/thickness interval for which the stable growth of delamination can be realized.
2. Equation (2.43) can be used for processing of test data and defining of the interlaminar fracture toughness of mixed II/I mode.
3. Relation between G_I and G_{II} can be obtained by using corresponding components of the strain energy.
4. There is sense to continue problem investigation including lab test.

3 DCB NONLINEAR SPECIMEN FOR DETERMINATION OF THE MODE I INTERLAMINAR FRACTURE TOUGHNESS. ANALYTICAL STUDY

3.1 Background

Specimens in the form of a DCB are most widely used in the practice of experimental determination of the interlaminar fracture toughness of layered composites for the I, II, and mixed I/II fracture modes. In the present study, the discussion is restricted to the application of a DCB specimen only to Mode I. The energetical theory, founded on the method of elastic compliance, for the basic description of release rate of the elastic energy upon propagation of delamination, employs the simple relations of the linear theory of bending of elastic beams of rectangular cross section (Euler beam), which makes this type of specimen attractive for investigating the interlaminar fracture toughness. However, this description is not quite perfect. First, the Euler beam theory is limited to small deflections. At rather large deflections, the arm of force changes relative to the cross section along the front of delamination, which affects the bending moment and strain energy of the specimen (the effect of large deflections). Second, displacements in the neighborhood of this cross section significantly differ from those in the case of perfect fixation. This cross section as though rotates, thus causing additional displacements of the point of application of the external force (the rotation effect). Third, characteristic of some types of layered composites is the bridging effect, which consists in the constraining influence of some part of unfailed fibers between delamination surfaces remaining upon propagation of delamination. The latter case is especially characteristic of unidirectional composites [8].

The problem of using DCBs for an experimental determination of the Mode I interlaminar fracture toughness G_{Ic} was first investigated [8]. A simple numerical method allows to calculate G for any configuration and provides examples of correction factors for multiple geometries. It is also shown that by measuring the horizontal distance from the load line to the end of the crack, G can be accurately found from the regular expression [76].

After correction of the DCB model and with account of other studies, the ASTM standard and then an international standard were elaborated, which regulate the processes of planning, preparation of specimens, realization of tests, methods of processing test results, and their interpretations [8]. This international standard specifies a method for determining the crack strength of Mode I interlayers. It can be used with carbon fiber and fiberglass reinforced thermoses and thermoplastics [68].

One of the most popular geometries of interlayer crack growth tests is the DCB specimen loaded by applying symmetrical tensile forces at the ends of the beam [49]. This test method is only applicable to composite materials consisting of unidirectional carbon fiber and glass fiber tape laminates with fragile and durable single-phase polymer matrices. This limited scope reflects the experience gained from the survey. This test method may be useful for other types and classes of composites [19].

In the quoted studies and standards, the effect of large deflections is taken into account by introduction of a dimensionless correction factor reflecting the effect of change in the arm of force relative to the line of delamination contour. The arm of force is approximately calculated as the projection of the deflection curve of the Euler beam on its initial longitudinal axis by using the first three terms of expansion of the function of rotation angle into a Taylor series. It is obvious that the applicability of this approach has its limits, which are not defined by standards. The correction factor also considers the way of application of forces to the ends of cantilevers [8].

The rotation effects are considered by using three variants of correction of the basic equation of energy release rate. The clearest of them is the MBT; it consists in using the effective length of delamination, which is determined from an analysis of the elastic compliance of the specimen as a function of delamination length. This procedure is similar to the application of the Saint-Venant principle to estimating the size of the stress concentration zone. Thus, for a DCB specimen, the correction of delamination length is proportional to the height of cross section [8].

The fracture toughness of Mode I interlayer for each fiber orientation was calculated using the MBT method and the MCC method [77, 78]. An alternative way to consider the rotation effect of the root cross section is employed in, where studies are performed to determine the resistance of the Mode I interlayer to fracture or the rate of release of critical energy. The calculated critical load and the corresponding displacement for the measured crack size for DCB specimens using the determined fracture energy are in good agreement with the published results [79]. Experimental evaluation of the energy release rate of critical strains in the composite opening mode (Mode I) using a specimen of a DCB has been studied. Fracture analysis was performed on DCB specimens made of glass / epoxy, carbon fiber / PEEK and carbon fiber / epoxy composites [80]. Another paper discusses the critical loads and corresponding displacements from a DCB for three different arrangements of glass / epoxy glass / epoxy composite specimens. Reduction schemes based on cubic and power law have also been proposed to determine the Young's modulus and energy release rate, and a good agreement was found with the published and test results [81].

The bridging effect can greatly affect the character of development of delamination. If the bridging zone is relatively large, it is necessary to use a more general criterion of destruction, namely the so-called R-curve, which has become the subject of numerous investigations [8].

The burning resistance of composite materials can be improved by using various transition mechanisms. The size of the bridge area is usually several times the thickness of the layer, so it is questionable to think of the resistance to lamination as a property of the material that does not depend on the size and geometry of the specimen [82].

It has been found that cracks in the composite materials of long fiber reinforced ceramic matrices that overlap with delamination reduce the fibers that awaken the crack at a shallow angle. This leads to a crack-closing force model that combines simple mechanics and Weibull statistics [83]. For the mixed-mode delamination of composites, a finite element model can be used. It takes into account the effects of the R-curve, such as fiber joints in cracked interfaces or plastic deformation at crack ends. Numerical modeling of standard delamination tests has been compared with experimental results showing the efficiency of the method [84]. The

obtained results show that in Mode I the growth of interlayer crack in the DCB specimens is related to the joining of the fibers behind the crack end and division at the end of the crack, but in Mode II – the formation of the damage zone at the end of the crack [85].

The dependence of R-curves on the geometry of DCB specimens for a unidirectional epoxy-carbon composite has been investigated. Extended crack formation was observed during crack propagation. The exact law connecting the studied composites was found. This data and the proposed numerical procedure allowed authors of the study to predict the R curve for any DCB specimen thickness [86].

To analyze the experimental results, an analytical model has been developed that can characterize the relationship between bridge voltage and microstructure, and a DCB analysis that includes the effect of bridge stress. The crack closure due to bridge stress is then calculated using the usual power law relationship and the new distribution bridge stress function developed in the study done by K.-S. Sohn, S. Lee, and S. Baik [87]. The bridging law is an important material parameter. The bridging law of a material is sensitive to the composition of the material and the fiber architecture. In the absence of established procedures, it is of interest to develop experimental and analytical methods for determining the bonding law and fracture energy of short-fiber polymer composites. All materials demonstrate mitigating transition rules [88].

From some experimental configurations, the bridging law of material can be obtained directly from measurements. No significant dependence of the specimen height was observed in the results. Therefore, the established transitional rules can be considered as material properties. Based on the observations, it was found that the concept of failure behavior in terms of bridging law is attractive because it can be used as a tool to adapt the microstructure to the desired fracture behavior [89]. When performing crack initiation and propagation tests, the well-known solution based on classical beam theory perfectly agrees with the experimental results in the case of crack excitation tests. In contrast, the classical model seems insufficient to evaluate the spread test data [90].

In the case of a small-scale bridging zone, the importance of this factor becomes secondary, and the resistance to the interlaminar fracture is estimated by the only constant – the interlaminar fracture toughness G_{Ic} [8].

As already mentioned, at a high flexural compliance of DCB specimens, the methods of determination of the quantity G_{Ic} by using the linear bending theory of Euler beams are not quite reliable because of the geometrical nonlinearity, which plays a significant role at large deflections. At present, some test methods with the use of DCB specimens made of layered composites of high flexibility are suggested. A simple expression is derived for estimating the energy release rate upon propagation of a delamination by calculating the invariant J-integral [8]. A specimen of a double cantilever beam was examined for fracture testing under high displacement conditions. J-expressions were obtained for arbitrary loading of beam ends. Two different loads, transverse force and bending moment, were studied as special cases. Direct relationships were obtained for use in experimental situations [91]. This made it possible for the authors of paper [66] to suggest a new method for determining the quantity G_{Ic} and to demonstrate its reliability for highly flexible layered composites too [73]. This method is most suitable for testing long, flexible, flexible specimens with delamination. The method is based

on the J-integral calculation of a well-known DCB specimen and does not require knowledge of the elastic properties of the tested material or crack length measurements. A comparison with a method based on beam theory and finite element simulations was made and a sufficiently good agreement was reached [92].

Another variant consists in artificially increasing the flexural rigidity of DCB specimens by gluing external strengthening patches to them [8]. A practical test method for determining the resistance of Mode I to adhesive joints with different substrates has been studied. This overcomes the limitations of existing methods, which preclude their use when testing compounds with different substrates. The test method is applicable to adhesive joints where, for geometrical and / or material reasons, the two joined substrates have different flexural strengths. The results indicate (Figure 3.1, 3.2) that the test method provides a practical means to characterize the resistance of Mode I to fractures in joints with different substrates [93].
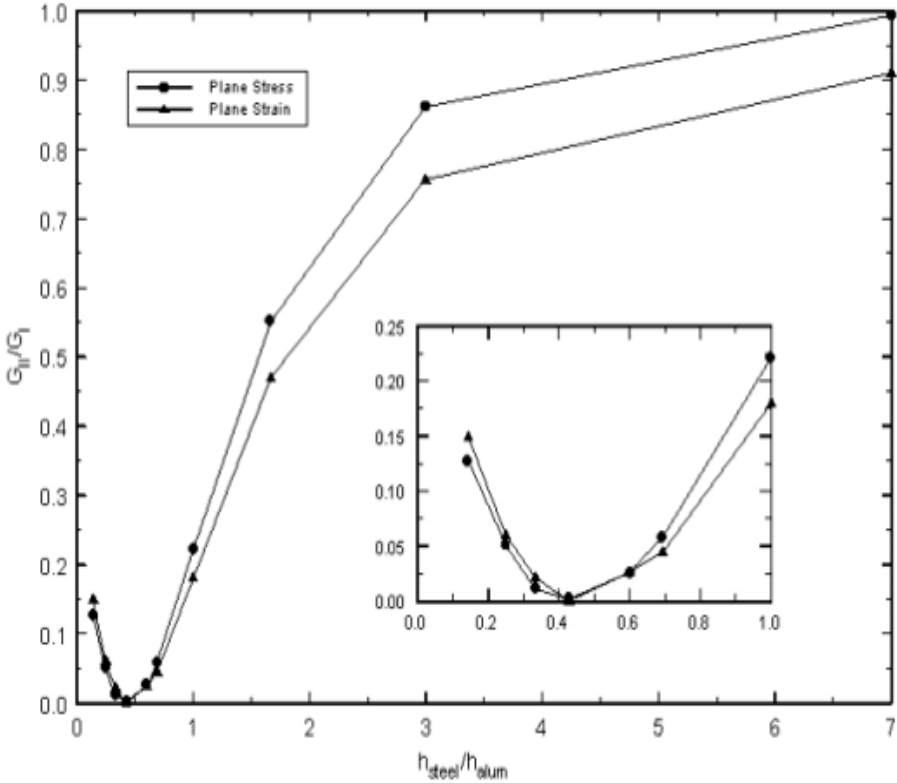
Figure 3.1. Finite element analysis depicting mode-mix versus the ratio of substrate heights for a steel-aluminum specimen [93].
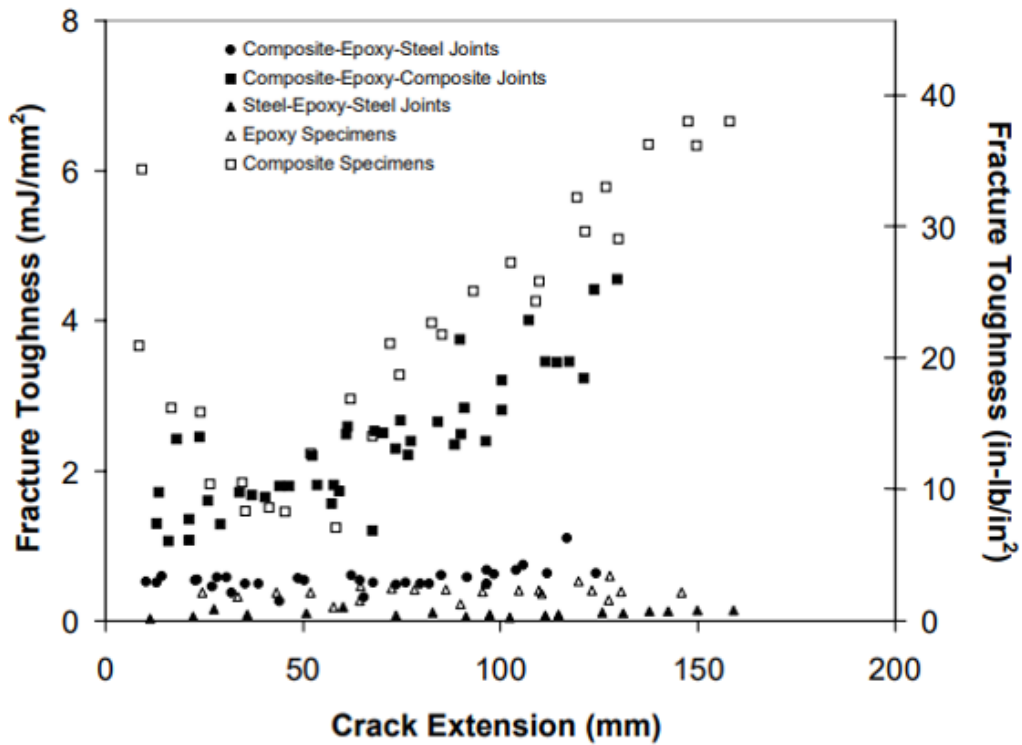
Figure 3.2. Fracture toughness as a function of crack length for similar and dissimilar joints. Each condition represents several specimens [93].

The parameters of the compound specimen can be chosen so that to ensure the acceptability of the linear bending theory of beams [8]. With fiber-reinforced polymer composites, environmental factors such as temperature and corrosion adversely affect their structural integrity. Study was done to characterize the fracture toughness resistance of glass / epoxy and glass-carbon hybrid fiber reinforced composites under unfavorable thermal aging conditions. The failure mechanism is initiated by cracking of the matrix at room temperature until the fibers break and the fibers rupture at low temperatures. Deficiencies of microstructures of ancient and thermally exposed specimens were studied according to the SEM image [94, 95].

It is obvious that the nonlinear bending theories of flexible beams are promising for perfection of the method of determination of G_{Ic} for layered composites based on DCB specimens (Figure 3.3) [8].
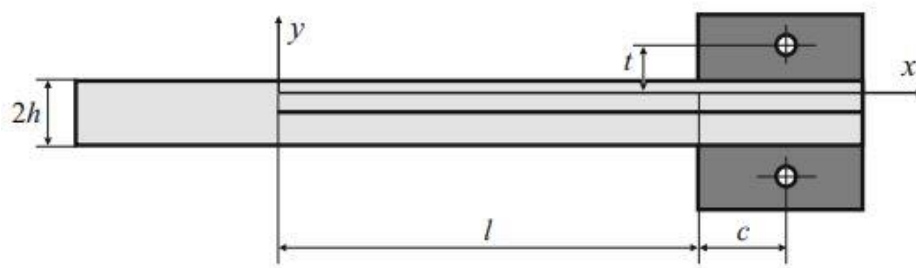
Figure 3.3. Scheme and main dimensions of a DCB specimen [8].

If the theory of elastic flexible plates with large displacements is used. The result of the total longitudinal deformation of the compressed force and the sublaminate is expressed as a complete elliptic integral that uniquely identifies the thickened shape of the sublaminate, the effect of curvature on the compressive strain, and the increase in compressive force in the explosion condition. The results of the analysis of the general delamination propagation and its compression-bending destruction in the bent state allows to determine the basic conditions of damage behavior of the compressed layered composite material [75].

The state of the Griffith type energy was used as a criterion for the delamination propagation of the 1D nonlinear model of thin plates. The model mentioned here is applied to the general type of delamination and allows to describe the curvature of the feet and the propagation of lesions [96].

The purpose of the present study is to investigate in more detail the effect of large deflections on the accuracy of determination of G_{Ic} for layered composites with the help of DCB based on the nonlinear bending theory of beams (Figure 3.4). An advantage of this approach is the rigorous description of the deflection curve of a beam at arbitrarily large deflections.
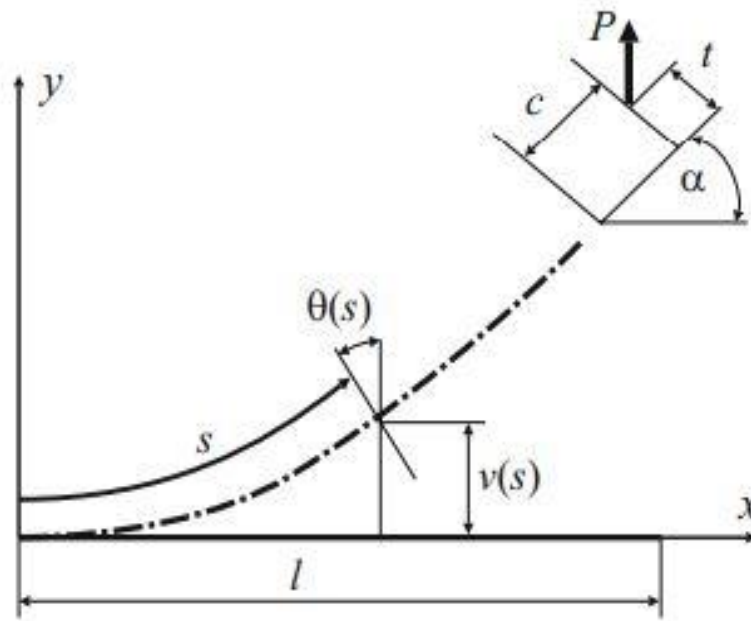
Figure 3.4. Deformation of a DCB specimen [8].

Our investigation is primarily focused on the creation of a tool for controlling the approximate methods based on the linear theory of Euler beam, a more accurate determination of limitations of the approximate methods, and the estimation of possible errors. The nonlinear theory of DCB specimens also allows one to directly determine the value of G_{Ic} for highly flexible layered composites [8]. A geometrically nonlinear model of sheet beams (cylindrical curvature of a plate) is presented to analyze the shrinkage behavior of a layered composite during delamination during compression. The main advantage of the model is an accurate description of the curved axis of the beam (plate) without linearization or other higher order approximation. The model only describes the geometrically nonlinear effect of the bending of

DCB specimens (global effect) and should be combined with the effective delamination extension procedure to correct the rotation of DCB specimens in front of the delamination (local effect). First, the nonlinear model can serve as a tool to estimate the possible error due to geometric nonlinearity compared to the linear solution. On the other hand, this model can be effectively used to determine the fracture toughness of interlayers using DCB specimens at large deviations [97].

The fact that the nonlinear theory does not contradict the standard, within the framework of its correct application, is shown by comparing its results with data obtained in experiments on a layered fiberglass [81]. In the present study, details of the theory are considered, and experimental results for highly flexible DCB specimens, which confirm the reliability and efficiency of the model suggested, are presented [8].

3.2 Analytical Investigation: Nonlinear mathematical model of DCB specimens

The basic nonlinear bending equation of cantilevers

A DCB specimen with a rectangular cross section of width *b* and height *2h*, made of a linearly elastic material (Figure 3.3), has a delamination in the horizontal plane of symmetry. Its cantilevers are loaded with a pair of equal, collinear, and oppositely directed forces. The loading is realized by means of blocks or piano hinges attached to the ends of cantilevers. According to the standard, the length of delamination is taken to be $a = l + c$ [8].

To estimate the value of G_{Ic}, the energy criterion of the linear fracture mechanics of Griffiths type is used, which implies determination of the elastic strain energy of a specimen under a load. If the blocks for loading are sufficiently rigid, the flexural strain of the part of the cantilever under the block can be neglected. In this case, the free parts of cantilevers of length *l* completely determine the elastic strain energy of the DCB specimen. Therefore, the basic element of analysis is the problem on bending of a cantilever beam of length *l* by a vertical concentrated force *P* whose application point is shifted relative to the free end of the beam, but its coordinates *c* and *t* remain constant in the reference system connected with the end section of the deformed part of the beam (Figure 3.4). The figure shows the deflection curve of the deformed part of the beam and the location of force, determined by the rotation angle α of the end section of the beam [8].

Usually, the width of the cross section of a specimen is much greater than its height ($b \gg h$), therefore, it can be assumed that the specimen is in a stress state close to the plane one. As stems from, [98] the differential equation of the deflection curve of a beam can be written as the equation (3.1) of a plane curve in the natural form:

$$D \frac{d\theta}{ds} = M(s), \tag{3.1}$$

where θ is the rotation angle of the cross section of the beam with a curvilinear coordinate *s*, *M(s)* is the bending moment in this section, and *D* is the cylindrical rigidity of the beam [8].

The bending moment can be expressed in terms of its value M_0 in the root cross section, the external active force P, and the axial displacement $u(s)$ in the cross-section s:

$$M(s) = M_o - P[s - u(s)].$$

After insertion of this expression into equation (3.1) and simple transformations, the differential equation (3.2) of the deflection curve takes the form:

$$\frac{d\theta}{ds} = k\sqrt{2}\sqrt{sin\alpha_0 - sin\theta},\tag{3.2}$$

where:

$$sin\alpha_0 = sin\alpha + \frac{(kl)^2}{2}(\bar{c}\,cos\alpha - \bar{t}\,sin\alpha)^2,$$

$$sin\alpha = \frac{1}{2}\left(\frac{M_0}{kD}\right)^2, k^2 = \frac{P}{D}, \bar{c} = \frac{c}{l}, \bar{t} = \frac{t}{l}.$$

Here, α is the rotation angle of the end section $s=l$ of the beam (see Figure 3.4); α_0 is the rotation angle in the cross section of the beam with a zero curvature of the deflection curve. For the configuration of the specimen at $c=t=0$, the cross section of zero curvature coincides with the beam end $s_0=l$. If $\bar{c}\,cos\alpha$ - $\bar{t}\,sin\alpha > 0$, this section corresponds to a curvilinear coordinate $s_0>l$, i.e., it does not exist in reality. In this case, the curvature of the beam is a positive decreasing function of the coordinate s. But if $\bar{c}\,cos\alpha$ - $\bar{t}\,sin\alpha < 0$, the curvilinear coordinate of the cross section of zero curvature $s_0 < l$, and this means that, upon transition through this section, the curvature changes its sign. It is obvious that the cross section with the zero curvature of the deflection curve coincides with the beam end if the condition shown in equation (3.3):

$$\alpha = \alpha_* = cotan(c/t)\tag{3.3}$$

is fulfilled. It follows from equation (3.2) that:

$$ds = \frac{d\theta}{k\sqrt{2}\sqrt{sin\alpha_0 - sin\theta}}.$$

If $\alpha < \alpha_0$, the rotation angle $\theta(s)$ grows monotonically. At $\alpha > \alpha_0$, the rotation angle θ grows in the interval $[0, s_0]$ from $zero$ to α_0 and then decreases in $[s_0, l]$ from α_0 to α. As a result, in the first case,

$$s = \int_0^s ds = \int_0^{\theta(s)} \frac{d\theta}{k\sqrt{2}\sqrt{sin\alpha_0 - sin\theta}},$$

and in the second one,

$$s = \begin{cases} \int_0^{\theta(s)} \dfrac{d\theta}{k\sqrt{2}\sqrt{sin\alpha_0 - sin\theta}} & at\ s \le s_0 \\ \int_0^{a_0} \dfrac{d\theta}{k\sqrt{2}\sqrt{sin\alpha_0 - sin\theta}} + \int_\theta^{a_0} \dfrac{d\theta}{k\sqrt{2}\sqrt{sin\alpha_0 - sin\theta}} & at\ s \le s_0 \end{cases}.$$

Calculations by these equations for the variable limit of integration $\theta(l) = \alpha$ make it possible to derive the dimensionless parameter kl of the external load as a function of the rotation angle α of the end section of the deformed part of the beam, as shown in equation (3.4):

$$kl = \frac{1}{\sqrt{2}}\begin{cases} I_l(0, \alpha) \ at \ \alpha \leq \alpha_* \\ I_l(0, \alpha_0) + I_l(\alpha, \alpha_0) \ at \ \alpha \leq \alpha_*, \end{cases} \tag{3.4}$$

where:

$$I_l(\alpha_1, \alpha_2) = \int_{\alpha_1}^{\alpha_2} \frac{d\theta}{\sqrt{sin\alpha_0 - sin\theta}}.$$

It is seen that the dimensionless parameter kl is uniquely related to the rotation angle α. The deflection curve of the beam can also be described in rectangular coordinates shown in equations (3.5 and 3.6):

$$x(\theta) = \frac{1}{k\sqrt{2}}\int_0^\theta \frac{cos\theta d\theta}{\sqrt{sin\alpha_0 - sin\theta}}, \tag{3.5}$$

$$y(\theta) = \frac{1}{k\sqrt{2}}\int_0^\theta \frac{cos\theta d\theta}{\sqrt{sin\alpha_0 - sin\theta}}. \tag{3.6}$$

It is obvious that the ordinate $y(\theta)$ coincides with deflection of the beam, $v(\theta)$. Equation (3.5) is simply integrated and takes the form, shown in equation (3.7):

$$\overline{x}(\theta) = \frac{x(\theta)}{l} = \begin{cases} \frac{\sqrt{2}}{kl}\left(\sqrt{sin\alpha_0} - \sqrt{sin\alpha_0 - sin\theta}\right) \ at \ s < s_0, \\ \frac{\sqrt{2}}{kl}\left(\sqrt{sin\alpha_0} + \sqrt{sin\alpha_0 - sin\theta}\right) \ at \ s > s_0 \end{cases}. \tag{3.7}$$

The deflection in equation (3.6) can be conveniently expressed in terms of integrals $I_1(\alpha_1, \alpha_2)$ and $I_2(\alpha_1, \alpha_2)$, shown in equation (3.8):

$$\overline{v}(\theta) = \frac{v(\theta)}{l} = \frac{1}{kl\sqrt{2}}\begin{cases} -l_2(0, \theta) + sin\alpha_0 I_l(0, \theta) \ at \ s < s_0 \\ -l_2(0, \alpha_0) + sin\alpha_0 I_l(0, \alpha_0) - \\ -l_2(\theta, \alpha_0) + sin\alpha_0 I_l(\theta, \alpha_0) \ at \ s > s_0 \end{cases}, \tag{3.8}$$

where:

$$l_2(\alpha_1, \alpha_2) = \int_{\alpha_1}^{\alpha_2} \sqrt{sin\alpha_0 - sin\theta} d\theta.$$

As seen from equations (3.4, 3.7 and 3.8), the geometrical form of the deflection curve of a cantilever beam is also uniquely determined by the rotation angle of its end section [8].

The elastic strain energy of a cantilever and a DCB specimen
If we assume that the effect of shear force on the elastic strain energy is weaker, then, at large deflections of the cantilever, this energy depends on two internal force factors: the bending moment and axial force. In what follows, the corresponding components of strain energy will be called the bending energy and the tension energy [8].

The bending energy of the cantilever can be presented in finite form as shown in equation (3.9):

$$U_b = \int_0^l \frac{M^2}{2D} ds = \frac{kD}{\sqrt{2}} \begin{cases} I_2(0,\alpha) \ at \ \alpha < \alpha_* \\ I_2(0,\alpha_0) + I_2(\alpha,\alpha_0) \ at \ \alpha < \alpha_* \end{cases}. \tag{3.9}$$

The tension energy is determined by the axial tensile force *N=P sinα*, which is projection of the external active force on the direction of tangent to the deflection curve of the beam, as shown in equation (3.10):

$$U_t = \int_0^l \frac{N^2}{2Eh} ds. \tag{3.10}$$

After simple transformations, we have equation (3.11):

$$U_t = \frac{D(kl)^4}{72hl^3} \begin{cases} I_1(\alpha_0) + sin\alpha_0 I_2(0,\alpha) \ at \ \alpha < \alpha_* \\ I_2(\alpha_0) + sin\alpha_0 [I_2(0,\alpha_0) + I_2(\alpha,\alpha_0)] \ at \ \alpha > \alpha_* \end{cases}. \tag{3.11}$$

In a dimensionless form, the components of strain energy read as in equations (3.12 and 3.13):

$$\bar{U}_b = \frac{U_b}{D/h} = \frac{kl}{\bar{l}\sqrt{2}} \begin{cases} I_2(0,\alpha) \ at \ \alpha < \alpha_* \\ I_2(0,\alpha_0) + I_2(\alpha,\alpha_0) \ at \ \alpha < \alpha_* \end{cases}, \tag{3.12}$$

$$\bar{U}_t = \frac{U_t}{D/h} = \frac{(kl)^4}{72\bar{l}^3} \begin{cases} I_1(\alpha_0) + sin\alpha_0 I_2(0,\alpha) \ at \ \alpha < \alpha_* \\ I_2(\alpha_0) + sin\alpha_0 [I_2(0,\alpha_0) + I_2(\alpha,\alpha_0)] \ at \ \alpha > \alpha_* \end{cases}, \tag{3.13}$$

where $\bar{l}=l/h$,

$$I_1(\alpha_0) = 2 - cos2\alpha_0 - \frac{\sqrt{2}}{kl}(\sqrt{sin\alpha_0} - cos\alpha\sqrt{sin\alpha_0 - sin\alpha}),$$

$$I_2(\alpha_0) = 2 - cos2\alpha_0 - \frac{\sqrt{2}}{kl}(\sqrt{sin\alpha_0} - cos\alpha\sqrt{sin\alpha_0 - sin\alpha}),$$

and the total strain energy of the DCB specimen is shown in equation (3.14):

$$\bar{U} = 2(\bar{U}_b + \bar{U}_t). \tag{3.14}$$

If $\alpha \leq \alpha_*$, the integrals, $I_1(\alpha_1,\alpha_2)$ and $I_2(\alpha_1,\alpha_2)$, are improper, and their numerical calculation requires a constant control of accuracy. This can be avoided by employing the transformation of the variable θ determined according to the equation (3.15):

$$sin\left[\frac{1}{2}\left(\theta + \frac{\pi}{2}\right)\right] = p \ sin\varphi, \tag{3.15}$$

where:

$$p = sin\left[\frac{1}{2}\left(\alpha_0 + \frac{\pi}{2}\right)\right].$$

As a result, the integrals mentioned turn into the incomplete elliptic integrals of the first and second kind, $F(\varphi_0, \varphi_*, p^2)$ and $E(\varphi_0, \varphi_*, p^2)$, respectively:

$$l_1(\alpha_1, \alpha_2) = \frac{1}{\sqrt{2}} F(\varphi_0, \varphi_*, p^2),$$

$$l_2(\alpha_1, \alpha_2) = 2\sqrt{2}[(p^2 - 1)F(\varphi_0, \varphi_*, p^2) + E(\varphi_0, \varphi_*, p^2)],$$

where:

$$F(\varphi_0, \varphi_*, p^2) = \int_{\varphi_0}^{\varphi_*} \frac{d\varphi}{\sqrt{1 - p^2 sin\varphi}},$$

$$E(\varphi_0, \varphi_*, p^2) = \int_{\varphi_0}^{\varphi_*} \sqrt{1 - p^2 \sin \varphi} \, d\varphi.$$

The limits of integration are determined by the basic transformation, as seen in equation (3.15) [8]:

$$sin\varphi_i = \frac{sin\left(\frac{a_i}{2} + \frac{\pi}{4}\right)}{sin\left(\frac{a_0}{2} + \frac{\pi}{4}\right)}.$$

Energy release rate G_I of a DCB specimen

According to definition,

$$G_I = -\frac{dU}{dl} = -\frac{D}{h^2}\frac{d\bar{U}}{d\bar{l}} = \frac{D}{h^2}\bar{G}. \tag{3.16}$$

In the particular case where the external force is applied to the end of the cantilever *(c=t=0)*, an accurate, but rather complex, formula for estimating the energy release rate of a DCB specimen can be obtained. Therefore, for practical applications, it is more convenient to use a numerical differentiation. In this case, it is necessary to bear in mind that the derivative of strain energy along the crack length has to be calculated at a constant opening of delamination [8].

It is obvious that, in testing a DCB specimen with controlled displacements in the state of critical equilibrium, the energy release rate is equal to the interlaminar fracture toughness. The initial data for determining the quantity G_{Ic} are the critical force P_c, the corresponding opening δ (relative displacement of the points of application of external forces), and the delamination length l_c at the instant of its next jump-like growth. These are the parameters measured in standard tests [4, 5]; they are redundant. Therefore, there are several variants of determination of the parameter G_{Ic} according to test data, which allow one to control the final result. In the present study, the determination of G_{Ic} according to the nonlinear model of DCB specimens implies an iterative procedure employing the opening and length of delamination. This procedure includes (I) joint solution of equations (3.4 and 3.8) with account of (3.3) for the measured values of opening δ and length l of delamination in order to find the dimensionless parameter of loading k_l and the corresponding rotation angle of the end section of cantilever; (II) determination of the elastic strain energy from equations (3.12–3.14); (III) repeated calculation of strain energy with a small increment of delamination at the same fixed deflection

of the ends of cantilevers; (IV) determination of the parameter G_{Ic} by equation (3.16) with the use of numerical differentiation. In this case, the information on the critical force allows one to estimate the cylindrical rigidity and, hence, to estimate the elastic modulus of the material along the longitudinal axis of the specimen. The algorithm for determining the strain energy, its release rate upon propagation of delamination, and the toughness G_{Ic} according to the nonlinear model of DCB specimen, was realized in the form of a MATLAB program code [8, 73] that can be seen in annex of this thesis.

4 DCB NONLINEAR SPECIMEN FOR DETERMINATION OF THE MODE I INTERLAMINAR FRACTURE TOUGHNESS. EXPERIMENTAL STUDY

4.1 Material, DCB specimen, and technological features

In [90], the suitability of the nonlinear model of DCB specimen developed was verified by comparing its predictions with test data for specimens of a layered fiberglass within the limits of applicability of the standard [19, 77].

A practically exact coincidence between the results obtained by the nonlinear model and standard method of a MBT was observed. However, the question of adequacy of the nonlinear model outside the limits of applicability of the standard methods remains open. There is known several attempts to resolve the problem of geometrical nonlinearity of DCB specimen. One of them is represented below. Modified DCB specimen is shown in the Figure 4.1 [94]. Here the levers of DCB are reinforced by metallic overlaps along of the significant part of their length. At the selection of appropriate material of overlap and its length and thickness can be obtained the modified DCB specimen for which linear description will be correct. However, the direct using of standard procedure of processing of measurement data for defining of the interlaminar fracture toughness will be incorrect. There will be needed or supplementary analysis of the modified DCB specimen properties or must be established special procedure of calibration.

(a)   (b)
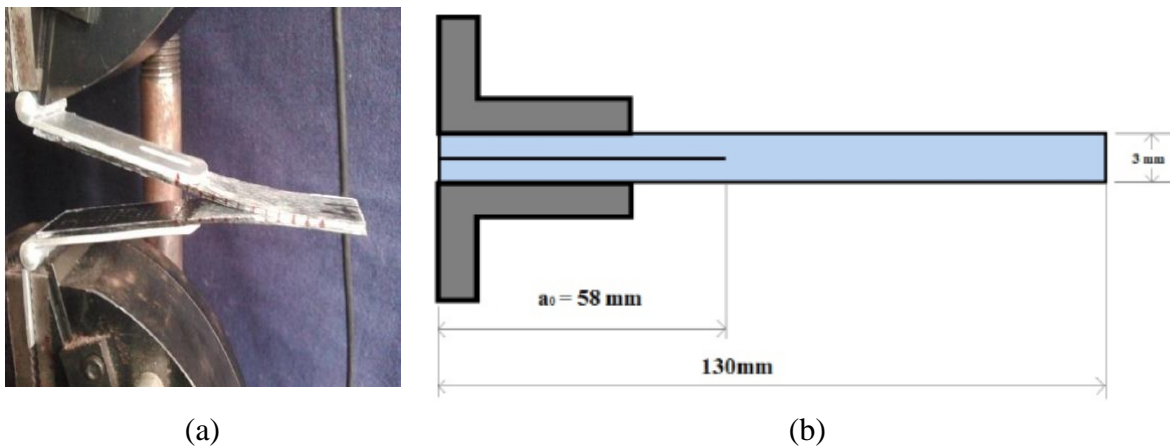
Figure 4.1. (a) DCB specimen at the stage of test (b) specimen dimensions used in test [94].

Other solution was proposed in [93] that requires of modified procedure of test data processing and significantly complicate procedure of testing. To make testing results more viable and precise, there are many photos taken in process of testing, Millimeter paper can be used in the background to better see the shape of specimens shown in Figure 4.2 [92].
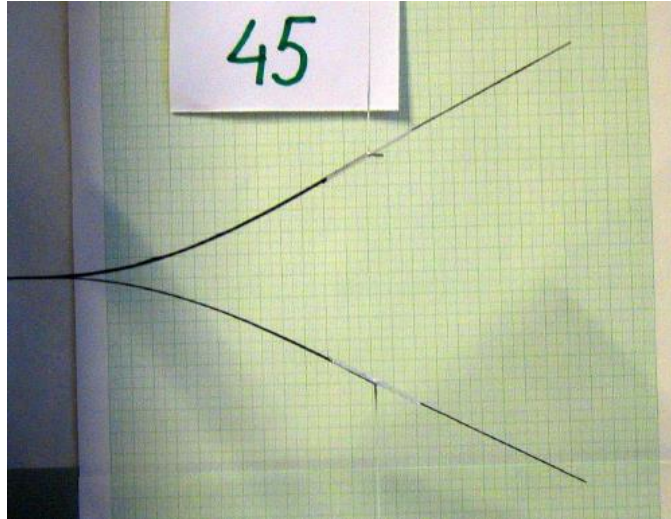
Figure 4.2. Millimeter paper used in background of specimen testing [92].

A 10-layer specimen had a total thickness of 2 mm and dimensions 20.5×200 mm in the plan. The initial delamination between the fifth and sixth layers was created by a Teflon interlayer in the specimen structure. Specimens were made with wet layup and high-quality epoxy resin. Vacuum was used in the process to make sure there are no air gaps in the structure. Some of specimens made can are shown in Figure 4.3.

Figure 4.3. Some of the Carbon fiber specimens made for testing.

To make up the deficiency, DCB specimens of increased flexibility were tested. We used a layered CFRP on the basis of carbon fabric 200 g/m^2 as the reinforced material and an epoxy resin as the binder. The specimens were manufactured by the vacuum technology with cure for 24 h at a temperature of 28 °C [8].

As there is always error in dimensions when making specimens with given technology, all were measured. The thickness *(H)* and width *(W)* were measured in 3 places: start, middle and end of the specimen, so the average can be taken. Results shown below in Table 4.1:

Table 4.1.

Results of measured specimens in mm and average results

No.	L (mm)	W1 (mm)	W2 (mm)	W3 (mm)	W_avg (mm)	H1 (mm)	H2 (mm)	H3 (mm)	H_avg (mm)
1	200.10	19.50	19.70	20.10	19.77	2.10	2.10	2.05	2.08
2	200.30	19.80	20.20	20.10	20.03	2.00	2.07	2.10	2.06
3	199.90	19.90	20.00	20.20	20.03	2.03	2.06	2.10	2.06
4	199.50	19.70	19.30	19.50	19.50	1.99	2.03	2.09	2.04
5	199.80	20.30	19.90	19.70	19.97	2.15	2.08	2.03	2.09
Avg.	199.92			Avg.	19.86			Avg.	2.07

The DCB specimen was subjected to the action of a splitting load by means of piano hinges pasted to the ends of cantilevers, so that the axes of hinges were located in the end cross section of cantilevers. To attach piano hinges to the specimen very strong glue was used, when using weaker glue, the bond was not strong enough to withstand initial load. To ensure the resolution of fine details for a more exact registration of the size of delamination, a thin layer of white ground was sprayed on the lateral surface of the specimen, and a scale was fixed (Figure 4.4).

(a)   (b)
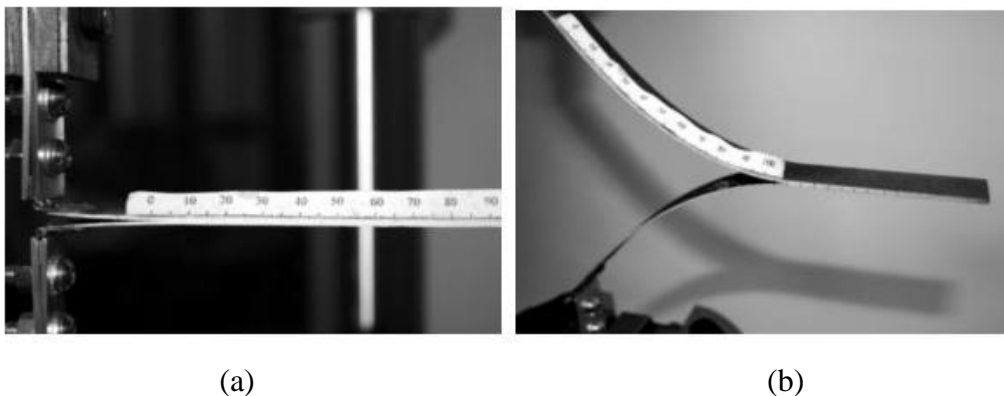
Figure 4.4**.** A DCB specimen at the initial stage of tests (a) and at a great opening of delamination (b).

The size of delamination was registered visually with the use of binocular optics (×8) and periodic photographing of the lateral surface of the specimen. The quasi-static tests of DCB specimens, according to the standard, were carried out on an Instron 8800 hydraulic testing machine (shown in Figure 4.5 from manufacturers materials) with controlled displacements at a constant loading rate of 3–5 mm / min [73].

Figure 4.5. *Instron 8800* hydraulic testing machine that are used in testing, manufacturers picture.

As per manual of manufacturer of *Instron 8800* hydraulic testing machine can support up to 100 kN axial force. It is equipped with many different grips and accessories to support different needs for testing purposes. It also features patented *Dynacell* load cell features than compensate for inertial loads caused by weight of grips and features. This all supports better and more accurate test results. For this test it was needed to equip a specimen with piano hinges to fix it to the testing machine.

S2M meter of small loads (HBM Test and Measurement), with the upper measurement limit of 1 kN, was connected in series in the loading circuit as the basic force transducer. After each jump-like growth in the size of delamination, the loading was interrupted, the delamination length was registered (Figure 4.4 (b)), the specimen was completely unloaded, and then the following loading stage was conducted. This procedure allowed us to obtain the full relation between the opening of delamination and the corresponding load at each registered delamination length [8].

4.2 Test results and analysis

To take into account the effect of rotation of the root cross section of cantilever in all three processing variants of tests results, the standard procedure for determination of the effective length of delamination, found by analyzing the elastic compliance of a specimen in relation to the delamination length (Figure 4.6), was used. A distinct feature was that, owing to nonlinearity, relations between the opening of delamination and load for the highly flexible specimens were determined from the slope of tangent to the opening–load curve at the initial loading stage. From the equation of the trend line, it follows that the correction for the delamination length has to be equal $\Delta l = 5.93\ mm$. The increased (effective) size of delamination, $a_e = a + \Delta l$, was used in all three variants of determination of the fracture toughness G_{Ic} [69].
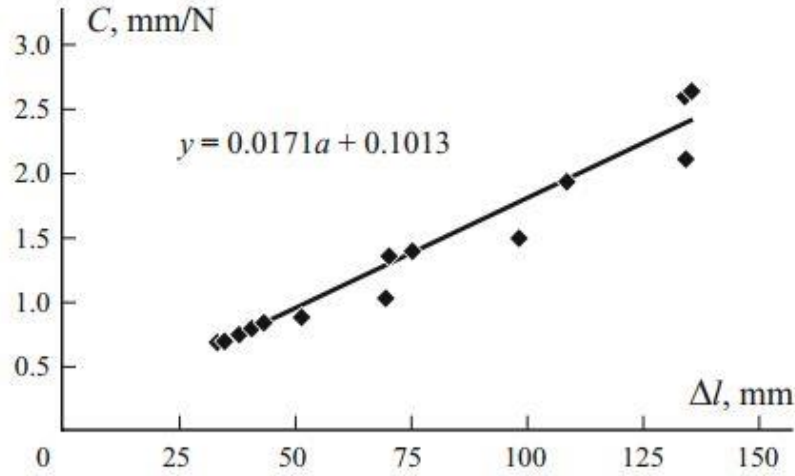
Figure 4.6. Compliance C of a DCB specimen vs delamination length Δl [8].

The first variant involved the use of the nonlinear DCB model developed according to the processing algorithm already described in brief. In the second variant, the standard MBT method was used for estimating the value of G_{Ic} within the limits of applicability of the Euler theory of bending of beams. The estimates showed that, for the DCB specimen considered, such a limit can be found from the condition that, in the critical configuration of DCB specimen, the ratio of the opening of delamination to its length must not exceed 0.25. This approximately corresponds to the ratio of critical length of delamination to the semi-thickness of specimens equal to 50. The third way of processing consists in a formal use of the linear theory of bending on the entire range of openings and correction of results according to recommendations of the standard. Namely, the quantity G_{Ic} was found from the critical load P_c and the critical effective length of delamination a_e shown in equation (4.1):

$$G_{lc} = G_{lc0}F\left(\frac{\delta}{a},\frac{a}{t}\right), \tag{4.1}$$

where G_{Ic0} is the toughness according to the linear model in terms of the critical force and the effective size of delamination, as shown in equation (4.2):

$$G_{lc0} = \frac{P_c^2 a_e^2}{D}, \tag{4.2}$$

but the second multiplier is the standard correction factor:

$$F\left(\frac{\delta}{a},\frac{a}{t}\right) = 1 - 0{,}3\left(\frac{\delta}{a}\right)^2 - \frac{3}{2}\cdot\frac{\delta t}{a^2}.$$

In equation (4.1), the cylindrical rigidity δ is the average value obtained in processing experimental data according to the nonlinear model. The basic results of measurements and calculations of the toughness G_{Ic} are presented in Table 4.2 [8].

Table 4.2.

Values of the interlaminar fracture toughness according to experimental results [8]

a, mm	P_c, H	δ, mm	$\left(\dfrac{\delta}{a}, \dfrac{a}{t}\right)$	G_{Ic}, J/m^2			
				Nonlinear model	MBT method	equation 4.1	equation 4.2
33,4	36,2	14,7	0.91	999	1077	1062	969
34,4	36,4	16,3	0.90	1080	1178	1128	1017
37,8	32,3	17,6	0.91	954	1035	1045	948
40,3	31,3	20,4	0.89	1014	1113	1100	984
43,2	28,5	21,4	0.90	905	988	1029	927
51,1	26,0	33,6	0.84	1107	1278	1155	972
68,7	18,9	48,4	0.83	878	1035	1043	863
74,6	19,9	60,2	0.78	1059	1315	1346	1050
97,1	14,5	90,0	0.72	890	1192	1170	843
106,9	14,3	106,2	0.68	942	1328	1372	937
135,0	13,5	167,0	0.52	1080	1961	1898	988
147,0	12,5	190,0	0.48	1037	2041	1916	918
135,0	12,1	151,0	0.61	891	1412	1525	924
138,0	12,7	161,0	0.57	970	1619	1752	1003

4.3 Comparison with DCB linear model

Results of investigation confirm the suitability of the nonlinear model of DCB specimen for determination of the quantity G_{Ic} of a composite within the limits of applicability of the standard test methods based on the Euler theory of bending of beams. Figure 4.7 shows a comparison between the estimates obtained by the nonlinear model and the standard MBT method. It is seen that, for the relative size of delamination, within the limits of 50, the estimates of G_{Ic} practically coincide: the difference is smaller than 0.025 %. As follows from the same diagram, the average value of G_{Ic}, on the entire range of delamination lengths, obtained according to the nonlinear model differs from that derived by the standard MBT method (within the limits of its applicability) by –2.32 %. Thus, we can conclude that the nonlinear model of DCB specimens makes it possible to obtain reliable values of G_{Ic} by testing highly flexible specimens [8].

The significant deviations of some experimental points from the average value, which are clearly seen from Figure 4.7, are most probably connected with a causal heterogeneity of the structure of the layered material used [8].
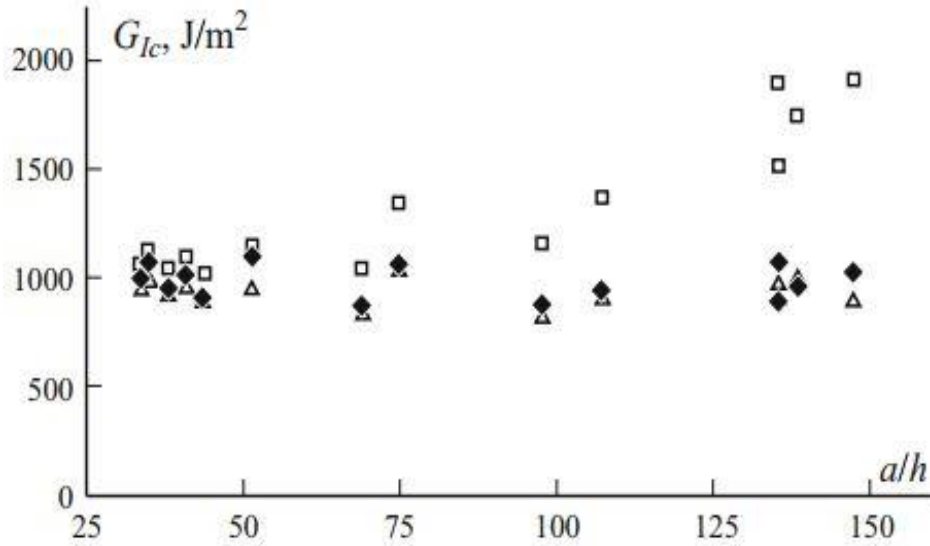
Figure 4.7. Interlaminar fracture toughness G_{Ic} vs the relative size a/h delamination according to the nonlinear (♦), linear (□), and corrected (41) (△) models [8].

The second basic conclusion concerns the use of correction, which is recommended by the standard for considering changes in the arm of force at large deflections. As follows from the results of our investigations, the direct correction envisaged by the standard may even worsen the estimate of G_{Ic} if the MBT method is employed. However, a satisfactory result can be obtained by using equation (4.2), which implies correction of the formal expression of G_{Ic} according to the linear model by its multiplication by the standard correction factor. In Figure 4.7, the estimate obtained by the nonlinear model is compared with those given by the uncorrected [90] and corrected [89] linear models. It is seen that the last estimate is rather close to that obtained by the nonlinear model. We should note, however, that there exists an upper limit of the relative delamination lengths above which the distinction between the estimates obtained by the nonlinear and corrected linear models grows sharply. Therefore, for testing highly flexible DCB specimens, the most reliable estimates of the parameter G_{Ic} can be obtained by using the exact nonlinear model [8].

5 THE EFFECT OF PLASTICITY TO INTERLAMINAR FRACTURE TOUGHNESS OF ADHESIVE BOND OF COMPOSITE

Adhesive joints of structural components are attractive as for manufacturing of the new aircraft or for repair of structural elements during operation. This type of joint is a good alternative to traditional joining systems (e.g., riveting or welding) for a wide class of components assembling to electronic, automotive, and aerospace industries. There are a huge number of publications in this field and a wide range of review-articles dedicated to different aspects of research and developments, production, and applications [7].

The influence of surface preparation, joint configuration, adhesive properties, and environmental factors on joint behavior is briefly described for bonded FRP composite material structures by Budhe S, Banea M D, de Barros S, and da Silva L F M. The analytical and numerical methods of stress analysis required before failure prediction are considered. Several methods used to predict joint joints were described. There is no general agreement on the method to be used to predict failure, as the strength and modes of collapse vary depending on the different bonding methods and parameters, but advanced lesion models are quite promising because important aspects of joint behavior can be modeled using this approach. However, there are still no reliable failure criteria, thus limiting the wider use of bonded joints in main load-bearing structures. In order to reduce the costly inspection at the design stage, it is important to accurately predict the strength of the joints to be bonded [99]. Durability and resistance to extreme temperatures has always been the main limit of adhesives, which, due to the nature of their polymer, degrade significantly at temperatures where other structural materials (e.g. metals, for example) have slight changes in mechanical properties. However, due to the inherent advantages of gluing, great efforts are being made to improve the temperature resistance of gluing joints [24]. The efforts of these researchers can all be put into practice, helping to solve complex problems in various high-tech industries, where light and strong components that can withstand large temperature gradients must be produced on an ongoing basis [28].

The damage profile will be dominated by fiber failure under load in the unidirectional composite (Figure 5.1). Compared to the matrix collapse strain, ε_f is very small [24].
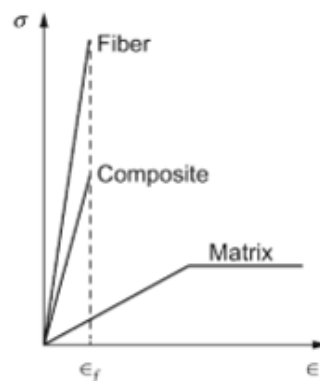
Figure 5.1. Damage controlled by the fiber failure [24].

Aerospace composites have relatively fewer defects than bulk materials. It is responsible for the high tensile strength of them. On the other hand, the calculated tensile strength of high-resolution fibers shows a significant statistical distribution observed in other fragile materials. This means that even if the fiber modulus may be identical, the maximum strain may be statistically different (Figures 5.1 and 5.2) [24].
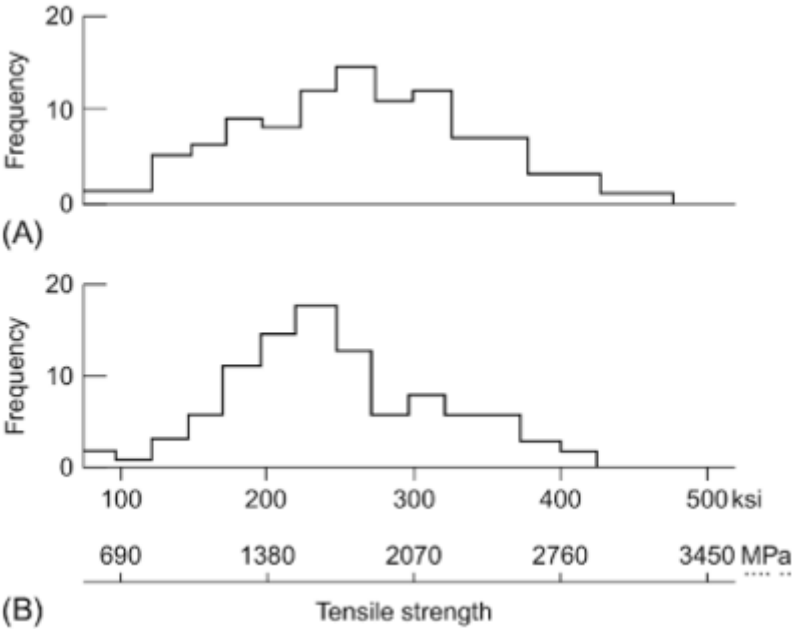
Figure 5.2. Statistical spread of tensile strength: (A) MODMOR I carbon fiber and (B) GY-70 carbon fiber [24].

Compared to aerospace bonded repairs, structural repair procedures in wind blades are not as well developed and thus face several challenges [100].

Adhesive bonding is a viable method for joining a wide range of materials. Today, however, there is a great demand to increase service life, reduce costs and improve structural safety. The industry is therefore very interested in developing new technologies and processes to easily recycle, heal or collaborate on connected structures.

The analysis of fatigue endurance and service life has attracted many researchers. Fatigue crack initiation is a very important topic, but it is difficult to address due to the difficulties associated with crack nuclear modeling and the ability to monitor and detect the initialization phase. Studies on the induction of cracks in adhesive joints are not yet sufficiently developed and could be considered as an early stage [23].

Tests characterizing Fracture mechanics for adhesive joints are analyzed and reviewed to understand their advantages and disadvantages. Both linear and nonlinear methods have been performed to obtain the rate of fracture energy release. There is no general agreement on the suitability of the test for the assessment of mixed-mode fractures of adhesive joints. A universal test that can be easily performed and give accurate results is essential to optimize costly testing at the design stage [26].

CZM have been used to determine the strength of adhesive joints in addition to FE analysis, which allows modeling of damage growth taking into account energy principles. On the other hand, when using fragile adhesives, the effect of the CZM shape can be disregarded without compromising the accuracy of the strength predictions too much [30].

There are many different parameters for strength introduction of the adhesive joints. One of the most important properties of this kind of joint is its resistance of debonding under mechanical load. Like delamination of composite laminates, it can be characterized by the interlaminar fracture toughness.

It is known that for the ideally brittle components of adhesive joints the Griffith theory can be used for prediction of strength of an adhesive joint with partial debonding. Only one parameter, the interlaminar fracture toughness, defines the condition of delamination propagation.

However, usually one-parametric estimation of crack (delamination) growth is not sufficient for different types of material and configuration of the damaged structural component. In these cases, the additional parameters and models are needed for adequate description of a damaged component fracture. Nowadays the most popular is the cohesive zone model, that was founded in and improved in many further research [7].

Yielding at the end of a slit in a sheet has been studied and the relationship between the degree of yield of the plastic and the applied external load is obtained. To test this relationship, the panels with internal and edge gaps were loaded and the lengths of the plastic zones were measured [101].

Interest in the problem of fragile fractures, and in particular crack theory, has grown significantly in connection with various technical applications. Many studies have been carried out, extending the classical gap concepts and analysis methods to important points. The qualitative features of the crack problems discovered in these studies, which are related to their specific nonlinearity, make crack theory different from all problems in terms of elasticity theory.

This model allows to describe small crack growth and is used also for describing the stable crack propagation (R-curve). The concept of the R-curve was developed for crack stable propagation in plane stress. Further development and applications of the CZM and the concept of the R-curve for layered composites and adhesive joints are given in [86, 100–102] and many other publications [7].

To study the separation of the viscoplastic block from the rigid substrate, a cohesive zone type interface model was used, taking full account of the limited geometry changes. Size considerations introduced a characteristic length in the wording. The specific limit value problem analyzed is the plane deformation stress with superficial hydrostatic stress. For an ideal interface, if the maximum thrust that the viscoplastic block can support is greater than the interface strength, the separation takes place mainly in the tensile mode. If this maximum traction is less than the interface strength, the predominant shear delamination begins at the edge of the block. Gaps in the shape of the unrelated part of the interface are taken into account [86, 101–104].

The excitation of crack growth and the subsequent resistance has been calculated for an elastic-plastic material with an idealized traction division law specified in the plane of the crack to characterize the fracture process. The results then applied three times: to predict the strength when the fracture process does not form and to unite, to predict the importance of plasticity for interface strength-like materials bonded together, and to illuminate the role of plasticity in improving the stiffness in the two-phase solids. The applicability regime of this model for ductile fracture due to void growth and fusion when multiple voids interact in the fracture process zone complements the applicability regime of models describing the interaction between a single void and the crack end [86, 102–108].

There has been a lot of research about the dependence of R-curves on the geometry of the DCB specimens with respect to the unidirectional epoxy-carbon composite. During crack propagation, expanded bridge formation is observed and R-curves for three different thicknesses obtained. A simple numerical procedure was proposed to model the crack propagation, taking into account linear and nonlinear transition laws. The results were compared with various approximate formulas for energy release rate calculations and a suitable formula was found. By measuring the deviation at two points of the DCB specimen and the applied load as a function of crack propagation, the exact law of bridge formation of the investigated composite was found. These data and the proposed numerical procedure allowed researchers to predict the R curve for any DCB specimen thickness [6, 7, 86].

A large nonlinear zone is formed during the fracture of a polyurethane adhesive bonded to a steel adhesive. The zone of the fracture process is later characterized by the law of traction separation, the so-called cohesive law. The law of cohesion was determined experimentally using specimens of double-console beam sandwiches filled with pure bending moment in an integrated approach to *J*. It was found that the uniform form of the law is very nonlinear. Cohesion tension increased with increasing separation, peaked and then decreased with increasing opening. The effect of load level and thickness of the adhesive layer on the cohesion law was later studied. An excellent agreement was reached between the measured fasteners of the connected panels, which have a central cut, and the strength predictions based on the uniform parameters of the law [102].

The general approach to determining cohesion laws is described by measuring the end aperture of the cohesion zone of J-integral and double cantilever specimens with pure bending moments. Two case stories have been looked at: degradation of adhesive compounds and unidirectional carbon fiber / epoxy composite decomposition. The degrees of strength of the measured compressed panels of the glued joints, which have a central cut, corresponded very well to the predicted parameters determined on the specimens. It has been found that the form of the cohesion law predicted by the micromechanical model fits well with the macroscopic cohesion law determined by the J-integral [103].

Analytical solutions for beam specimens used in mechanical tests of fractures of composite materials and bonded joints generally use a beam on a resilient base model, assuming that the beam on the resilient base has unlimited linear resilience in the region in front of the end of the crack. Therefore, such an approach requires a model of elasticity and stiffness, but it is not necessary to assume a critical $\sigma\,max$ value for the crack tip region. Thus, they give one fracture

parameter, namely the fracture energy G_c. However, the corresponding value of σ *max* obtained, of course, can be calculated from the knowledge of the value of G_c. On the other hand, fracture models and criteria have been developed based on the approach that there are two parameters to describe the fracture process: namely, G_c and σ *max*. Here σ *max* is considered critical in limiting the maximum stress value in the fault area before the crack and is often assumed to have some physical significance. A general representation of the two-parameter failure criterion approach is for the CZM. The main objectives have been to investigate whether the value of σ max has a unique value for a given problem and whether this parameter can be assigned a physical significance. In some cases, both FEA and analytical methods are used to provide a useful comparison of two different approaches and two different methods of analysis [104].

Cohesion crack model, one of the basic models used so far to describe the fracture of concrete and other easily perceptible materials. The evidence presented and the discussion are based on considering the cohesion gap model as a constitutional assumption and not as an ad hoc model for behavior before the existing gap. Topics covered include fracture of loose specimens, mixed fracture, diffuse crack, anomalous stress-strain curves, size effect and asymptotic analysis, as well as strength of structural elements with notches [105].

Problem of adhesively bonded joints with ductile adhesive materials is investigated much less [106, 107].

Developed and implemented interface elements for the analysis of finite elements of adhesive compounds within the framework of interface element modeling (CZM) methods and introduced a new law of traction separation, which reflects the constitution of ductile adhesive material. The proposed law is based on the embedded process area approach and is designed to address the mixed mode load and fracture of glued joints. This law is first used to describe pure Mode I (opening) and pure Mode II (sliding) loads and fractures, and then integrated into the developed mixed-mode model to account for the dependence of the individual pure mode. laws. The increasing part of the law of traction is characterized by an exponential function, while the softening part is characterized by a linear decrease. The forecast of the onset of the fault is determined by the criterion of the nominal square voltage, while the propagation of the fault is determined by the linear energy criterion. Experimental results from a single steel and steel belt connection configuration have been used to validate the proposed law and mixed mode model. Comparisons from finite element analysis with the already known trapezoidal law and the PRP (Park – Paulino – Roesler) model are also provided (Figure 5.3). The proposed law adequately reflects the elastoplastic behavior of the tested adhesive compounds in terms of their overall reaction. In addition, the strength of the tested compounds is predicted with great accuracy [106].
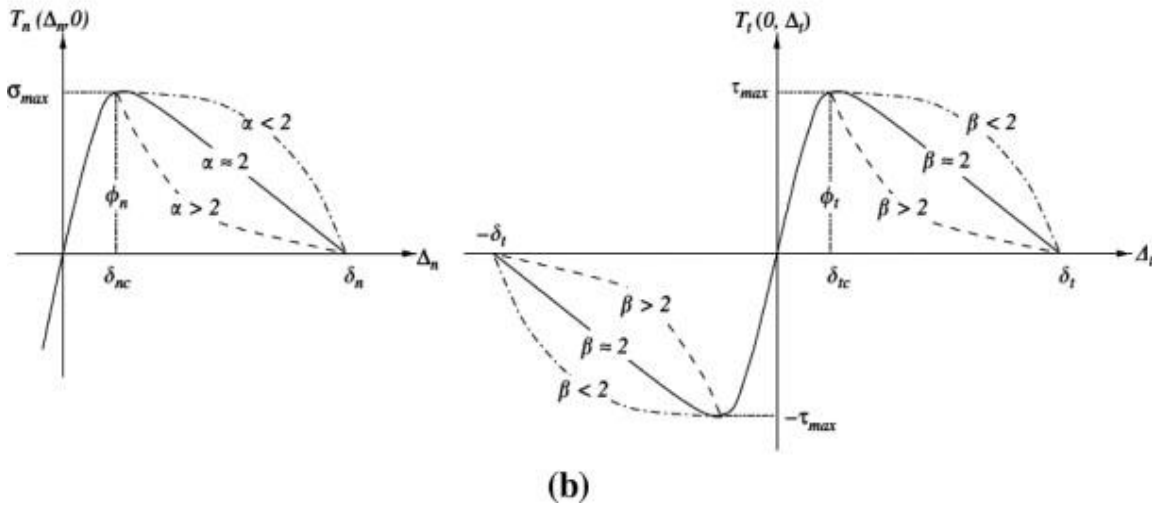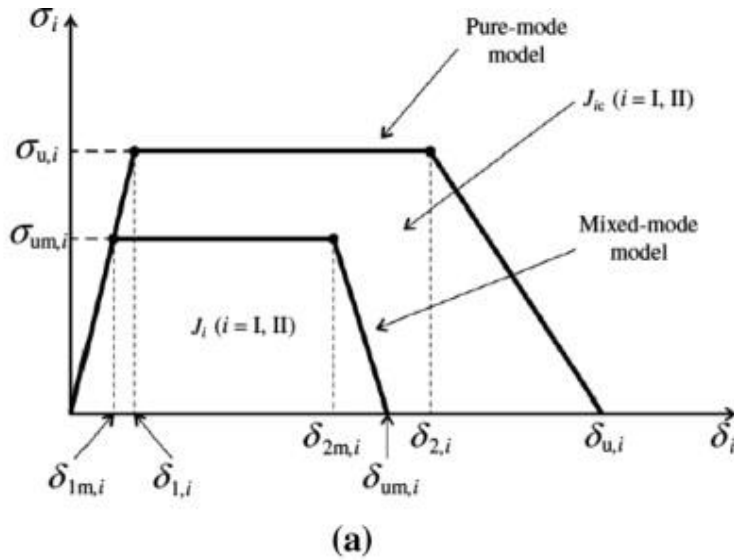
Figure 5.3. Trapezoidal laws (a) and Park–Paulino–Roesler laws (b) [106].

To describe the elastoplastic load of the adhesive layer and the fracture reaction under mode I and II conditions, a recently developed mixed mode law is used. This model is implemented in the interface elements used to replace the usual continuity elements to model the gluing area. The potential of the proposed model for analysis and design purposes is demonstrated using experimentally tested CFRP and steel adhesive compound simulations taken from the literature. In addition, a numerical parametric study has been conducted in an effort to investigate the effect of overlap length and adhesive thickness on joint strength [7, 107].

The elongation of the crack at the end of the crack is governed by an additional condition. As a result, the problem of the "fine" structure of the crack tip is considered. The general additional condition of any continuity model is obtained using the law of energy saving and the physical concept of fracture energy. The dynamic cracks in elastic rigid parts and quasi-static cracks in elastic and rigid plastics, as well as the problem of crack expansion when dispersing viscoelastic bodies are briefly considered. The general approach is also applied to cases of fatigue and "fluctuation" cracks [69].

In this research the effect of plasticity of an adhesive to interlaminar fracture toughness of adhesive bond of thin-walled layered composite is investigated. The characteristics of failure of low toughness adhesive layer were obtained using the DCB specimen [7].

5.1 Experimental Study

Test setup, specimen material and sizes

The glass/epoxy laminate reinforced by glass fabric was used for preparation of the test specimens. The 25x125 mm strips were cut from the GFRP 2 mm thick plate and they were used as the adherents of adhesive joint manufacturing in the form of the DCB specimen (Figure 5.4) with initial deboning 55-60 mm. The adherents were connected by the two-component epoxy paste EPON 828/EPICURE 3140 and were cured at room temperature. The curing time for specimens of group 1 was 1 day but for group 2 it was more than 7 days. The thickness of the adhesive layer was not more than 0.5 mm. Operating forces are applied to the specimen by means of the loading blocks [7].
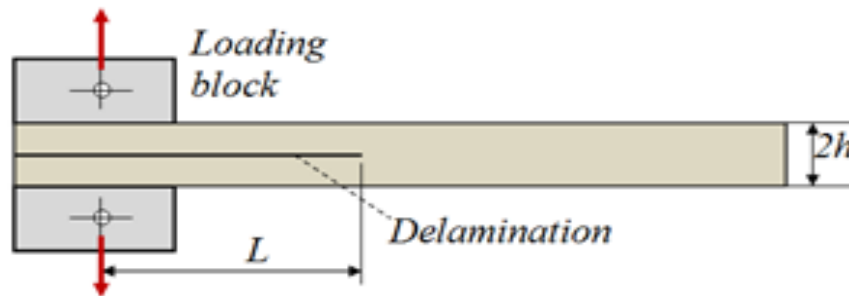
Figure 5.4. Schematic view of the DCB specimen [7].

During the test with the controlled displacement of 3 mm/min rate the data force /extension (load points relative displacement) was digitally stored permanently with periodic stops for accurate fixing of the current size of delamination, further unloading and determination of residual extension of specimen. Delamination continues growth during loading was observed without the unstable increment of delamination front in contrast, for example, with the high-strength laminate. The significant residual extension after unloading also was indicated [7].

Procedure of testing and primary test data

The quasi-static tests of DCB specimens, according to the standard, were carried out on an Instron 8800 hydraulic testing machine with controlled displacements at the constant rate of movable clamp 3 mm/min. To increase the accuracy of measurement of small values of the load, the S2M meter of small loads (HBM Test and Measurement), with the upper measurement limit of 1 kN, was connected in series in the loading circuit as the basic force sensor [7].

The test procedure generally corresponds to the ASTM Standard method is intended for use only with composite materials consisting of unidirectional carbon fiber and glass fiber tape laminates with fragile and durable single-phase polymer matrices. This limited scope reflects the experience gained from the survey. This test method may be useful for other types and

categories of composite materials; however, some disorders are noted [19]. There are some deviations caused by specific features of elastic-plastic deformation during the test of the DCB specimen of group 1 [7].

The standard provides for a continuous loading of the specimen at a constant rate moving jaws until a final increment of delamination. A closing step test is supposed to discharge with the same speed as the loading rate. In the present experiment, the step-to-step loading/unloading after each 5-7 mm increment of the delamination length was realized. Such modification of the test procedure provides an adequate definition of the elastic compliance on the linear portion of the force/extension record, as well as a more accurate measurement of the initial crack length at the beginning of each loading step [7].

The curves of loading are shown in Figures 5.5 and 5.6 for a specimen of group 1 and group 2 respectively. In the legend of the plot on the right side the delamination initial length before each next step of loading is shown [7].
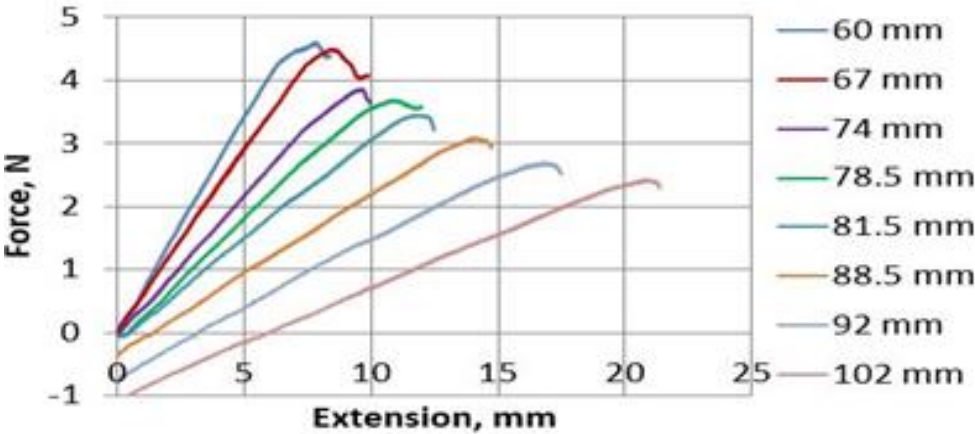
Figure 5.5. Force/extension function for a specimen of group 1 [7].
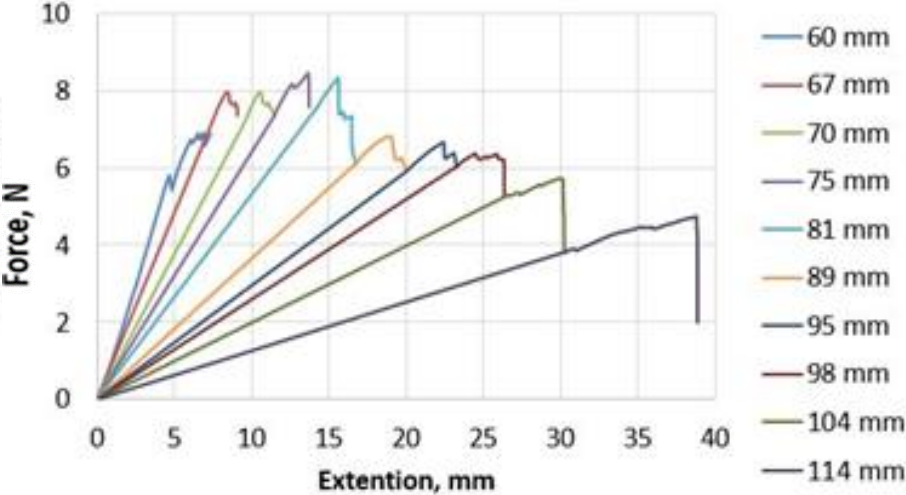
Figure 5.6. Force/extension function for a specimen of group 2 [7].

5.2 Test data processing, analysis and discussion

General comparison of test results of two groups of specimens

Common for both groups is a linear relationship between the extension and the load before the start of the delamination growth. However, there is a significant difference in the behavior of specimens under stress. The delamination of a specimen of group 1 grows smoothly without sudden jumps of load. In contrast, in the specimen of the group 2 the jump-like growth of delamination and sharp drop of load is observed. The linear dependence of load/extension remains up to a jump [7].

Another feature of behavior of the specimen of group 1 is also observed: if there is large increment of delamination, the compressive load is needed for complete closure of the specimen unloading (in Figure 5.5). Obviously, this behavior is caused by plastic deformation of the adhesive layer and the roughness of surface delamination due to residual strain [7].

In general, it can be concluded that the adhesive layer in the specimens of group 1 have pronounced elastoplastic properties. A specimen of the group 2 is characterized by an elastic behavior and brittle fracture of the adhesive layer (Figure 5.6) [7].

Interlaminar fracture toughness

The standard normally is used in practice of the determination of the Mode I interlaminar fracture toughness of a brittle adhesive joint. Here this standard is used formally also for the elastoplastic adhesive joint. Three options of processing were used: MBT, CC and MCC. It is known that the MBT method assumes use of the effective length of delamination to correct DCB arms rotation at the delamination front. In Figure 5.7 the cubic root of a DCB elastic compliance is presented as a function of delamination length for the specimen of group 1. So, the elastic compliance of the DCB specimen can be introduced as follows in equation (5.1) [7]:

$$C = \frac{\delta}{P} = (\alpha L + \beta)^3, \qquad (5.1)$$

where P is applied load, δ is load point extension, and are regression coefficients (in Figure 5.7) [7].
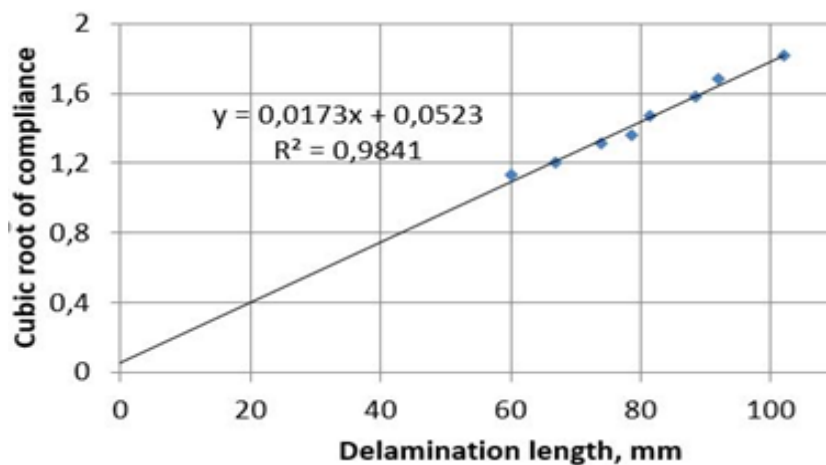
Figure 5.7. Function of effective length of delamination [7].

The DCB elastic compliance was obtained as the slope of the linear part of the experimental function extension/ delamination length (Figure 5.7). It shows that there is close correlation of these two variables [7].

The exponential regression equation (Figure 5.8) was used for determining the effective length of delamination during the linear portion of a specimen loading, and to estimate the actual length of delamination at its growth [7].

$$G_{Ic} = 51{,}23e^{-0{,}009L}$$
$$R^2 = 0{,}6658$$
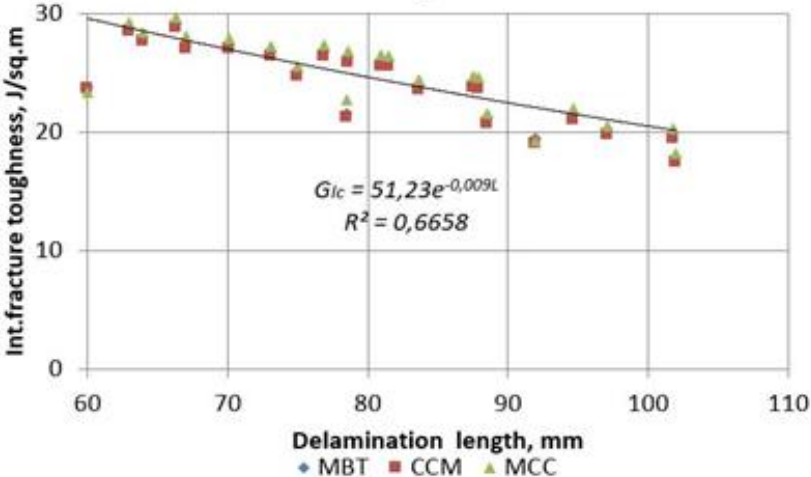
Figure 5.8. Interlaminar fracture toughness as a function of delamination length of the group 1 specimen [7].

In Figure 5.8 the results of test data processing are presented for specimens of group 1. Each point of this graph corresponds to the maximum of the experimental curve load/extension of the corresponding step of test. The length of delamination is estimated using the mentioned regression equation [98].

In Figure 5.9 the outcome of test data processing is presented for specimens of group 2. It is seen that for the specimens of group 2 beginning since the 70 mm delamination length G_{Ic} approximately is constant about 150 J/m^2.
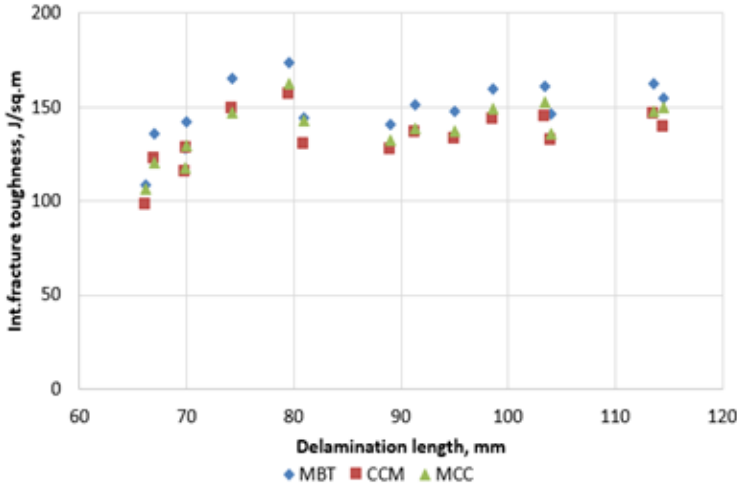
Figure 5.9. Interlaminar fracture toughness as a function of delamination length of the group 2 specimen [7].

Only for the initial length of delamination the G_{Ic} is smaller. Usually, this effect is called an R-curve [7].

For the specimens of group 1, this parameter is significantly lower, and the monotonic decrease is observed with the increase of delamination length [7].

Analysis of unsteady growth of delamination

In Figures 5.8 and 5.9 the stress energy release rate is defined by standard procedure for the steady state at which the force is maximal. But because test loading is process with extension non-zero rate, there is some specific evolution both the force and the length of delamination [7].

After some simple operations, the rate of delamination growth can be expressed in equation (5.2):

$$\frac{dL}{dt} = \frac{1 - C\frac{dP}{d\delta}d\delta}{3P\frac{dC}{dL}dt}. \tag{5.2}$$

The $P(\delta)$ is the main outcome of the test of the DCB specimen. Nonlinear portion measured function (growth of delamination) $P(\delta)$ were approximated by fifth-degree polynomial for determination of a derivative $dP/d\delta$. The derivative dC/dL is defined by equation (5.1). So, the rate of delamination growth was calculated as a time function and integrating equation (5.2) gives current delamination length [7].

As a result, the strain energy release rate can be also calculated for any time moment. The MBT approach gives equation (5.3):

$$G_I = \frac{3P\delta}{2H(L+\Delta)}, \tag{5.3}$$

where $\Delta = \beta/\alpha$ is the correcting member of delamination length [7].

In Figure 5.10 the evolution of load and rate of delamination growth is presented for 67 mm initial length of crack. Note that because the rate of extension is constant, then the evolution of mentioned parameters in time is similar [7].
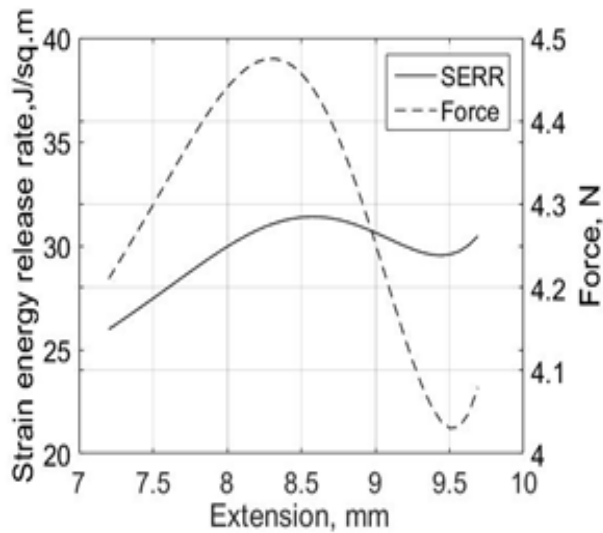
Figure 5.10. Evolution of load and rate of delamination for its initial length 67 mm [7].

It is seen that the rate of delamination increases a few increases before load maximum, but its peak is reached significantly later. In Figure 5.11 comparison of two processes (force and strain energy release rate) evolution is presented for the same step of loading. It is seen that maximum of the strain energy release rate corresponds the downward part of the $P(\delta)$ function [7].
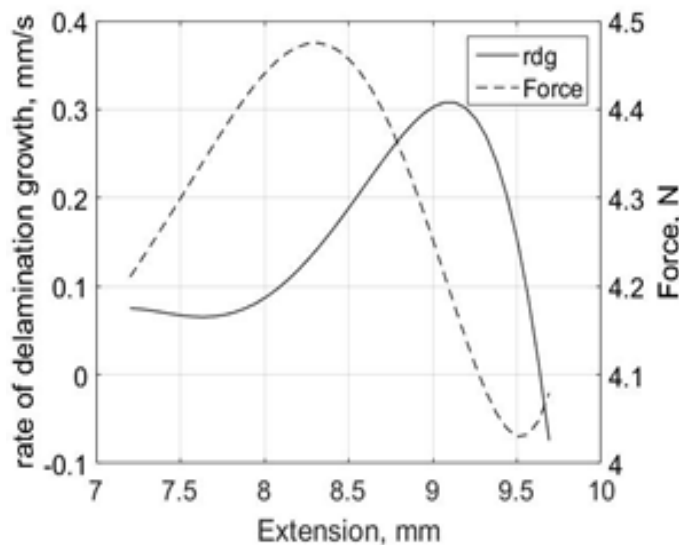
Figure 5.11. Evolution of load and rate of delamination for its initial length 67 mm [7].

Integrating of equation (5.2) was done using MATLAB code *ode45*. As a result, the evolution of delamination was predicted for unsteady growth at all steps of loading. Finally, the resistance curve can be obtained. In Figure 5.12 the nonlinear parts of function $G_I(L)$ for each step of loading is introduced. It is seen that for all steps of the test there is an unsteady process of delamination growth: stable increasing of the strain energy release rate, its maximum, and next decreasing (sometime to the minimum) [7].

The increment of delamination length to maximum of the strain energy release rate for all steps of loading is presented in Figure 5.13 [7].
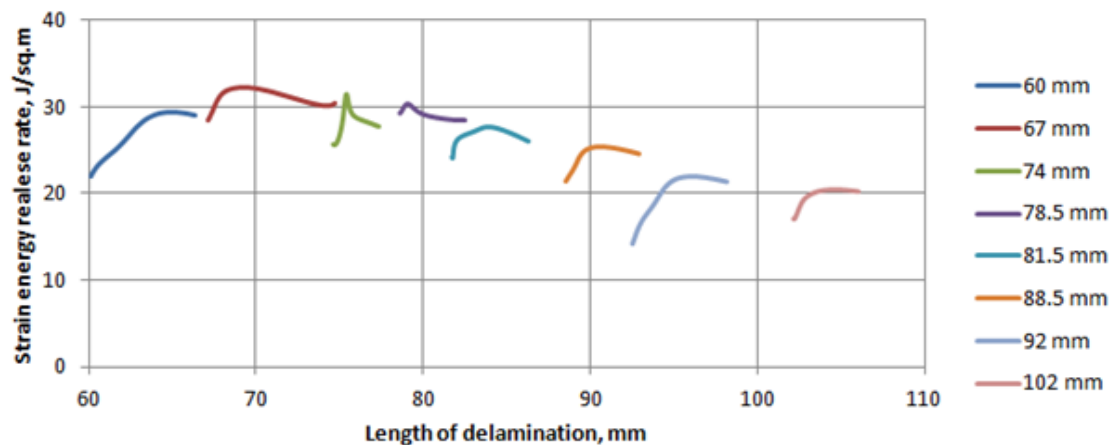
Figure 5.12. The strain energy release rate as function of delamination incement at different initial length of delamination [7].

The approximate evaluation of the critical parameters of interlaminar fracture

Results of this research show that at elastic-plastic behavior of adhesive material there is specific continuous smooth growth of delamination without jump-like propagation that is observed for brittle material. Formally, the interlaminar fracture toughness can be evaluated also at the elastic-plastic behavior of the adhesive material, if to use the maximum load and corresponding extension or length of delamination. As easy see in Figure 5.12 the maximum strain energy release rate at each step of loading only a few more than defined by Standard procedure (Figure 5.8). But from other hand, in both cases the critical strain energy release rate can be dependent from delamination length [7].

It could be assumed that this effect is defined by bending moment/shear force relation in the cross-section of the DCB arm at the front of delamination. For the DCB specimen this relation is equal to a length of delamination.
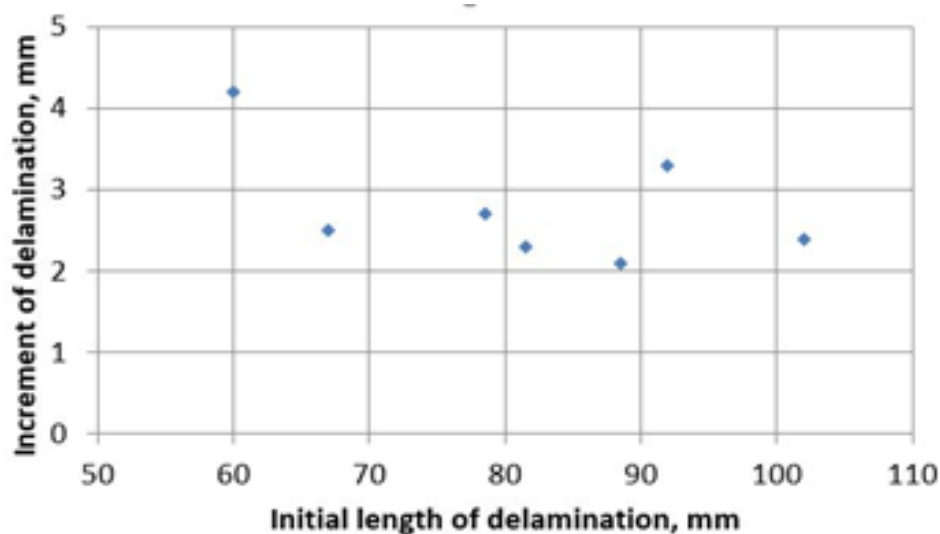
Figure 5.13. The increment of delamination length as a function of its initial length [7].

Therefore, adhesive joint strength at a given initial length of delamination is determined by the maximum strain energy release rate. But since this time a stable growth of the delamination is preceded, the calculation should take into account the actual length of the delamination. It means that adhesive joint strength of some structure should be defined by the following equation (5.4) [7]:

$$G_I = (l, l_0, m) = G_{Ic}(L, L_0), \qquad (5.4)$$

where l_0 is initial length of delamination of analysed structure (initial value), its critical value, but $L_0 = m$ and $L = L_0 + \Delta L$ are initial and critical delamination lengths of DCB respectively [7].

5.3 Summary

Adhesive materials based on epoxy resins, most often, are brittle. To evaluate the interlaminar strength of these type of adhesive joints is required to know a single constant – interlaminar fracture toughness. If the adhesive material is elastoplastic, then the process of progressive delamination is much more complicated. In the present study, the effect of plasticity on its interlaminar strength was investigated. A comparative analysis of the test data was carried out for two groups of specimens from the same two-component adhesive material. For one of the groups the curing time was reduced in comparison with the standard. As a result, it became possible to assess the influence of technological faults to the strength of the adhesive joint. However, the main purpose of the analysis was to examine the patterns of delamination growth caused by plasticity of the adhesive material.

Plasticity effect has been studied in the DCB specimen for Mode 1 interlaminar fracture. The main conclusions about the features of the delamination process of the elastoplastic adhesive layer are presented below.

Finally, it should be noted that the proposed means of fracture parameters estimation is applicable only to the DCB specimen and the Mode 1 of its loading. For practical application to other configurations of adhesive joints the specifics of the delamination progress should be investigated additionally [7].

CONCLUSIONS

Above presented results of research show that global aims of doctoral thesis are completely achieved. All planning analytical and experimental studies are performed:

1. Literature analysis of composite materials, testing methods and standards, as well as research of tests performed so far showed that physic-chemical, mechanical, structural, and other properties of layered composites are defined as their advantages, as also specific scientific, technique, technological and operation problems.

2. Analysis of the effect of DCB specimen non-linearity to the interlaminar fracture toughness measurement is performed and shows that existing Standard methods of DCB specimen use for this purpose is approximate and there are a number of restrictions for use of these methods.

3. Development of theoretical model of the interlaminar fracture toughness for mixed I/II mode, based on the nonlinear theory of flexible plates.

4. Development of mathematical model of non-linear DCB specimens for the interlaminar fracture toughness measurement is achieved using nonlinear theory of flexible beam bending.

5. Experimental study of the interlaminar fracture toughness measurement of layered composite of high flexibility using the DCB specimen: material selection, specimen designing and manufacturing technology, procedure of testing is performed.

6. Algorithm and MATLAB software of test results processing using non-linear DCB specimen was created.

7. Results confirm the suitability of the nonlinear model of DCB specimen for determination of the G_{Ic} quantity of a composite within the limits of applicability of the standard test methods based on the Euler theory of bending of beams [8].

8. A satisfactory result can be obtained by using an equation that implies correction of the formal expression of G_{Ic} according to the linear model by its multiplication by the standard correction factor [8].

9. To test highly flexible DCB specimens, the most reliable estimates of the parameter G_{Ic} can be obtained by using the accurate nonlinear model [8].

10. Experimental study: effect of plasticity to process interlaminar delamination propagation in the layered composite of the elastic-plastic material of a matrix is performed.

11. Test results processing and main features extraction on the effect of plasticity to the interlaminar fracture toughness of layered composites showed that:

    11.1. The delamination of a specimen grows smoothly, without sudden jumps of size and load (in contrast the jump-like growth of delamination for brittle adhesive) [7].

    11.2. The compressive load is needed for complete closure of the specimen at unloading caused by plastic deformation of the adhesive layer and the roughness of surface of delamination due to residual strain [7].

    11.3. Formally defined, the mode-I interlaminar fracture toughness is not a material constant and monotonically decreases as a function of delamination length [7].

    11.4. At constant extension rate the relationships between strain energy release rate, load and rate of delamination growth in the elastoplastic stage of loading are complex and mutually disproportionate [7].

    11.5. A possible means for an approximate evaluation of the critical parameters of interlaminar fracture of the DCB specimen involves the use of a regression between the maximum of strain energy release rate and the size of delamination, corrected for its increment in a stable stage of growth [7].

REFERENCES

1) Guoqing Wu, Qingqing Zhang, Xue Yang, Zheng Huang, Wei Sha. Effects of particle/matrix interface and strengthening mechanisms on the mechanical properties of metal matrix composites. *Composite Interfaces*. 2013, vol.21, no.5, pp.415-429. Available from: doi: 10.1080/15685543.2014.872914

2) Sinmazçelik T. Avcu E. Bora, MO. Çoban O. A review: Fibre metal laminates, background, bonding types and applied test methods. *Materials and Design*. 2011, vol.32, no.7 pp.3671-3685. Available from: doi: 10.1016/j.matdes.2011.03.011

3) Shehzad, Khurram. Xu, Yang. Gao, Chao. Duan, Xiangfeng. Three-dimensional macro-structures of two-dimensional nanomaterials. *Chemical Society Reviews*. 2016 no.20, pp.5541-5588. Available from: doi: 10.1039/c6cs00218h

4) Keten Sinan. Xu, Zhiping. Ihle, Britni. Buehler, Markus J. Nanoconfinement controls stiffness, strength and mechanical toughness of β-sheet crystals in silk. *Nature Materials*. 2010, vol.9, pp.359- 367. Available from: doi: 10.1038/nmat2704

5) Kim Hyoung Seop. On the rule of mixtures for the hardness of particle reinforced composites. *Materials Science and Engineering*. 2000, vol.289, no.1-2, pp.30-33. Available from: doi: 10.1016/S0921-5093(00)00909-6

6) Glessner A.L., Takemori M.T., Vallance M.A., Gifford S.K. Mode I Interlaminar Fracture Toughness of Unidirectional Carbon-Fiber Composites Using a Novel Wedge-Driven Delamination Design" in: Composites Materials: Fatigue and Fracture, 2nd Volume, Lagace P.A., editor, American Society for Testing and Materials, ASTM. 1989, STP 1012:181-200.

7) Pavelko V., Lapsa K., Pavlovskis P. The Effect of Plasticity to Interlaminar Fracture Toughness of Adhesive Bond of Composite. IOP Conference Series: *Materials Science and Engineering*. 2017, vol.251: 3rd International Conference on Innovative Materials, Structures and Technologies (IMST 2017), 012081.-012081.lpp. ISSN 1757-8981. e-ISSN 1757-899X. Available from: doi:10.1088/1757-899X/251/1/012081

8) Pavelko V., Lapsa K., Pavlovskis P. Determination of the Mode I Interlaminar Fracture Toughness by using a Nonlinear Double-Cantilever Beam Specimen. *Mechanics of Composite Materials*. 2016, vol.52, no.3, pp.347.–358. Available from: doi: 10.1007/s11029-016-9587-y

9) M. A. Mcevoy, N. Correll. Materials that couple sensing, actuation, computation and communication. *Science*. 2015, vol.347, no.6228. Available from: doi: 10.1126/science.1261689

10) William D. Jr. Callister. Materials Science and Engineering: An Introduction, 7th Edition. 2006.

11) Wu Xiangguo. Yang Jing. Mpalla Issa B. Preliminary design and structural responses of typical hybrid wind tower made of ultra high performance cementitious composites. *Structural Engineering and Mechanics*. 2013, vol.48, pp.791-807. Available from: doi: 10.12989/sem.2013.48.6.791

12) Aghdam, M.M. Morsali, S.R. Damage initiation and collapse behavior of unidirectional metal matrix composites at elevated temperatures. *Computational Materials Science*. 2013, vol.79, pp.402-407. Available from: doi: 10.1016/j.commatsci.2013.06.024

13) Matzkanin, George A. Yolken, H. Thomas. Techniques for the Nondestructive Evaluation of Polymer Matrix Composites. The AMMTIAC Quarterly. 2008, vol.2, no.4, pp.3-7.

14) Davies P. Blackman B.R.K., Brunner A.J. Standard Test Methods for Delamination Resistance of Composite Materials: Current Status. *Applied Composite Materials 5.* 1998, pp.345-364.

15) Tay T.E. Characterization and analysis of delamination fracture in composites – a review of developments from 1990 to 2001. *Applied Mechanics Reviews*. 2003, vol.56, no.1, pp.1-23. Available from: doi: 10.1115/1.1504848

16) J. M. Hodginson. Mechanical Testing Of Advanced Fibre Composites. Cambridge, England. 2000, pp.170-210.

17) Chen B.Y., Tay T.E., Baiz P.M., Pinho S.T. Numerical analysis of size effects on open-hole tensile composite laminates. *Composites Part A: Applied Science & Manufacturing*. 2013, vol.47, pp.52-62. Available from: doi: 10.1016/j.compositesa.2012.12.001

18) Martin R.H. Incorporating interlaminar fracture mechanics into design. *Journal of Materials: Design and Applications*. 2000, vol.214, no.2, pp.91-97. Available from: doi: 10.1177/146442070021400204

19) Standard Test Method for Mode I Interlaminar Fracture Toughness of Unidirectional FibreReinforced Polymer Matrix Composites, D 5528, *American Society for Testing and Materials International*. ASTM. 1994.

20) Hiroshi Yoshihara Holzforschung. Simple estimation of critical stress intensity factors of wood by tests with double cantilever beam and three-point end-notched flexure. *De Gruyter*. 2007, vol.61, pp.182–189. Available from: doi: 10.1515/HF.2007.032

21) A.j. Brunner, B.R.K. Blackman, P. Davies. A status report on delamination resistance testing of polymer-matrix composites. *Engineering Fracture Mechanics*. 2008, vol.75, no.9, pp.2779-2794. Available from: doi: 10.1016/j.engfracmech.2007.03.012

22) Fischer SKF., Jäschke P., Frauenhofer M., Kracht D., Dilger K. Laser surface Pre-treatment of CFRP for adhesive bonding in consideration of the absorption behaviour. *The Journal of Adhesion*. 2012, vol.88, no.4-6, pp.350-363. Available from: doi: 10.1080/00218464.2012.660042

23) Banea MD., da Silva LFM., Campilho RDSG., Sato C. Smart adhesive joints: an overview of recent developments. *The Journal of Adhesion*. 2014, vol.90, no.1, pp.16-40. Available from: doi: 10.1080/00218464.2013.785916

24) Katnam KB., da Silva LFM., Young TM. Bonded repair of composite aircraft structures: a review of scientific challenges and opportunities. *Progress in Aerospace Sciences*. 2013, vol.61, pp.26-42. Available from: doi: 10.1016/j.paerosci.2013.03.003

25) S. Budhea, M.D. Banea, S. de Barrosa, da Silva LFM. An updated review of adhesively bonded joints in composite materials. *International Journal of Adhesion & Adhesives*. 2017, vol.72, pp.30-42. Available from: doi: 10.1016/j.ijadhadh.2016.10.010 JAAD1914

26) Abdel Wahab MM. Fatigue in adhesively bonded joints: a review. *ISRN Material Sciences*. 2012, vol.3, pp.1-25.

27) J. Andersons, M. Konig. Dependence of fracture toughness of composite laminates on interface ply orientations and delamination growth direction. *Composite Science and Technology*. 2004, vol.64, no.13-14, pp.2139-2152. Available from: doi: 10.1016/j.compscitech.2004.03.007

28) Rosa MM. Paiva, Marques EAS., da Silva LFM., António CAC., Arán-Ais F. Adhesives in the footwear industry. *Journal of Materials: Design and Applications*. 2015, pp.1-18. Available from: doi: 10.1177/1464420715602441

29) Barbosa AQ., da Silva LFM., Banea MD., Öchsner A. Methods to increase the toughness of structural adhesives with micro particles: an overview with focus on cork

particles. *Materialwissenschaft und Werkstofftechnik*. 2016, vol.47, pp.307–325. Available from: doi: 10.1002/mawe.201600498

30) da Silva LFM., das Neves PJC., Adams RD., Spelt JK. Analytical models of adhesively bonded joints—Part I: literature survey. *International Journal of Adhesion and Adhesives*. 2009, vol.29, no.3, pp.319-330. Available from: doi: 10.1016/j.ijadhadh.2008.06.005

31) Roger A. Sauer. A survey of computational models for adhesion. *The Journal of Adhesion*. 2016, vol.92, no.2, pp.81-120. Available from: doi: 10.1080/00218464.2014.1003210

32) Meneghetti G., Quaresimin M., Ricotta M. Influence of the interface ply orientation on the fatigue behaviour of bonded joints in composite materials. *International Journal of Fatigue*. 2010, vol.32, no.1, pp.82-93. Available from: doi: 10.1016/j.ijfatigue.2009.02.008

33) Kanerva M., Saarela O. The peel ply surface treatment for adhesive bonding of composites: a review. *International Journal of Adhesion and Adhesives*. 2013, vol.43, pp.60–69. Available from: doi: 10.1016/j.ijadhadh.2013.01.014

34) Mohan J., Ivanković A., Murphy N. Mode I fracture toughness of co-cured and secondary bonded composite joints. *International Journal of Adhesion and Adhesives*. 2014, vol.52, pp.13–22. Available from: doi: 10.1016/j.ijadhadh.2014.02.008

35) Mohan J., Ivanković A., Murphy N. Mixed-mode fracture toughness of co-cured and secondary bonded composite joints. *Engineering Fracture Mechanics*. 2015, vol.134, pp.148–167. Available from: doi: 10.1016/j.engfracmech.2014.12.005

36) Mohan J., Ivanković A., Murphy N. Effect of prepreg storage humidity on the mixed-mode fracture toughness of a co-cured composite joint. *Composites Part A: Applied Science and Manufacturing*. 2013, vol.45, pp.23–34. Available from: doi: 10.1016/j.compositesa.2012.09.010

37) Khoshravan M., Mehrabadi FA. Fracture analysis in adhesive composite material/ aluminum joints under mode-I loading; experimental and numerical approaches. *International Journal of Adhesion and Adhesives*. 2012, vol.39, pp.8–14. Available from: doi: 10.1016/j.ijadhadh.2012.06.005

38) Kanerva M., Sarlin E., Hoikkanen M., Rämö K., Saarela O., Vuorinen J.. Interface modification of glass fibre–polyester composite–composite joints using peel plies. *International Journal of Adhesion and Adhesives*. 2015, vol.59, pp.40–52. Available from: doi: 10.1016/j.ijadhadh.2015.01.016

39) Budhe S. Effect of pre-bond moisture on the static and fatigue behavior of bonded joints between CFRP laminates for structure repairs. Spain: University of Girona. 2014.

40) da Silva LFM., Ferreira NAMJ., Richter-Trummer V., Marques EAS. Effect of grooves on the strength of adhesively bonded joints. *International Journal of Adhesion and Adhesives*. 2010, vol.30, no.8, pp.735–743. Available from: doi: 10.1016/j.ijadhadh.2010.07.005

41) Dawood M., Rizkalla S. Environmental durability of a CFRP system for strengthening steel structures. *Construction and Building Materials*. 2010, vol.24, no.9, pp.1682–1689. Available from: doi: 10.1016/j.conbuildmat.2010.02.023

42) Heshmati M., Haghani R., Al-Emrani M. Environmental durability of adhesively bonded FRP/steel joints in civil engineering applications: state of the art. *Composites Part B: Engineering*. 2015, vol.81, pp.259–275. Available from: doi: 10.1016/j.compositesb.2015.07.014

43) Azari MPS., Spelt JK. Effect of Surface Roughness on the Performance of Adhesive Joints Under Static and Cyclic Loading. *The Journal of Adhesion*. 2010, vol.86, no.7, pp.742–764. Available from: doi: 10.1080/00218464.2010.482430

44) Boutar Y., Naimi S., Mezlini S., da Silva LFM., Hamdaoui M., Ali MBS. Effect of adhesive thickness and surface roughness on the shear strength of aluminium one component polyurethane adhesive single-lap joints for automotive applications. *Journal of Adhesion Science and Technology*. 2016, vol.30, no.17, pp.1913–1929. Available from: doi: 10.1080/01694243.2016.1170588

45) da Silva LFM., de Magalhaes FACRG., Chaves FJP., de Moura MFSF. Mode II fracture toughness of a brittle and a ductile adhesive as a function of the adhesive thickness. *The Journal of Adhesion*. 2010, vol.86, no.9, pp.889–903. Available from: doi: 10.1080/00218464.2010.506155

46) Banea MD., da Silva LFM. Mechanical characterization of flexible adhesives. *The Journal of Adhesion*. 2009, vol.85, no.4, pp.261-285. Available from: doi: 10.1080/00218460902881808

47) Banea MD., da Silva LFM. Static and fatigue behavior of room temperature vulcanising silicone adhesives for high temperature aerospace applications. *Materialwissenschaft und Werkstofftechnik*. 2010, vol.41, no.5, pp.325–335. Available from: doi: 10.1002/mawe.201000605

48) Banea MD., da Silva LFM., Campilho RDSG. The effect of adhesive thickness on the mechanical behavior of a structural polyurethane adhesive. *The Journal of Adhesion.* 2015, vol.91, no.5, pp.331–346. Available from: doi: 10.1080/00218464.2014.903802

49) S. Hashemi, A. J. Kinloch, J. G. Williams. Corrections needed in double-cantilever beam tests for assessing the interlaminar failure of fibre-composites. *Journal of Materials Science Letters.* 1989, vol.8, pp.125-129.

50) Marzi S., Biel A., Stigh U. On experimental methods to investigate the effect of layer thickness on the fracture behavior of adhesively bonded joints. *International Journal of Adhesion and Adhesives*. 2011, vol.31, no.8, pp.840–850. Available from: doi: 10.1016/j.ijadhadh.2011.08.004

51) JABP Neto, Campilho RDSG, da Silva LFM. Parametric study of adhesive joints with composites. *International Journal of Adhesion and Adhesives*. 2012, vol.37, pp.96–101. Available from: doi: 10.1016/j.ijadhadh.2012.01.019

52) Lousdad A., Megueni A., Bouchikhi AS. Geometric edge shape-based optimization for interfacial shear stress reduction in fiber reinforced polymer plate retrofitted concrete beams. *Computational Materials Science*. 2010, vol.47, no.4, pp.911-918. Available from: doi: 10.1016/j.commatsci.2009.11.023

53) Mahi BE., Benrahou KH., Belakhdar K., Tounsi A., Bedia EAA. Effect of the tapered end of a FRP plate on the interfacial stresses in a strengthened beam used in civil engineering applications. *Mechanics of Composite Materials*. 2014, vol.50, no.4, pp.467–476. Available from: doi: 10.1007/s11029-014-9433-z

54) Nanda Kishore A., Siva Prasad N. An experimental study of Flat-Joggle-Flat bonded joints in composite laminates. *International Journal of Adhesion and Adhesives*. 2012, vol.35, pp.55–58. Available from: doi: 10.1016/j.ijadhadh.2012.02.003

55) Campilho RDSG., de Moura MFSF., Domingues JJMS. Numerical prediction on the tensile residual strength of repaired CFRP under different geometric changes. *International Journal of Adhesion and Adhesives.* 2009, vol.29, no.2, pp.195–205. Available from: doi: 10.1016/j.ijadhadh.2008.03.005

56) Renart J., Vicens J., Budhe S., Rodríguez-Bellido A., Comas J., Mayugo JA., Costa J. An automated methodology for mode II delamination tests under fatigue loading based on the real time monitoring of the specimen's compliance. *International Journal of*

Fatigue. 2016, vol.82, pp.634–642. Available from: doi: 10.1016/j.ijfatigue.2015.09.021

57) Chaves FJP., de Moura MFSF., da Silva LFM., Dillard DA. Fracture characterization of bonded joints using the dual actuator load apparatus using the dual actuator load apparatus. *Journal of Adhesion Science and Technology*. 2014, vol.28, no.5, pp.512–524. Available from: doi: 10.1080/01694243.2013.845357

58) Reis PNB., Soares JRL., Pereira AM., Ferreira JAM. Effect of adherends and environment on static and transverse impact response of adhesive lap joints. *Theoretical and Applied Fracture Mechanics*. 2015, vol.80, pp.79-86. Available from: doi: 10.1016/j.tafmec.2015.07.004

59) Li H, Xian G, Lin Q, Zhang H. Freeze-thaw resistance of unidirectional-fiber-reinforced epoxy composites. *Journal of Applied Polymer Science*. 2012, vol.123, no.6, pp.3781–3788. Available from: doi: 10.1002/app.34870

60) Zhang Y., Vassilopoulos AP., Keller T. Effects of low and high temperatures on tensile behavior of adhesively-bonded GFRP joints. *Composite Structures*. 2010, vol.92, no.7, pp.1631–1639. Available from: doi: 10.1016/j.compstruct.2009.11.028

61) Celemin J.A., Llorca J. The embrittlement of Nicalon/alumina composites at intermediate and elevated temperatures. *Composites Science and Technology*. 2000, vol.60, no.7, pp.1067-1076. Available from: doi: 10.1016/S0266-3538(00)00007-5

62) A. Szekrényes. Overview on the Experimental Investigations of the Fracture Toughness in Composite Materials. *Submitted to HEJ*. 2002, pp.1-9. Manuscript no.: MET-020507-A

63) Denis Roach, Randy Duvall. Detection of Hail Impact Damage in Composite Structures at the Failure Threshold Energy. *Sandia National Labs, FAA Airworthiness Assurance Center.*

64) Kenane M., Benzeggagh M.L. Mixed-mode delamination fracture toughness of unidirectional glass/epoxy composites under fatigue loading. *Composites Science and Technology*. 1997, vol.57, pp.597-605. Available from: doi: 10.1016/S0266-3538(97)00021-3

65) Dahlen C., Springer G.S. Delamination in composites under cyclic loads. *Journal of Composite Materials*. 1994, vol.28, no.8, pp.732-781. Available from: doi: 10.1177/002199839402800803

66) Filatows G.J., Sadler R.L., EL-Shiekh A.H.M. Fracture behavior of 3-D braid graphite/epoxy composite. *Journal of Composite Materials*. 1994, vol.28, no.6, pp.526-542. Available from: doi: 10.1177/002199839402800603

67) Lawcock G., YE L., Mai Y.-W., Sun C.-T. The effect of adhesive bonding between aluminium and composite prepreg on the mechanical properties of carbon-fiber-reinforced metal laminates. *Composites Science and Technology*. 1997, vol.57, no.1, pp.35-45. Available from: doi: 10.1016/S0266-3538(96)00107-8

68) International Organization for Standardization, ISO 15024. Fibre-reinforced plastic composites – Determination of mode I interlaminar fracture toughness, G_{IC}, for unidirectionally reinforced materials. 2001.

69) Cherepanov G. Cracks in solids. *International Journal of Solids and Structures*. 1968, vol.4, no.8, pp.741-835. Available from: doi: 10.1016/0020-7683(68)90059-0

70) Jianing Zhang, Shiqiang Deng, Lin Ye1, Zhong Zhang. Interlaminar Fracture Toughness and Fatigue Delamination Growth of CF/EP Composites with Matrices Modified by Nano-silica and CTBN rubber. *13th International Conference on Fracture*, June 16-21, 2013, Beijing, China

71) A.J. Brunner, B.R.K. Blackman, P. Davies. A status report on delamination resistance testing of polymer-matrix composites. *Engineering Fracture Mechanics*. 2008, vol.75, no.9, pp.2779-2794. Available from: doi: 10.1016/j.engfracmech.2007.03.012

72) Schueker C., Davidson B.D. Evaluation of the accuracy of the four-point bend end-notched flexure test for mode II delamination toughness determination. *Composites Science and Technology*. 2000, vol.60, no.11, pp.2137-2146. Available from: doi: 10.1016/S0266-3538(00)00113-5

73) Miller T.C., LIU C.T. Pressure effects and fracture of a rubbery particulate composite. *Experimental Mechanics*. 2001, vol.41, pp.254-259. Available from: doi: 10.1007/BF02323142

74) V. Pavelko, I. Pavelko, M. Smoļaņinovs. Large Deformation and Failure of Thin-Walled Film at the Post-Buckling Delamination. *Key Engineering Materials*. 2014, vol.577-578, pp.497-500. Available from: doi: 10.4028/www.scientific.net/KEM.577-578.497

75) V. Pavelko. Behavior of Thin-Film-Type Delamination of Layered Composite in Post-Buckling. *Advanced Materials Research*. 2013, vol.774-776, pp.1312-1321. Available from: doi: 10.4028/www.scientific.net/AMR.774-776.1312

76) J. G. Williams. Large displacement and End Block Effects in the DCB Interlaminar Test in Modes I and II. *Journal of Composite Materials*. 1987, vol.21, no.4, pp.330-347. Available from: doi: 10.1177/002199838702100403

77) J. Tsai, C. Guo, C. Sun. Dynamic delamination fracture toughness in unidirectional polymeric composites. *Composite Science and Technology*. 2001, vol.61, pp.87-94. Available from: doi: 10.1016/S0266-3538(00)00197-4

78) J. G. Williams. End corrections for orthotropic DCB specimens. *Composite Science and Technology*. 1989, vol.35, no.4, pp.367-376. Available from: doi: 10.1016/0266-3538(89)90058-4

79) B. N. Rao, A. R. Acharya. Evaluation of fracture energy, G_{Ic}, using a double cantilever beam fibre composite specimen. *Engineering Fracture Mechanics*. 1995, vol.51, no.2, pp.317-322. Available from: doi: 10.1016/0013-7944(94)00251-C

80) B. N. Rao, A. R. Acharya. Maximum load at the initiation of delamination growth in a double cantilever beam specimen. *International Journal of Materials Research*. 2021, vol.86, no.6, pp.428-433. Available from: doi: 10.1515/ijmr-1995-860609

81) V. A. Franklin, T. Christopher. Fracture energy estimation of DCB specimens made of glass/epoxy: An experimental study. *Advances in Materials Science and Engineering*. 2013, pp.1-7. Available from: doi: 10.1155/2013/412601

82) Z. Suo, G. Bao, B. Fan. Delamination R-curve phenomena due to damage. Journal of the Mechanics and Physics of Solids. 1992, vol.40, no.1, pp.1-16. Available from: doi: 10.1016/0022-5096(92)90198-B

83) D. Kaute, H. R. Shercliff, M. F. Ashby. Modeling of fibre bridging and toughness of ceramic matrix composites. *Scripta Metallurgica et Materialia*. 1995, vol.32, no.7, pp.1055-1060. Available from: doi: 10.1016/0956-716X(95)00074-6

84) A.-M. Yan, E. Marechal, H. Nguyen-Dang. A finite element model of mixed-mode delamination in laminated composites with an R-curve effect. *Composite Science and Technology*. 2001, vol.61, no.10, pp.1413-1427. Available from: doi: 10.1016/S0266-3538(01)00041-0

85) S. Hashemi, J. Kinloch, J. G. Williams. Mechanics and mechanisms of delamination in a polyether sulphone-fibre composites. *Composite Science Technology*. 1990, vol.37, no.4, pp.429-462. Available from: doi: 10.1016/0266-3538(90)90013-U

86) V. Tamuzs, S. Tarasovs, U. Vilks. Progressive delamination and fiber bridging modeling in double cantilever beam composite specimen. *Engineering Fracture*

Mechanics. 2001, vol.68, no.5, pp.513-525. Available from: doi: 10.1016/S0013-7944(00)00131-4

87) K.-S. Sohn, S. Lee, S. Baik. Analysis of bridging stress effect of polycrystalline alumina using double cantilever beam method. *Acta Materialia*. 1997, vol.45, no.8, pp.3445-3457. Available from: doi: 10.1016/S1359-6454(97)00012-8

88) J. E. Lindhagen, L. A. Berglund. Application of bridging-law concepts to short-fibre composites. Part 1: DCB test procedures for bridging law and fracture energy. *Composite Science and Technology*. 2000, vol.60, no.6, pp.871-883. Available from: doi: 10.1016/S0266-3538(00)00004-X

89) S. O. Fernberg, L. A. Berglund. Bridging law and toughness characterization of CSM and SMC composites. *Composite Science and Technology*. 2001, vol.61, no.16, pp.2445-2454. Available from: doi: 10.1016/S0266-3538(01)00167-1

90) A. Szekrernyes, J. Uj. Advanced beam model for fibre-bridging in unidirectional composite double-cantilever beam specimens. *Engineering Fracture Mechanics*. 2005, vol.72, no.17, pp.2686-2702. Available from: doi: 10.1016/j.engfracmech.2005.05.001

91) F. Nilsson. Large displacements aspects on fracture testing with double cantilever beam specimens. *International Journal of Fracture*. 2006, vol.139, no.2, pp.305-311. Available from: doi: 10.1007/s10704-006-8376-3

92) V. Tamužs, S. Tarasovs, U. Vilks, I. Rumkovska. Development of test methods for adhesion measurements of flexible elastic materials. 2008. Proc. ECCM-13.

93) R. G. Boeman, D. Erdman, L. Klett, R. Lomax. A practical test method for mode I fracture toughness of adhesive joints with dissimilar substrates. *Advanced Composite Conference*, Detroit, MI, September 27-28 1999, pp.1-9.

94) C. Prasanth, S. Ravindranath, A. Samraj, T. Manikandan. Mode-I fracture analysis of thermally aged of glass and glass-carbon hybrid composites. *International Journal of Innovative Technology and Exploring Engineering*. 2014, vol.3, no.10, pp.84-89.

95) Whitcomb J.D. Finite Element Analysis of Instability Related Delamination Growth. *Journal of Composite Materials*. 1981, vol.15, pp.403-426. Available from: doi: 10.1177/002199838101500502

96) V. Pavelko. Analytical 1D model of delamination development and strength of layered composite beam in postbuckling. *Key Engeering Materials*. 2014, vol.627, pp.325-328. Available from: doi: 10.4028/www.scientific.net/KEM.627.325

97) V. Pavelko. Application of the nonlinear model of a beam for investigation of interlaminar fracture toughness of layered composite. *Key Engineering Materials*. 2015, vol.665, pp.273-276. Available from: doi: 10.4028/www.scientific.net/KEM.665.273

98) S. P. Timoshenko, J. M. Gere. Theory of Elastic Stability 2nd Edition. *McGraw-Hill Book Company*, Toronto (1961) Chapter 2.

99) Budhe S., Banea M. D., de Barros S., da Silva L. F. M. Adhesively bonded joints in composite materials: An overview. *Journal of Materials and Design*. 2016, vol.223, no.1, pp.1-18. Available from: doi: 10.1243/14644207JMDA219

100) Katnam K. B., Comer A. J., Roy D., da Silva L. F. M. Composite Repair in Wind Turbine Blades: An Overview. *The Journal of Adhesion*. 2015, vol.91, no.1-1, pp.113-139. Available from: doi: 10.1080/00218464.2014.900449

101) Needleman A. An analysis of tensile decohesion along an interface. *Journal of the Mechanics and Physics of Solids*. 1990, vol.38, no.3, pp.289-324. Available from: doi: 10.1016/0022-5096(90)90001-K

102) Sørensen B. F. Cohesive law and notch sensitivity of adhesive joints. *Acta Materialia*. 2002, vol.50, no.5, pp.1053-1061. Available from: doi: 10.1016/S1359-6454(01)00404-9

103) Sørensen B. F., and Jacobsen T. K. The determination of cohesive laws by the J integral approach. *Engineering Fracture Mechanic*. 2003, vol.70, no.14, pp.1841-1858. Available from: doi: 10.1016/S0013-7944(03)00127-9

104) Blackman B. R. K., Hadavinia H., Kinloch A. J., Williams J. G. The use of a cohesive zone model to study the fracture of fibre composites and adhesively bonded joints. *International Journal of Fracture*. 2003, vol.119, no.1, pp.25-46. Available from: doi: 10.1023/A:1023998013255

105) Planas J., Elices M., Guinea G. V., Gómez F. J., Cendón D. A., Arbilla I. Generalizations and specializations of cohesive crack models. *Engineering Fracture Mechanics*. 2003, vol.70, no.14, pp.1759-1776. Available from: doi: 10.1016/S0013-7944(03)00123-1

106) Anyfantis K. N., Tsouvalis N. G. A novel traction–separation law for the prediction of the mixed mode response of ductile adhesive joints. *International Journal of Solids and Structures*. 2012, vol.49, no.1, pp.213-226. Available from: doi: 10.1016/j.ijsolstr.2011.10.001

107) Anyfantis K. N. Finite element predictions of composite-to-metal bonded joints with ductile adhesive materials. *Composite Structures*. 2012, vol.94, no.8, pp.2632-2639. Available from: doi: 10.1016/j.compstruct.2012.03.002

108) Tvergaard V., Hutchinson J.W. The relation between crack growth resistance and fracture process parameters in elastic-plastic solids. *Journal of the Mechanics and Physics of Solids*. 1992, vol.40, no.6, pp.1377-1397. Available from: doi: 10.1016/0022-5096(92)90020-3

ANNEX

```matlab
MATLAB code: NL_DCB
%MATLAB code: NL_DCB (processing of test result with obtained with the
non-linear DCB sample
%1. Input data
a=12.5; % local coordinate of the point of force applying, mm (c in Figure
3.4)
t=1.5;    %local coordinate of the point of force applying, mm (t in Figure
3.4) mm
d=1;    % tickness of the lever of DCB, mm
b=20.5;   % widthof of cross-cection of DCB, mm
P0=36.2; % force, N
ex=14.7; % extension, mm
%s0=10;
l0=33.4;  % currant cracl length,mm
del=4.35;% correction of crack length,mm
%del=2*sqrt(P0/s0/l0*b)+del;
l=l0+del;%length of delamination, mm
% 2.Transformation of input data to dimensionless form and initial data
P=P0/b*1000;
ad=a/d;
td=t/d;
ld0=(l-a)/d;
ld=ld0;
dl=0.5/d;
v0l=ex/l/2;
al=ad/ld;
tl=td/ld;
alf0=0.5;
alr0=alf0*pi/180;
alz=atan(a/t);
alr=alr0;
kl0=0.005;dkl=1;dv=0.5;
%3.Solution of equations (4) and (8) taking into account condition (3)
% Numbering of equations corresponds to article
while abs(dv)>0.0001
 if alr<alz
while abs(dkl)>0.0001
    alr=alr0;
    sina=sin(alr);
    cosa=cos(alr);
sna0=sina+(kl0*(al*cosa-tl*sina))^2/2;
al0=asin(sna0);
        p=sqrt((1+sna0)/2);
        fi0=asin(1/p/sqrt(2));
        fiz=asin((sin(alr/2)+cos(alr/2))/p/sqrt(2));
sal1 = @(x) 1./sqrt(2*(sna0-sin(x)));
kl =quad(sal1,0,alr);
dkl=abs(kl-kl0)/kl;
kl0=kl;
end
 end
 kl0=0.0;dkl=1;
   if alr==alz
   while abs(dkl)>0.0001
       alr=alr0;
       e=0.0001*alr;
     sina=sin(alr);
```

```matlab
    cosa=cos(alr);
        sna0=sina+kl0^2/2*(al*cosa-tl*sina)^2;
        al0=asin(sna0);
        p=sqrt((1+sna0)/2);
    sal1 = @(x) 1./sqrt(2*(sna0-sin(x)));
    fi0=asin(1/p/sqrt(2));
        fiz=asin((sin(alr/2)+cos(alr/2))/p/sqrt(2));
    kl =quad(sal1,0,alr-e)+sqrt(2*e/cosa);
    dkl=abs(kl-kl0)/kl;
    kl0=kl;
      end
      end


    kl0=0.1;dkl=1;
    if alr>alz
   while abs(dkl)>0.0001
        alr=alr0;
        e=0.0001*alr;
     sina=sin(alr);
     cosa=cos(alr);
        sna0=sin(alr)+kl0^2/2*(al*cos(alr)-tl*sin(alr))^2;
        al0=asin(sna0);
        p=sqrt((1+sna0)/2);
        fi0=asin(1/p/sqrt(2));
        fiz=pi-asin((sin(alr/2)+cos(alr/2))/p/sqrt(2));
        sal2 = @(x) 1./sqrt(1-p^2*sin(x).^2);
        kl=quad(sal2,fi0,fiz);
    dkl=abs(kl-kl0)/kl;
    kl0=kl;
      end
      end
    va0=v0l-al*sina+tl*(1-cosa);
    sal = @(x) sqrt((sna0-sin(x))/2);
    va =sna0-quad(sal,0,alr)/kl;
    if alr>alz
     va =sna0-(quad(sal,0,alr)+quad(sal,alr,al0))/kl;
    end
    ss1 = @(x) 1./sqrt(1-p^2*sin(x).^2);
        ss2 = @(x) sqrt(1-p^2*sin(x).^2);
     vaa= sna0-2/kl*((p^2-1)*quad(ss1,fi0,fiz)+quad(ss2,fi0,fiz));
     vaa0=vaa;
    dv=(va0-va)/va0;
    alr0=alr*va0/va;dkl=1;
    end
    %4.Calculation of strain energy
    if alr<=alz
    ub=kl/ld*quad(sal,0,alr);    % binding energy, direct integration (DI)
    sl = @(x) (sna0+sin(x)).*sqrt((sna0-sin(x))/2);
    ut=kl^4/24/ld^3*(sna0^2-1/kl*quad(sl,0,alr));% tensile  energy,   direct
integration (DI)
    sll = @(x) sqrt(sna0-sin(x));
    utt=kl^4/72/ld^3*(1+2*sna0^2-
sqrt(2)/kl*(sna0*quad(sll,0,alr)+sqrt(sna0)-cos(alr)*(sqrt(sna0-
sin(alr)))));% tensile energy, direct integration (DI)by transformed equation
    end
    if alr==alz
    ub=kl/ld*(quad(sal,0,alr-e)+sqrt(2*e/cosa));
    sl = @(x) (sna0+sin(x)).*sqrt((sna0-sin(x))/2);
    ut=kl^4/24/ld^3*(sna0^2-1/kl*quad(sl,0,alr));
    end
    if alr>alz
```

```matlab
    ub=kl/ld*(quad(sal,0,alr0)+quad(sal,alr,alr0));   % binding energy, direct
integration (DI)
    sl = @(x) (sna0+sin(x)).*sqrt((sna0-sin(x))/2);
    ut=kl^4/24/ld^3*(sna0^2-1/kl*(quad(sl,0,alr0)+quad(sl,alr,alr0)));%
tensile energy, direct integration (DI)
    sll = @(x) sqrt(sna0-sin(x));
    utt=kl^4/72/ld^3*(1+2*sna0^2-
sqrt(2)/kl*(sna0*quad(sll,0,alr0)+sna0*quad(sll,alr,alr0)+sqrt(sna0)+cos(al
r)*(sqrt(sna0-sin(alr))))));% tensile  energy,  direct  integration  (DI)by
transformed equation
    end
    sal2 = @(x) 1./sqrt(1-p^2*sin(x).^2);
    sal3 = @(x) sqrt(1-p^2*sin(x).^2);
    ub0=kl/ld*2*((p^2-1)*quad(sal2,fi0,fiz)+quad(sal3,fi0,fiz));
    sll = @(x) sqrt(sna0-sin(x));
    ut0=kl^4/72/ld^3*(1+2*sna0^2-
sqrt(2)/kl*(sna0*quad(sll,0,alr)+sqrt(sna0)-cos(alr)*(sqrt(sna0-
sin(alr))))));% tensile energy, eliptic integration (EI)

    u00=2*(ub0+ut0);
    u0=2*(ub+ut);
    Dt2=P*(ld/kl)^2;
    kl;
    ld1=ld0+dl;
    va0=va0*ld/ld1;
    ld=ld1;
    al=ad/ld;
    tl=td/ld;
    kl0=0.005;dkl=1;dv=0.5;
    alf0=0.5;
    alr0=alf0*pi/180;
    while abs(dv)>0.0001
        if alr<alz
    while abs(dkl)>0.0001
        alr=alr0;
        sina=sin(alr);
        cosa=cos(alr);
    sna0=sina+(kl0*(al*cosa-tl*sina))^2/2;
    p=sqrt((1+sna0)/2);
            ap=1/p/sqrt(2);
            fi0=asin(ap);
            fiz=asin((sin(alr/2)+cos(alr/2))/p/sqrt(2));
    sal1 = @(x) 1./sqrt(2*(sna0-sin(x)));
    kl =quad(sal1,0,alr);
    dkl=abs(kl-kl0)/kl;
    kl0=kl;
    end
        end
    if alr==alz
       while dkl>0.0001
            alr=alr0;
            e=0.0001*alr;
        sina=sin(alr);
        cosa=cos(alr);
            sna0=sina+kl0^2/2*(al*cosa-tl*sina)^2;
        p=sqrt((1+sna0)/2);
            ap=1/p/sqrt(2);
            fi0=asin(ap);
            fiz=asin((sin(alr/2)+cos(alr/2))/p/sqrt(2));
    sal1 = @(x) 1./sqrt(2*(sna0-sin(x)));
    kl=quad(sal1,0,alr-e)+sqrt(2*e/cosa);
```

97

```matlab
    dkl=abs(kl-kl0)/kl;
    kl0=kl;
        end
        end


    kl0=2;dkl0=1;
     if alr>alz
   while dkl>0.0001
         alr=alr0;
         e=0.0001*alr;
      sina=sin(alr);
      cosa=cos(alr);
         sna0=sin(alr)+kl0^2/2*(al*cos(alr)-tl*sin(alr))^2;
         al0=asin(sna0);
         p=sqrt((1+sna0)/2);
         fi0=asin(1/p/sqrt(2));
         fiz=pi-asin((sin(alr/2)+cos(alr/2))/p/sqrt(2));
         sal2 = @(x) 1./sqrt(1-p^2*sin(x).^2);
         kl=quad(sal2,fi0,fiz);
    dkl=abs(kl-kl0)/kl;
    kl0=kl;
      end
       end
    sal = @(x) sqrt((sna0-sin(x))/2);
    va =sna0-quad(sal,0,alr)/kl;
     vad=va;
    ss1 = @(x) 1./sqrt(1-p^2*sin(x).^2);
        ss2 = @(x) sqrt(1-p^2*sin(x).^2);
     vaa= sna0-2/kl*((p^2-1)*quad(ss1,fi0,fiz)+quad(ss2,fi0,fiz));
     vaad=vaa;
    dv=(va0-va)/va0;
    alr0=alr*va0/va;dkl=1;
    end
    if alr<=alz
    ub1=kl/ld*quad(sal,0,alr);     % bending energy, direct integration (DI)
    sl = @(x) (sna0+sin(x)).*sqrt((sna0-sin(x))/2);
    ut1=kl^4/24/ld^3*(sna0^2-1/kl*quad(sl,0,alr));% tensile energy, direct
integration (DI)
    sll = @(x) sqrt(sna0-sin(x));
    utt1=kl^4/72/ld^3*(1+2*sna0^2-
sqrt(2)/kl*(sna0*quad(sll,0,alr)+sqrt(sna0)-cos(alr)*(sqrt(sna0-
sin(alr)))));% tensile energy, direct integration (DI)by transformed equation
    end
    if alr>alz
    ub1=kl/ld*(quad(sal,0,alr0)+quad(sal,alr,alr0));      % binding energy,
direct integration (DI)
    sl = @(x) (sna0+sin(x)).*sqrt((sna0-sin(x))/2);
    ut1=kl^4/24/ld^3*(sna0^2-1/kl*(quad(sl,0,alr0)+quad(sl,alr,alr0)));%
tensile energy, direct integration (DI)
    sll = @(x) sqrt(sna0-sin(x));
    utt1=kl^4/72/ld^3*(1+2*sna0^2-
sqrt(2)/kl*(sna0*quad(sll,0,alr0)+sna0*quad(sll,alr,alr0)+sqrt(sna0)+cos(al
r)*(sqrt(sna0-sin(alr)))));% tensile energy, direct integration (DI)by
transformed equation
    end

    sal2 = @(x) 1./sqrt(1-p^2*sin(x).^2);
    sal3 = @(x) sqrt(1-p^2*sin(x).^2);
    ub01=kl/ld*2*((p^2-1)*quad(sal2,fi0,fiz)+quad(sal3,fi0,fiz));

    sll = @(x) sqrt(sna0-sin(x));
```

```matlab
    ut01=kl^4/72/ld^3*(1+2*sna0^2-
sqrt(2)/kl*(sna0*quad(sll,0,alr)+sqrt(sna0)-cos(alr)*(sqrt(sna0-
sin(alr)))));% tensile energy, eliptic integration (EI)

    u01=2*(ub1+ut1);
    u001=2*(ub01+ut01);
    %5.Definition of interlaminar fracture toughness(IFT)
    Gc=(u0-u01)/dl*Dt2;% IFT by non-linear model
    Gc0=(u00-u001)/dl*Dt2;% IFT by non-linear model
    % 6. Additional estimations (linear estimates)
    Gc1=9/4*Dt2*(ex/d)^2/(l/d)^4;% IFT  by  linear  model  using  cylindrical
stiffness
    Gc2=3*P*(ex/l)/2;% IFT by MBT method
```